Understanding the molecular basis of regulation of class I PI3Ks by activation signals, oncogenic mutations, and post-translational modifications

by

Harish Ranga-Prasad
Bachelor of Technology, SRM University 2016

A Thesis Submitted in Partial Fulfillment
of the Requirements for the Degree of

MASTER OF SCIENCE

in the Department of Biochemistry and Microbiology

Supervisory Committee

Understanding the molecular basis of regulation of class I PI3Ks by activation signals, oncogenic mutations, and post-translational modifications

by

Harish Ranga-Prasad
Bachelor of Technology, SRM University 2016

Supervisory Committee

Dr. John E Burke
Department of Biochemistry and Microbiology
Supervisor

Dr. Julian J Lum
Department of Biochemistry and Microbiology
Departmental Member

Dr. Bob Chow
Department of Biology
Outside Member

Abstract

Class I Phosphoinostide-3 Kinases (PI3K) generate Phosphatidylinositol-3, 4, 5 Trisphosphate (PIP_3), which regulates important cellular tasks such as proliferation, cell growth, survival and metabolism through membrane recruitment and activation of downstream targets that bear PIP_3 recognizing domains. Misregulation of class I PI3K signaling is found in several human diseases, such as cancer, immunological disorders, neurological disorders, diabetes, localized tissue overgrowth, and cardiovascular disease. Due to the essential roles of class I PI3Ks, their activity is held under tight control through molecular interactions with various activating partners and post- translational modifications (PTM). The aim of my thesis is to study the regulation of class I PI3Ks by activation signals, post-translational modifications (PTM), and oncogenic mutations. To this end, we have utilized a combination of cutting-edge biophysical and biochemical techniques like Hydrogen- Deuterium Exchange Mass Spectrometry (HDX-MS), lipid kinase assays and protein- lipid Fluorescence Resonance Energy Transfer (FRET) assays. Our results provide insights into novel aspects of regulation of PI3Kα by oncogenic mutations and the role of PTMs in modulating the activity of PI3Kγ. This work provides an excellent framework for understanding how PI3Ks are involved in human diseases.

Table of Contents

List of Tables

List of Figures

Acknowledgments

I would like to start with thanking my supervisor, Dr. John Burke for his continuous scientific and moral support over the past three years. I am grateful for all the experience I was able to get in his lab.

Next, I would like to thank my committee members, Dr. Julian Lum and Dr. Bob Chow for their guidance and feedback which have greatly helped shape my thesis. I would also like to thank Dr. Alisdair Boraston for his feedbacks.

I would like to extend my gratitude to everyone in the John Burke lab, Manoj, Meredith, Alex, Noah, Kaelin, Sushant, Matthew Parson, Matthew Thibodeau, and Edward. I would like to use this opportunity to thank Manoj for all the support during my initial days as I was learning to work during COVID and other troubling times. I would also like to thank Meredith for all her help and guidance right from experimental setup to analysis. I treasure all our wing nights, and the enjoyable work atmosphere.

I would like to thank all my friends for the fun times and for helping me get through these past three years: Kavina, Vishnu, Amruta Gupta, Antra, Raj, Prathyusha, Prerna and Pavitra. I find myself extremely lucky to have all these wonderful people supporting me in my academic and personal lives. Finally, I would like to thank my brother Rishi and my father for all their emotional support and moral guidance.

List of Abbreviations

aa	Amino acid
ABD	Adaptor binding domain
ADP	Adenosine diphosphate
ATP	Adenosine triphosphate
BLI	Biolayer interferometry
β-Me	Beta mercaptoethanol
CHAPS	3-[(3-Cholamidopropyl) dimethylammonio]-1-propanesulfonate
Cryo-EM	Cryogenic electron microscopy
DMSO	Dimethyl sulfoxide
DNA	Deoxyribonucleic acid
EM	Electron Microscopy
FBS	Foetal Bovine Serum
GBD	Gβγ binding domain
GDP	Guanosine diphosphate
GFB	Gel filtration buffer
GPCR	G-protein coupled receptor
GTP	Guanosine triphosphate
HDX-MS	Hydrogen deuterium exchange mass spectrometry
IgE	Immunoglobulin E
kDa	Kilodalton
mTOR	Mammalian target of rapamycin
MS	Mass spectrometry
MS/MS	Tandem mass spectrometry
MWCO	Molecular weight cut off
Ni-NTA	Nickel nitrotriacetic acid
NB	Nanobody
PBD	p110γ binding domain
PBS	Phosphate buffer saline
PC	Phosphatidylcholine
PCR	Polymerase chain reaction
PDB	Protein data bank
PDGFR	Platelet derived growth factor receptor
PDK1	Phosphoinositide dependent kinase 1
PE	Phosphatidylethanolamine
PH	Pleckstrin homology
PI	Phosphoinositide
PI3K	Phosphoinositide 3-kinase
PIP_2	Phosphatidylinositol-4,5-bisphophate
PIP_3	Phosphatidylinositol-3,4,5-trisphosphate
PM	Plasma membrane
PKA	Protein kinase A
PKC	Protein kinase C
PS	Phosphatidylserine
PTM	Post-Translational Modification

PTEN	Phosphatase and tensin homolog
pY	Phosphorylated tyrosine
RBD	Ras binding domain
RTK	Receptor tyrosine kinase
SDS-PAGE	Sodium dodecyl sulphate polyacrylamide gel electrophoresis
Sf9	*Spodoptera frugiperda* 9
SH2	Src homology 2
SM	Sphingomyelin
Strep	Streptavidin
TAM	Tumor-associated macrophage
TCEP	Tris(2-carboxyethyl)phosphine)
TLR	Toll-like receptor
TOF	Time of flight
TSC2	Tuberous sclerosis complex 2
VEGF	Vascular endothelial growth factor
WT	Wild type

Thesis Format and Manuscript Claims

This thesis was written to follow the format of a manuscript. Chapter one summarizes relevant background information and the thesis' rationale and objectives. Chapter two follows a manuscript format and contains an abstract, introduction, materials and methods, results, and discussion sections. Chapter three also follows a manuscript format and contains an abstract, introduction, materials, and methods, results and discussion sections. The last chapter highlights the findings of the thesis, provides a conclusion, and suggests possible future directions for this work.

Chapter two adapted from: Ranga-Prasad H, Jenkins ML, Parson M. AH, Rathinaswamy MK and John E Burke (2022). Oncogenic mutations of PIK3CA lead to increased membrane recruitment driven by reorientation of the ABD, p85 and C-terminus.

(bioRXiv link: https://www.biorxiv.org/content/10.1101/2022.04.05.487205v1.full)

Chapter 1: Introduction

1.1 Overview: PI3K signalling

Membrane bound phosphoinositides (PIs) are critical regulators of several cellular processes and biological responses such as growth, proliferation, survival, mobility, and differentiation. The structure of PIs consists of a glycerol backbone bound to a *myo*-inositol ring and two fatty acid chains; stearic acid at sn-1 position and arachidonic acid at sn-2 positions in the glycerol backbone[1] (Fig 1.1A). These lipids control cellular processes through reversible phosphorylation at the 3, 4, and 5 positions of the inositol ring. Such reactions are orchestrated through recruitment of several phosphatidylinositol kinases and phosphatases. These enzymes catalyse the phosphorylation either at a single site or in combination to generate seven different PI species namely, PI3P, PI4P, PI5P, PI(3,4)P2, PI(4,5)P2, PI(3,5)P2 and PI(3,4,5)P3.

PI3Ks are enzymes that can phosphorylate the 3' position of the inositol ring. Phosphatidylinositol 3,4,5 trisphosphate (PIP_3) is formed by the activity of class I Phosphoinositide 3-Kinase (PI3K), when stimulated by signal molecules that activate cell surface receptors like receptor tyrosine kinases (RTKs) and G-protein-coupled receptors (GPCRs). PIP_3 is a potent signaling molecule and is responsible for the regulation of a repertoire of downstream targets of cellular activities, such as growth, proliferation, differentiation, migration, and metabolism, including activation of AKT, an oncogenic protein. PI3Ks are divided into three classes based on their primary structure and substrate specificity. These classes are class I, II and III, and only class I PI3Ks can generate PIP_3. The Class II PI3Ks synthesize PI3P and $PI(3,4)P_2$ and studies have shown their importance in cell proliferation, migration, and metabolism[2]. Class III PI3Ks

generates only PI3P which is an important regulator of membrane trafficking and an mTOR signaling mediator[3].

Class I PI3Ks are heterodimers consisting of a catalytic subunit and a regulatory subunit. The members of this family are bound to regulatory subunits, which determine the signals operating its activity. They are classified into two sub classes based on their interaction with the regulatory subunit as Class IA PI3Ks, consisting of p110α, p110β and p110δ, while the class IB consists of a sole member called p110γ[4]. The class IA catalytic subunits interact with p85 like regulatory subunits that consists of SH2 domains that stabilizes the catalytic subunit, locking the protein in an inactive confirmation and potentiates activation by regulatory signals[5]. p110γ of Class IB interacts with either p101 or p84, and unlike class IA the interaction with the regulatory subunit does not inhibit the enzyme activity and potentiates activation downstream of activation signals [6–8]. The members of class I p110s differ in their cellular distribution; p110α and p110β can be found across all cell types, whereas p110δ and p110γ are found to be enriched in specialized cells such as immune cells[3]. Irregularities in the class I PI3K pathway driven by either activating or inactivating mutations and deletions have been implicated in a broad spectrum of human diseases, such as cancer, immunological disorders, neurological disorders, diabetes, localized tissue overgrowth, and cardiovascular disease. This thesis focuses on the regulation of PI3Kα and PI3Kγ by activation signals, oncogenic mutations and PTMs.

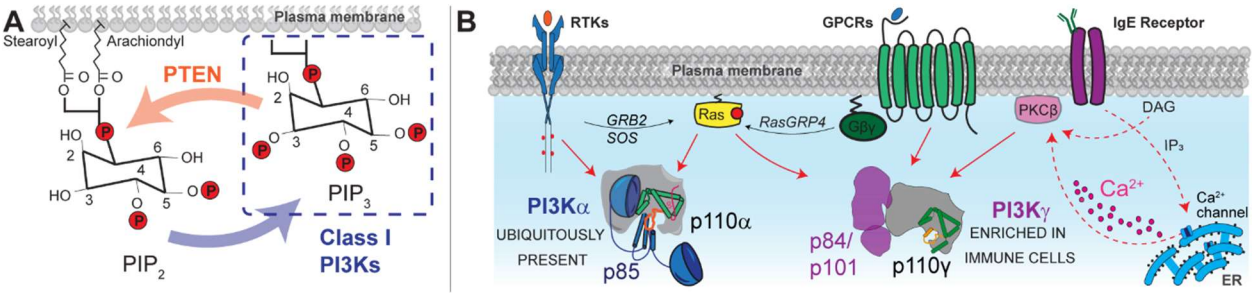

Fig 1.1: Activation of class I PI3Ks generate PIP_3 (A) PIP3 is generated at the plasma membrane (PM) by the action of class I PI3K that phosphorylates at the 3' position on the inositol ring of PIP_2. PTEN is a phosphatase that has been shown to dephosphorylate PIP_3 to generate PIP_2 **(B)** Cartoon model showing the various activation signals that regulate class I PI3Ks. PI3Kα is activated by RTKs and Ras. PI3Kγ complexes are activated by Ras and GPCRs with p110γ/p101 being more sensitive to GPCR activation over p110γ/p84. p110γ/p84 can also be activated by PKC downstream of IgE receptors.

1.2 Structural features that dictate regulation of PI3K

PI3Kα is a heterodimer composed of a catalytic (p110α) and a regulatory subunit (p85α), encoded by PIK3CA and PIK3R1, respectively (refer Fig 1.2a). The catalytic subunit consists of an N-terminal adaptor binding domain (ABD) that mediates binding to the iSH2 domain of p85α, a Ras binding domain (RBD) that interacts with switch I and II regions of RAS to stabilize p110α/p85α on the membrane [9,10], a C2 domain (C2) that participates in membrane binding, a helical domain, which interacts with nSH2, and a kinase domain, which hosts functionally important regions including the PIP_2 and the ATP binding pockets. The RBD, C2, helical, and kinase domains together form the catalytic core of PI3Ks, which is conserved through the class I, II, and III PI3Ks[7,11]. The ABD of class IA PI3Ks binds irreversibly to the iSH2 coiled coil domain present in all class IA regulatory subunits[12] and forms an inhibitory intra-subunit interface with the N-lobe of the kinase domain.

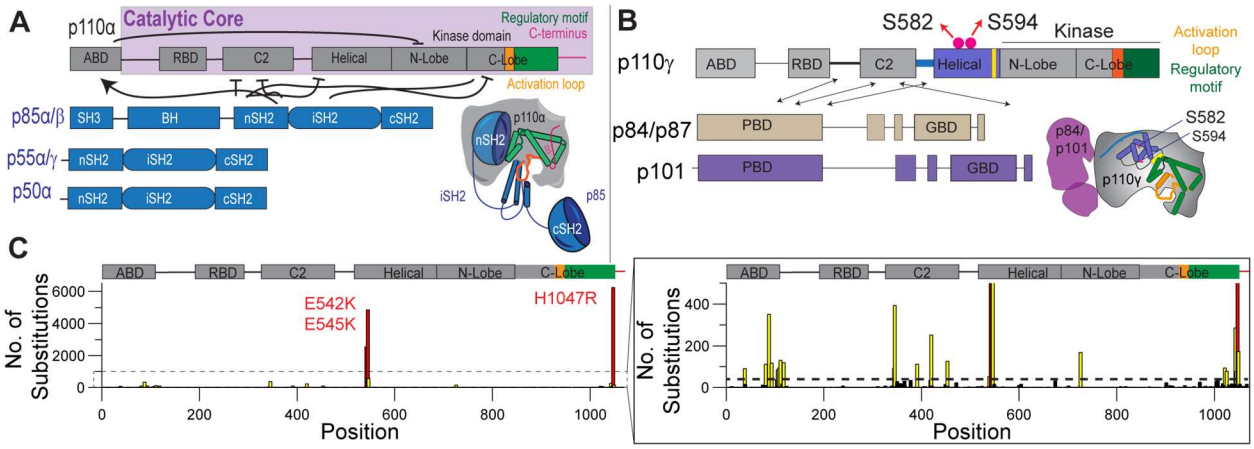

Fig 1.2: The activity of class I PI3Ks are regulated by the binding of regulatory partners, PTMs and oncogenic mutations. Domain schematics of (A) class IA isoform p110α and its regulatory partners and (B) class IB enzyme p110γ along with p84 and p101. The cartoon schematic of the enzyme showing the various regions including the regulatory motif and regulatory partner binding sites colored according to the domain organization. The arrows indicate the binding sites and inhibition coming from the regulatory partner binding. The pink dots in p110γ domain schematics indicates the phosphorylation sites for PKCβ. (C) Frequency of mutations across the primary sequence of *PIK3CA* from the **C**atalog **o**f **S**omatic **M**utations **i**n **C**ancer (COSMIC) database (data from January 2022).

The regulatory subunits of Class IA consist of five isoforms namely p85α, p85β, p55γ, p50α and p50γ. These contain two Src homology 2 (SH2) domains, namely nSH2 and cSH2, that bind to the pYXXM motifs of the phosphorylated RTK, and an inter coiled-coil domain (iSH2) between them, which mediates the high-affinity interaction to ABD of the catalytic subunit. These domains are preceded by a Src homology 3 domain (SH3), a Bar cluster region homology domain (BH), and two proline-rich regions, PR1 and PR2 surrounding the BH domain in p85α and p85β (refer Fig 1.2a)[13,14]. It is also reported that these domains could facilitate the homodimerization of p85α[15]. Apart from p85α, *PIK3R1* also encodes for p55α and p50α, which are functional splice variants that lack the domains required for homodimerization (they lack the proline-rich region, BH and SH3 domains) (see Fig 1.2a). The SH2 domains mediate the inhibition of p110 through several

reversible inhibitory interactions. These contacts occur between the nSH2 of p85 with the C2, helical, and kinase domains of p110 and the iSH2 domain packing up against the activation loop. In p110β and p110δ, the cSH2 domain also interacts and inhibits the kinase domain, this interaction is not found in p110α. Cellular studies from the Cho lab have indicated that multiple lipids bind the C-terminal of SH2 domains in a spatiotemporal manner[16]. Further Hydrogen-Deuterium Exchange Mass Spectrometry (HDX-MS) experiments have also indicated that the region spanning residues 405-420 in nSH2 showed decreased hydrogen-deuterium exchange upon membrane binding with HRAS-coupled vesicles, suggesting that nSH2 could not only bind to the RTKs but potentially to the membrane[17].

Extensive biophysical experiments on the free p110γ catalytic subunit and studies from our lab with the p110γ-p101 complex have revealed insight into the architecture and regulation of p110γ by the two different regulatory subunits. The p110γ subunit exists as a heterodimer with p101, while it forms a weaker/transient interaction with p84 [7], but the molecular basis for this was not understood, until recently[8]. Both subunits contain a N-terminal helical p110γ binding domain (PBD), a central α/β barrel domain, and a C-terminal beta-sandwich Gβγ binding domain (GBD). p84 and p101 binds to the C2 domain and the RBD-C2 and C2-helical linkers of p110γ. The primary interface for p110γ in p84 was located at the N-terminal helical region of p84, with additional interactions involving the GBD and C-terminus. One of the primary differences between p101 and p84 regulatory subunits is their differential ability to be recruited by lipidated Gβγ subunits. Cryo-EM studies with p110γ/p101 revealed the presence of an addition Gβγ binding site which was labelled as Gβγ binding domain (GBD)[7]. Further cryo-EM and HDX-MS

analysis of p110-p84 revealed that p110-p101 can bind two Gβγ molecules while p110-p84 binds to single Gβγ subunits[8].

The key structural elements controlling the enzyme activity lies in the C-terminal kinase domain called the regulatory motif (Fig 1.2a). This consists of helices kα7-12 that surrounds the activation loop and keeps the enzyme in an inactive state[18,19]. This region is kept in an inactive confirmation by their interaction with cSH2 domain (in p110β and p110δ) or through an internal tryptophan lock (in p110α and p110γ). In addition, the regulatory motifs of class IA catalytic subunits are also inhibited by their interactions with the nSH2 domain.

The full molecular mechanism of how PI3Kα is recruited to the membrane and becomes activated remains unclear. RTKs activate PI3Kα through binding of the SH2 domains to the pY residues (pYXXM motifs) located in the activated RTK. The activation of PI3Kα leads to dissociation of nSH2 from the helical domain triggering a series of allosteric changes. In the inactivated conformation of PI3Kα, nSH2 interacts with the C2, helical and kinase domains[20]. Upon the nSH2 binding to the receptor, these interactions cease to exist. The transition of PI3Kα from an inactive cytosolic state to an activate membrane bound state entails four distinct events. The interface between nSH2 and the helical domain which includes charge interactions between the negatively charged helical domain and the positively charged nSH2 get disrupted. The nSH2 release is partially destabilizing the iSH2-C2 and ABD-Kinase interfaces revealing its inhibitory role[20,21]. Conformational changes in the iSH2-C2 interface and the ABD/RBD linker may be mechanistically linked according to HDX-MS data. It was also observed that mutations in

the ABD-RBD linker caused similar conformational changes to those located at the iSH2-C2 interface [21].

One of the most functionally important structural elements of PI3Kα is the C-terminal tail. Mutations in the C-terminal tail may influence the allosteric regulation of enzyme activity, the lipid binding, the phosphoryl-transfer, or the product release during catalysis[13]. The hotspot H1047R mutation alters membrane recruitment as it leads to a large rearrangement of the C-terminus into an active conformation leading to enhanced membrane recruitment[21]. The HDX-MS data comparing the H1047R oncogenic mutant against WT revealed exposures in the membrane-binding regions at residues 848-859 (Active site), 859-872, 930-956 (Activation loop) and 1039-1068 (C-terminus). Mandelker *et all* reported the crystal structure of the mutated heterodimer and observed that R1047 points toward the cell membrane, perpendicular to the orientation of H1047 in the WT enzyme [22] (refer chapter 2 for more details). They also performed biochemical assays that revealed that the enzymatic activity of the p110α H1047R mutant is differentially regulated by lipid membrane composition[22]. Hon *et al.* have shown that the activated c-terminal mutants H1047L, H1047R and G1049R mutants increase electrostatic interactions with lipids[23]. Within the foci of H1047, there are other high frequency mutations: M1043 L/V/I, G1049 R/ S/A (identified from the COSMIC database) and the recently identified frame shift mutations. These C-terminal mutants together account for >50% of total PIK3CA-related oncogenic mutations. Although the activation potential of these mutants has been tested using non-cancerous cell lines[24,25], the structural implications and the mechanism of activation are still unknown.

1.3 Post-translational modifications

Apart from activation signals, the activity of PI3K can also be regulated by PTMs. Studies have identified PTMs found within both the catalytic and regulatory subunits of class I PI3Ks, but the structural implications of these modifications are yet to be studied. Post-translational modifications of p85α regulate the catalytic activity of PI3Kα. Phosphorylation of S361 in nSH2, and of S652 in cSH2, by Protein Kinase C (PKC), and phosphorylation of S690 in cSH2, by IkB kinase (upstream regulator of NFkB and promotes expression of anti-apoptotic genes), prevent these domains from binding to phosphorylated tyrosine receptors. On the contrary, phosphorylation of Y688 in cSH2 may activate PI3Kα by facilitating an intramolecular interaction with nSH2. Moreover, phosphorylation of S83 in the SH3 domain by protein kinase A (PKA) promotes binding of 14-3-3z, which leads to increased membrane binding and PI3Kα activity[26]. The catalytic subunit, p110α can phosphorylate the regulatory subunit, p85α, at S608, although this autophosphorylation is not a significant regulator of the lipid kinase activity of PI3Kα[27]. Moreover, p85α is phosphorylated on Y508 by the Platelet Derived Growth Factor Receptor (PDGFR)[28]. Cruz-Herrera *et al.*[31] suggested that small ubiquitin like modifiers (SUMO1 and SUMO2) modulate p85 function by reducing the levels of tyrosine-phosphorylated-p85. Different lysine residues located at the iSH2 domain are putative SUMOylation sites. However, the post-translational modifications in other regulatory subunits for Class I isoforms are currently unknown.

Class IB PI3K catalytic subunit, p110γ has been previously shown to be phosphorylated in the helical domain upon activation of the IgE receptors. In response to the clustering of IgE receptors and Ca^{2+} influx from store operated Ca^{2+} channels, PKCβ

has been shown to phosphorylate p110γ at S582, which has been shown to be essential for mast cell degranulation[30]. Interestingly, this event also correlates with the release of the p84 subunit and has been shown to operate PI3Kγ downstream of Ca^{2+} and PKCβ[31]. The regulatory subunit p84 undergoes phosphorylation at T607 which has been shown to be important for p110γ-p84 dimerization and the tumour suppressor role of p84[32].

1.4 Activation of PI3Ks

Class I PI3Ks are activated downstream of three membrane bound activation signals namely: RTK, GPCRs and GTP bound Ras. PI3Kα is primarily activated downstream of RAS (leading to membrane recruitment) and RTK signalling (relieves nSH2 mediated inhibition and iSH2 packing up against the C2 and the activation loop). The phosphopeptide sequence of the RTKs binds to the nSH2 domain, disrupting the charge-charge interaction between the nSH2 domain and the helical domain of p110α[13,33]. pY also binds to cSH2, however, cSH2 does not have an inhibitory role in PI3Kα[20]. Two conserved FLVR motifs (res. 355-358 in nSH2 domain and 646-649 in cSH2 domain) are critical for binding to the phosphorylated RTK[26]. Upon activation, p110α is recruited to the membrane where it interacts with Ras to synthesize $PI(3,4,5)P_3$ by transferring the γ-phosphate group of ATP to $PI(4,5)P_2$. Previous work from our lab has shown that the synergistic activation from both these signals are required for the complete activation of the enzyme[17].

Gβγ subunits from GPCR has been shown to activate PI3Kγ. Work with mouse neutrophils have shown that p110γ/p101 and p110γ/p84 control distinct functions of the

PI3Kγ pathway. The p110γ/p101 complex has been shown to promote cell migration whereas the p110γ/p84 complex leads to Reactive Oxygen Species production (highly reactive metabolites of oxygen including superoxide, hydrogen peroxide, hydroxyl radical, and hypochlorous acid)[34]. These signaling outputs are dependent on PI3Kγ activation that occurs downstream of GPCRs, Ras superfamily of GTPases and post-translational modifications. Activation of the p110γ-p101 complex is dependent on Gβγ[6], whereas the p110γ-p84 complex requires Ras as a co-stimulator along with Gβγ for complete activation[35].

The generation of PIP_3 upon subsequent activation and membrane recruitment of PI3K leads to the recruitment of multiple PIP3 effector proteins to the plasma membrane. These include protein kinases such as pyruvate dehydrogenase kinase 1(PDK1), Akt/ protein kinase B, Bruton's tyrosine kinase (BTK), etc. and guanine nucleotide-exchange factors (GEFs)/GTPase activating proteins (GAPs) of Ras superfamily GTPases. One of the well-studied effectors of the PI3K pathway is AKT. Upon generation of PIP_3, AKT is translocated to the membrane mediated by its pH domain and cascades signalling pathway through phosphorylation of numerous substrates that regulate crucial cellular functions. These functions include protein synthesis (through activation of TSC2 and PRAS40), glucose metabolism (AS160 and TXNIP), apoptosis (FOXO), abundance of acetyl-COA[36,37] etc. Signal cascades downstream of these effectors play key roles in growth, metabolism, and survival and are important in immune cell development.

1.5 Role of PI3Ks in human diseases and drug discovery

Class I PI3Ks are frequently mutated in human disease, with both activating and inactivating mutations identified in multiple diseases. Mutations in class IA catalytic and regulatory subunits (p110α, p110δ, p85α, and p85β) cluster at both intra- and inter-subunit inhibitory interfaces (Fig 1.2C). The *PIK3CA* gene encoding p110α is one of the most frequently mutated oncogenic drivers in cancer ([38,39]), with >17,000 somatic mutations in the Catalog Of Somatic Mutations In Cancer (COSMIC) database[40]. The majority of *PIK3CA* mutations cluster at one of the two hotspot regions; the nSH2-helical interface (E542K, E545K) and the c-terminus of the kinase domain (H1047R). Other mutations cluster at the C2-iSH2, nSH2-helical, and ABD-kinase regulatory interfaces and the regulatory motif. In addition to the role of *PIK3CA* in cancer, the same mutations are also found in overgrowth syndromes[35,41,42] distributed throughout the primary sequence including the hotspot mutations. These conditions are pooled under one umbrella term called the PIK3CA Related Overgrowth Syndrome (PROS)[43]. These mutations activate kinase activity through both disrupting inhibitory inter-domain interactions and increasing recruitment to membrane substrate[21]. However, the exact mechanism through which these mutations activate the enzyme is currently unknown except for the hotspot mutations. The p110β subunit is not commonly somatically mutated in cancer; however, its activity is critical in promoting tumorigenesis in cancers driven by the loss of the PIP_3 phosphatase PTEN[44]. Somatic activating mutations also occur in the p85α subunit in cancer[45] and overgrowth syndromes[46]; however, mutations in p85α unable to bind p110 (R348*) are also oncogenic, presumably through misregulations of p110 free p85α and its interaction with other binding partners[47].Activating point mutations in the p110δ isoform have been identified in

primary immunodeficiency patients, with this disease called activated PI3K delta syndrome (APDS1)[48]. These mutations are in similar positions to oncogenic mutations in p110α. A splice site mutant in PIK3R1 that leads to an internal deletion at the N terminus of the iSH2 has also been identified in primary immunodeficiency patients, referred to as APDS2[49]. Biochemical studies of the p85α splice mutant reveal that it primarily activates p110δ over p110α[50].

Similar to class IA isoforms, p110γ has been implicated in multiple human diseases and its inhibition have shown to provide protection against tumour and auto-immune disorders. Pharmacological or genetic inhibition of PI3Kγ led to reduced atherosclerotic lesions in mouse models[51]. It also plays a vital role in inflammation in obesity-induced insulin resistance. This was seen in PI3Kγ KO mice that provided protection against β-cell apoptosis and improved fasting insulin levels[52]. Although p110γ has a low number of oncogenic mutations in comparison to p110α, blocking PI3Kγ signalling resulted in anti-angiogenic effects in tumour. Targeting p110γ has also shown protection against inflammatory diseases such as allergy, anaphylaxis[53], pulmonary fibrosis, cystic fibrosis and respiratory infection[54].

Targeting PI3Ks has been a challenging as the various PI3K isoforms are structurally related to each other and other PI3K related kinases such as mTOR. Multiple preclinical studies and clinical trials have resulted in only seven FDA approved drugs namely Everolimus and Temsirolimus (mTOR inhibitors), Alpelisib (PI3Kα inhibitor), Idelalisib (PI3Kδ inhibitor), Copanlisib (PI3Kα/δ inhibitor), Duvelisib (PI3Kγ/δ inhibitor) and Umbralisib (PI3Kδ/CK1ε inhibitor). Isoform-selective ATP competitive PI3K inhibitors have been developed, with high-resolution structural information being critical in defining

the molecular mechanism of specificity. Complicating the use of PI3Kα inhibitors is that they can lead to insulin feedback, which can reactivate the PI3K-mTOR signaling pathway. Inhibition of PI3K signalling with Alpelisib led to PI3Kα pathway inhibition with both WT and mutants which caused a spike in blood insulin levels (hyperglycemia) which led to reactivation of the pathway. Interestingly pharmaceutical, or dietary suppression of insulin feedback can enhance the effectiveness of PI3K inhibitors in animal models, revealing a potential novel approach for clinical trials of PI3K inhibitors[55]. This warrants the development of novel strategies to mitigate and/or manage on- target and off- target toxicities, identifying PI3K dependent tumours and enhancing the specificity of the small molecules. Ongoing examinations and the future of PI3K inhibitors in cancer are focused on oncogenic mutant-specific compounds[37], combination therapies, and the use of PI3K inhibitors as immunomodulators of the tumor microenvironment[56,57]. For instance, PI3Kγ inhibition has been shown to promote pro-immune macrophages and increased CD8+ T-cell signalling against tumour cells[56].

1.6 Research Objectives

The Class I PI3Ks play an important role in maintaining cellular homeostasis and growth, however misregulations in p110s have been implicated in tumours, immunity disorders and other overgrowth syndromes. The activity of class I PI3Ks can be altered by activation signals, binding of regulatory partners, post-translational modifications, and oncogenic mutations. Through my research, I want to understand such regulatory mechanisms that control the enzyme activities of class I isoforms PI3Kα and PI3Kγ. Specifically, I intend to answer the following questions:

1. What are the molecular mechanisms of activation for the oncogenic mutations in PIK3CA?

   For this, we hypothesize that oncogenic mutations in PIK3CA would either disrupt ABD-p85 inhibition or regulatory motif inhibition. This was based on mapping these frequently mutated residues on the protein structure, which revealed that these residues occurred at the interface of these inhibitory contacts (Fig 2.1b). To test this, we will be assessing the difference between WT and the mutants with respect to their structural changes and membrane recruitment using HDX-MS and protein-lipid FRET experiments respectively.
2. What are the implications of the PKCβ mediated phosphorylation event in p110γ?

   For this, we hypothesize that the activating modification leads to allosteric changes in the kinase domain causing enhanced enzyme activity. This will be tested using a series of biochemical assays and HDX-MS experiments to compare the structural and biochemical changes in p110γ upon phosphorylation.

The development of mutant selective compounds is an essential goal in PI3K therapeutic development. Recently, Genentech reported a compound that led to mutant selective degradation of mutant p110α/p85β over wild type[58], with additional mutant H1047R selective compounds recently reported by Petra and Relay Therapeutics. Therefore, understanding the molecular mechanism of how the full complement of all oncogenic mutants activate PI3K activity is fundamental for future therapeutic development. Similarly, there are potential challenges for selective p110γ inhibitors, as immune side effects may be difficult to avoid which is highlighted in patients with inactivating primary immunodeficiency clinical p110γ mutations[59,60]. Therefore,

understanding the molecular basis for regulation of p110γ-p84 and p110γ-p101 complexes by activation signals and PTMs would provide valuable information for developing specific inhibitors against the two complexes which may be beneficial for reducing the side effects.

Chapter 2: Molecular basis for activation and regulation of PI3Kα

Adapted from:

Harish Ranga-Prasad, Meredith L Jenkins, Matthew AH Parson, Manoj K Rathinaswamy, John E Burke (2022). Oncogenic mutations of PIK3CA lead to increased membrane recruitment driven by reorientation of the ABD, p85 and C-terminus.

Contributions:

JEB, HR-P and MKR designed all biophysical/biochemical experiments. HRP, MKR and MLJ cloned all the constructs used in this study (except WT p110α and p85α), Protein expression and purification were carried out by HR-P with assistance from MKR and MLJ. Biochemical assays were performed by HR-P. All HDX-MS samples were made by HR-P and M.K.R prepared samples for experiments shown in Fig 2.4 A,C and D with assistance from M.L.J and M. AH. P. HDX-MS analysis was done by HR-P, M.L.J and JEB. Sushant Suresh – Purified free p85α used in Fig 2.3B; HP and JEB wrote the manuscript with input from all authors.

2.1 Abstract

PIK3CA encoding the phosphoinositide 3-kinase (PI3K) p110α catalytic subunit is frequently mutated in cancer. The full set of mechanisms underlying how PI3Ks are activated by oncogenic mutations on membranes are still undefined. Using a synergy of biochemical assays and hydrogen deuterium exchange mass spectrometry (HDX-MS), we reveal unique regulatory mechanisms underlying PI3K activation. Engagement of p110α on membranes leads to disengagement of the ABD of p110α from the catalytic core, and the C2 domain from the iSH2 domain of the p85 regulatory subunit. PI3K activation also requires reorientation of the p110α C-terminus, with mutations that alter the inhibited conformation of the C-terminus increasing membrane binding. Mutations at

the C-terminus (M1043I/L, H1047R, G1049R, and N1068KLKR) activate p110α through distinct mechanisms, with this having important implications for mutant selective inhibitor development. This work reveals unique mechanisms underlying how PI3K is activated by oncogenic mutations and explains how double mutants can synergistically increase PI3K activity.

2.2 Introduction

Activating mutations in the gene *PIK3CA*, which encodes the class IA phosphoinositide 3-kinase (PI3K) catalytic subunit p110α are among the most common mutations across human cancers[61–64]. Class I PI3Ks are composed of four isoforms (class IA [p110α, p110β, p110δ] and class IB [p110γ]), which together generate the lipid second messenger phosphatidylinositol 3,4,5 trisphosphate (PIP_3) downstream of multiple cell surface receptors, including receptor tyrosine kinases (RTKs), G-protein coupled receptors (GPCRs), and Ras superfamily GTPases. PIP_3 recruits multiple effectors, including kinases and regulators of G protein signalling which play critical roles in regulating growth, survival, proliferation, and metabolism[65–67].

PI3Kα is a heterodimer composed of a p110α catalytic subunit and a p85 regulatory subunit, of which there are 5 isoforms: p85α, p55α and p50α (encoded by *PIK3R1*), p85β (encoded by *PIK3R2*) and p55γ (encoded by *PIK3R3*). The class IA regulatory subunits play three key roles in regulating class IA PI3Ks: they stabilize and inhibit the p110 catalytic subunits[68,69], and they allow for activation through the direct engagement of the nSH2 and cSH2 domains of regulatory subunits with pYXXM motifs in RTKs[70]. In unstimulated cells, the p110α protein is kept in an inactive and stable

cytosolic configuration due to its interactions with the regulatory subunit, with full activation and membrane recruitment of the PI3Kα complex requiring binding to both GTP loaded Ras, and engagement of both the nSH2 and cSH2 of regulatory subunits by bis-phosphorylated pYXXM motifs present in RTKs and their adaptors[71–73]. However, the full molecular mechanisms underpinning activation and membrane binding of class IA PI3K are not completely understood.

Extensive biochemical and biophysical studies have revealed how p110α is inhibited by regulatory subunits[74–80]. The p110α catalytic subunit is composed of five domains (an Adaptor Binding Domain (ABD), Ras Binding Domain (RBD), C2, helical, and a bi-lobal kinase domain)[74,81] (Fig. 1A). The RBD, C2, helical, and kinase domains together form the catalytic core of PI3Ks, which is conserved through the class I, II, and III PI3Ks[82,83]. The ABD of class IA PI3Ks binds irreversibly to the iSH2 coiled coil domain present in all class IA regulatory subunits[75], and also forms an inhibitory intra-subunit interface with the N-lobe of the kinase domain (Fig. 2.1A, 2.1B). The iSH2 also makes inhibitory contacts with the C2 and activation loop of the kinase domain[76,84]. The nSH2 domain of regulatory subunits binds reversibly to the C2, helical and kinase domains[75,77], with these contacts broken when the nSH2 binds to pYXXM motifs[79]. The cSH2 of regulatory subunits is strictly required for high affinity association with bis-phosphorylated receptors and their adaptors[71], and in p110β and p110δ forms an inhibitory interface with the kinase domain, however, this interaction is either absent or transient in p110α[85,86]. Recently Cryo-EM analysis of p110α bound to p85α showed that upon binding to phosphopeptides there appeared to be complete disengagement of the ABD and regulatory subunit from the catalytic core[87], which was not fully supported

by previous HDX-MS analysis of phosphopeptide binding[76,79]. However, disengagement of the catalytic core from the ABD and regulatory subunits is consistent with HDX-MS results studying PI3K membrane binding[72].

The *PIK3CA* and *PIK3R1* genes encoding p110α and p85α are both frequently mutated in human cancers[61,62,88]. The majority of mutations lead to amino acid substitutions (Fig. 2.1C)[89], although, more complex insertions and deletions also occur[90]. Oncogenic transformation by p85α mutations is driven by activation of the p110α isoform[91]. For p110α the most frequent mutations are located at two hot spots located at the helical-nSH2 interface (E542K, E545K) and the C-terminus of the kinase domain (H1047R) (Fig. 2.1B). The E545K disrupts the nSH2-helical interface[75] while H1047R alters the membrane binding surface of the kinase domain (Fig. 2.1D and E)[77]. However, there also are relatively high frequency mutations at the ABD-kinase interface, the ABD-RBD linker, the C2-iSH2/C2-nSH2 interfaces, the putative membrane interface of the N-lobe with membranes, and in a region of the kinase domain C-terminal to the activation loop, referred to as the regulatory motif (Fig. 2.1C)[92]. We have previously found that oncogenic mutations mimicked and enhanced conformational changes observed in the catalytic cycle of WT PI3Kα[76], with different mutants showing unique conformational changes. Different *PIK3CA* mutations activating lipid kinase activity through unique mechanisms is supported by the discovery of tumours harbouring double *PIK3CA* mutations *in cis*, with these tumours showing enhanced sensitivity to PI3K inhibition[93].

Here, using a combination of hydrogen deuterium exchange mass spectrometry (HDX-MS) and membrane binding assays, we provide a molecular model for how

oncogenic mutants in p110α activate both kinase activity and membrane binding. This has revealed the critical role of disengagement of the inhibitory contacts of the ABD domain and the p85 regulatory subunit, as well as the importance of reorganisation of the membrane binding C-terminus in PI3K activation. Intriguingly, mutations at the C-terminal tail activate PI3K through distinct molecular mechanisms and provide unique insight into how this might be utilised in mutant selective inhibitor design. Overall, this work provides unique insight into the molecular mechanisms mediating PI3K activation by oncogenic mutations.

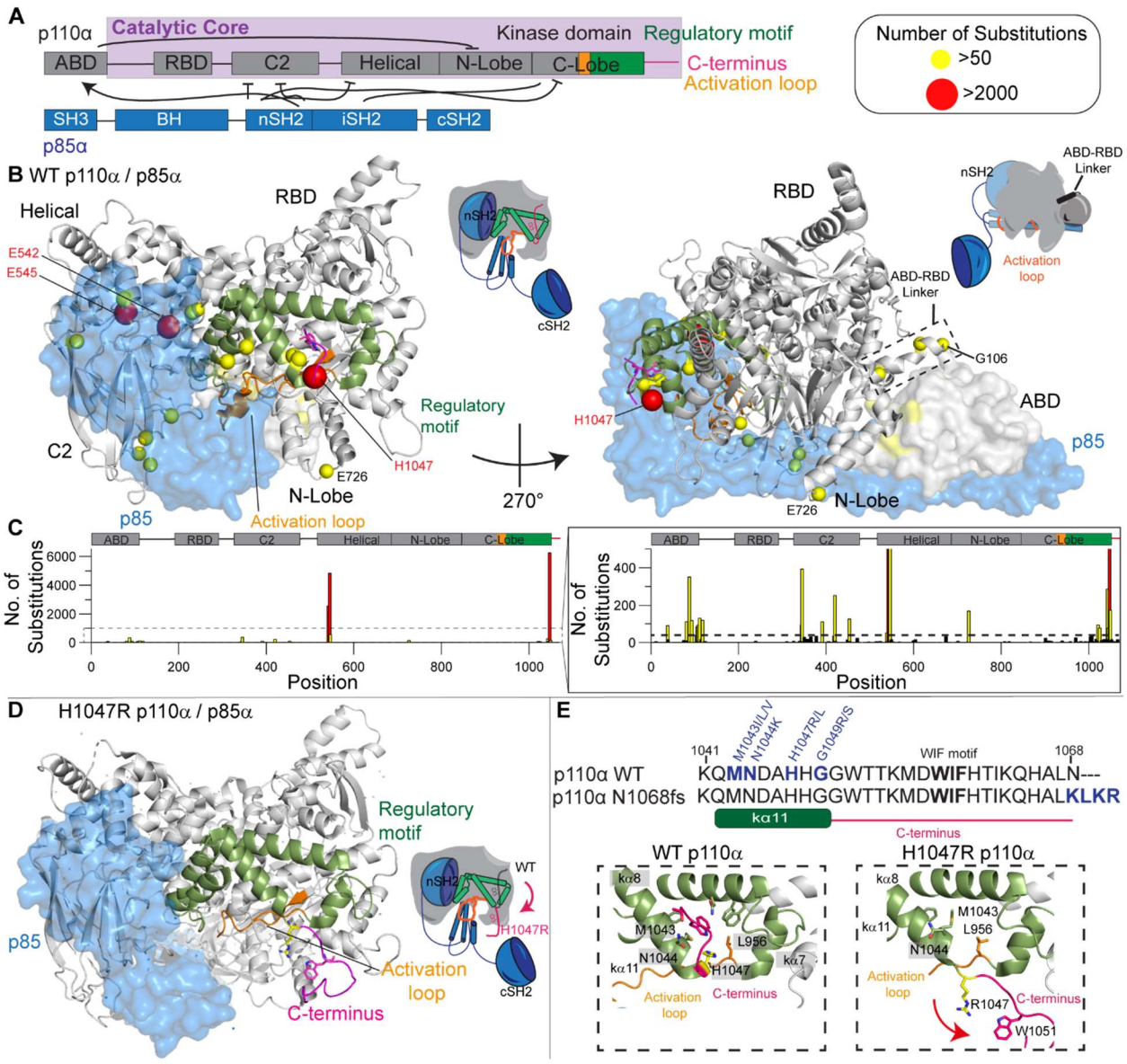

Figure 2.1. Structure of p110α/p85α and location of *PIK3CA* oncogenic mutations

A. Domain schematic of both p110α/p85α, with their respective domains highlighted. P110α consists of five domains namely adaptor binding domain (ABD), Ras binding domain (RBD), helical domain and the bi-lobal kinase domain. The important features namely catalytic core, activation loop (orange), regulatory motif (green), and C-terminus (magenta) of p110α are annotated. P85 consists of two Src homology-2 (SH2) domains separated by an inter coiled-coil SH2 (iSH2) domain. In p85α and β, nSH2 is preceded by SH3 and Bcr Homology (BH) domains. Same color scheme has been used to map these features on the structures below.

B. Oncogenic mutations in p110α mapped on the structure of WT p110α/p85α (PDB: 4OVU[94]). The frequency of oncogenic mutations from the COSMIC database[95] as described in panel **C** is colored according to the legend with any mutation with a frequency >50 indicated as a sphere. Other features are colored according to the domain schematic in panel A. The p85 subunit is

shown as a transparent blue surface. Cartoons of the two views of PI3K highlighting these features are shown to the right of each structural model. These same cartoon views are used to map all further HDX-MS data.
C. Frequency of mutations across the primary sequence of *PIK3CA* from the **C**atalog **o**f **S**omatic **M**utations **i**n **C**ancer (COSMIC) database (data from January 2022)[95].
D. C-terminus in H1047R adopts a unique confirmation compared to WT (PDB: 3HHM)[77]. Features are colored the same as in panel B.
E. Above: The sequence of the C-terminus is shown, with mutants colored blue, and the membrane binding WIF motif in bold[96]. The sequence of a frameshift mutant (N1068KLKR)[90] is also shown. Below: Orientation of the C-terminus in the WT (PDB:4OVU) and H1047R (PDB:3HHM) crystal structures. The relative positioning of additional oncogenic mutants (M1043I/L, N1044K, G1049R/S) are indicated. The reorientation of the C-terminus (colored in magenta) that occurs upon H1047R mutation is indicated by the red arrow.

2.3 Materials and Methods

2.3.1 Plasmid Generation

Genes of interest were inserted into the pFastBac1 vector to allow baculovirus expression in *Spodoptera frugiperda* (Sf9) cells. The plasmids containing p110 and free p85α isoforms also expressed N-terminal to the protein a 10X histidine tag, followed by a 2X Strep tag, followed by a tobacco etch virus protease cleavage site. Single substitution mutations (D915N, H1047R, M1043L, G1049R and N1068fs) and p110 truncations (p110α core and ΔC) were generated using site-directed mutagenesis according to published commercial protocols (QuickChange Site-Directed Mutagenesis, Novagen). DNA oligonucleotides spanning the desired region and either containing the altered nucleotides (single substitutions) or lacking the truncated region were ordered (Sigma). PCR reactions were performed on the WT p85α, and PCR purified (Q5 High-Fidelity 2X MasterMix, New England Biosciences #M0492L; QiaQuick PCR Purification Kit, Qiagen #28104). Single colonies were grown overnight and purified using QIAprep Spin Miniprep

Kit (Qiagen #27104). Plasmid identity was confirmed by Sanger Sequencing (Eurofins Genomics).

2.3.2 Virus Generation and Amplification

The plasmids harbouring p110α WT and other variants and p85α were transformed into DH10MultiBac cells (MultiBac, Geneva Biotech) containing the baculovirus viral genome (bacmid) and a helper plasmid expressing transposase to transpose the expression cassette harbouring the gene of interest into the baculovirus genome. Bacmids with successful incorporation of the expression cassette of pFastBac/ pACEBac1 into the viral genome was identified by blue-white screening and were purified from a single white colony using a standard isopropanol-ethanol extraction method. Briefly, colonies were grown overnight (~16 hours) in 3-5 mL 2xYT (BioBasic #SD7019). Cells were pelleted by centrifugation and the pellet was resuspended in 225 µL P1 buffer (Qiagen MiniPrep Kit, #27106), chemically lysed by the addition of 225 µL buffer P2, and the lysis reaction was neutralized by addition of 300 µL buffer N3. Following centrifugation at 21130 rcf and 4°C (Rotor #5424 R), the supernatant was separated and mixed with 600 µL isopropanol to precipitate the DNA out of solution. Further centrifugation at the same temperature and speed pelleted the bacmid DNA, which was then washed with 500 µL 70% Ethanol three times. The bacmid DNA pellet was then dried for 1 minute and re-suspended in 50 µL Buffer EB.

Purified bacmid was then transfected into Sf9 cells. 2 mL of Sf9 cells between 0.3-0.5X10^6 cells/mL were aliquoted into the wells of a 6-well plate and allowed to attach, creating a monolayer of cells at ~ 70-80% confluency. Transfection reactions were

prepared by the addition of 2-10 µg of bacmid DNA to 100 µl 1xPBS and 12 µL polyethyleneimine (PEI) at 1 mg/mL (polyethyleneimine “Max” MW 40.000, Polysciences #24765, USA) to 100 µL 1xPBS. The bacmid-PBS and the PEI-PBS solutions were mixed, and the reaction occurred for 20-30 minutes before addition drop-by-drop to an Sf9 monolayer containing well. Transfections were allowed to proceed for 5-7 days before harvesting virus containing supernatant as a P1 viral stock.

Viral stocks were amplified by adding P1 viral stock to suspension Sf9 cells between 1-2x10^6 cells/mL at a 1/100 volume ratio. This amplification produces a P2 stage viral stock that can be used in final protein expression. The amplification proceeded for 4-5 days before harvesting, with cell shaking at 120 RPM in a 27°C shaker (New Brunswick). Harvesting of P2 viral stocks was carried out by centrifuging cell suspensions in 50 mL Falcon tubes at 2281 RCF (Beckman GS-15), collecting the supernatant in a fresh sterile tube, and adding 5-10% inactivated foetal bovine serum (FBS; VWR Canada #97068-085).

2.3.3 Expression and purification of recombinant proteins

All PI3K constructs were purified by expressing the catalytic subunit and the regulatory subunit using the pFASTBAC/ pACEBac1 expression system in Sf9 cells. After expressing the cells at 27°C (42 hours for Kinase active variants and 55 hours for Kinase dead), the cells were harvested at 2800 rpm and 4°C using Eppendorf Centrifuge 5810R and the cells were flash frozen using liquid nitrogen and stored in -80°C. The proteins were purified by a series of affinity chromatography techniques that includes Nickel affinity, Streptavidin and Q column.

The frozen pellets were resuspended in lysis buffer containing 20 mM Tris pH 8, 10 mM Imidazole, 100 mM NaCl, 5% glycerol [v/v], 2 mM βME, protease inhibitor [Protease Inhibitor Cocktail Set III, Sigma]) and sonicated for 2 min (15 s on, 15 s off, level 4.0, Misonix sonicator 3000). Triton-X was added to the lysate at a final concentration of 0.1% and then clarified by spinning at 14, 000 rpm for 45 min (Beckman Coulter JA-20 rotor). The supernatant was loaded onto a 5 ml crude Ni-NTA column (GE healthcare) equilibrated in NiNTA A buffer containing 20 mM Tris pH 8, 100 mM NaCl, 10 mM Imidazole and 5% glycerol [v/v]. The column was washed using high salt buffer containing 20 mM Tris, 1 M NaCl, 10 mM Imidazole, 5% Glycerol [v/v] followed by NiNTA buffer wash (20 mM Tris pH 8, 100 mM NaCl, 21 mM Imidazole and 5% Glycerol). The protein was eluted using 100% NiNTA B buffer (20 mM Tris pH 8, 100 mM NaCl, 200 mM Imidazole and 5% Glycerol). The elute from the nickel column was loaded onto Streptavidin column (GE healthcare) and subjected to buffer wash using Hep A buffer (20 mM Tris pH 8, 100 mM NaCl, 5% Glycerol and 0.5 mM tris(2-carboxyethyl) phosphine [TCEP]). The column was incubated on ice for 3 hours in the presence of TEV protease and then eluted by a wash with Hep A buffer. The eluent was loaded onto Q column equilibrated with Hep A buffer. The column was washed with Hep A buffer to remove TEV protease and the final PI3K was eluted by passing Hep B elution buffer (20 mM Tris pH 8, 325mM NaCl, 5% glycerol [v/v] and 0.5 mM TCEP). The protein was exchanged to the final buffer containing 20 mM HEPES pH 7.5, 100 mM NaCl, 10 % Glycerol [v/v] and 0.5 mM TCEP using a desalting column. The protein was concentrated to 1 mg/ml using a 50,000 molecular weight cut-off (MWCO) Amicon Concentrator (Millipore), flash frozen and stored at -80°C.

For HDX experiments involving WT, p110α core, H1047R, M1043L, ΔCter and free p85α were further subjected to gel filtration using Superdex^{TM} 200 10/300 GL Increase from GE healthcare. After gel filtration, the protein was concentrated, aliquoted, frozen, and stored at −80°C.

2.3.4 Lipid Vesicle Preparation

To measure membrane recruitment using Protein-Lipid FRET two sets of lipid vesicles were prepared: PE/PS/PIP_2 containing 5 % brain PIP_2, 65% egg yolk PE, 25 % brain PS and 10% Dansyl-PS (Avanti, #810225C) and PM mimic consisting of 5% brain PIP_2, 20% brain PS, 10% Dansyl-PS, 45% egg yolk PE, 15% egg yolk phosphatidylcholine (PC) (Avanti #840051C), 10% cholesterol (Sigma Aldrich, #47127-U), and 5% egg yolk sphingomyelin (Sigma Aldrich, #S0756). To generate vesicles the lipid mixtures were combined in organic solvent. The mixture was then evaporated using a stream of argon gas followed by desiccation under vacuum for 45 minutes. The lipids were resuspended in a lipid buffer (25 mM HEPES pH 7, 100 mM NaCl, 10% Glycerol [v/v] and the solution was subjected to sonication for 15 mins. The vesicles were subjected to five freeze thaw cycles and extruded 11 times through a 100 nm filter (T and T Scientific: TT-002–0010). The extruded vesicles were sonicated again for 5 min, aliquoted and stored at −80°C.

2.3.5 Protein-Lipid FRET Assay

Protein-lipid FRET experiments were carried out either at a saturating protein concentration (Fig. 2.3 and 2.5) or as a dose response with PI3K (Fig. Appendix 3A).

Protein-lipid FRET assays with saturating PI3K were initiated by mixing 2.5 µL PI3K (4 µM) with 2.5 µL of pY peptide (final conc) for 15 mins at 20°C. 5 µL of lipid vesicles (either PIP_2/PS/PE or PM mimic vesicles, both at final conc. 33.33 µg/mL) was added to the protein-pY mixture and were incubated for 15 mins at 20°C. Dose experiment was carried out exactly the same, except PI3K amount varied from 0.015 µM to 1 µM. The plate was then read using a SpectraMax M5 plate reader using a 280-nm excitation filter with 350nm and 520 nm emission filters to measure Tryptophan (Trp) and Dansyl-PS FRET emissions, respectively. The FRET signal shown in the figures has $I-I_o$ along the Y axis where I is the intensity of 520 with protein and I_o is the intensity of lipid alone.

2.3.6 HDX-MS analysis: Sample Preparation

HDX-MS experiments for all conditions were conducted as follows: reactions comparing full-length p110α/p85α and p110α core were conducted in 13.5 µl reaction volumes with a final PI3K amount of 10 pmol. Prior to HD exchange, 3.5 µl of either protein was incubated with 3.5 µl of PIP_2/PS/PE lipid at 1 mg/ml or lipid buffer for 2 minutes at room temperature. To initiate HD exchange, a mixture of either 6.5 µl of the same lipid at 1 mg/ml or lipid buffer and 36.5 µl of D_2O buffer [20 mM HEPES (pH 7.5), 100 mM NaCl, 94.3% D_2O (v/v)] was added to the protein-lipid/buffer mix (final D_2O concentration of 69%). Exchange was carried out for 3, 30, and 300s at 20°C.

HDX reactions comparing full-length p110α/p85α WT against M1043L, H1047R and ΔC were conducted in 20µl reaction volumes with a final PI3K amount of 9 pmol. Prior to HD exchange, 3 µl of protein was incubated with 1 µl of 50 µM pY peptide or protein buffer and allowed to incubate for 15 minutes on ice. Exchange was initiated by the

addition of 16 µl of D_2O buffer to the protein +/- pY mixture (final D_2O concentration of 75%). Exchange was carried out for 3, 30, 300, and 3000s at 20°C and 0.3s (3s on ice).

HDX reactions comparing full-length p110α/p85α WT against G1049R were conducted in 20µl reaction volumes with a final PI3K amount of 15 pmol. HD exchange was initiated by the addition of 16 µl of D_2O buffer to 4 µl of protein (final D_2O concentration of 75%). The reaction proceeded for 3, 30, 300, and 3000s at 20°C.

HDX reactions comparing full-length p110α/p85α WT against N1068fs were conducted in 20 µl reaction volumes with a final PI3K amount of 11 pmol. HD exchange was initiated by the addition of 17.2 µl of D_2O buffer to 2.8 µl of protein (final D_2O concentration of 81%). The reaction proceeded for 3, 30, 300, and 3000s at 20°C.

HDX reactions comparing full-length p110α/p85α WT kinase active vs kinase dead were conducted in 50 µl reaction volumes with a final PI3K amount of 10 pmol. Prior to HD exchange, 4 µl of either protein was incubated with 10 µl of PIP_2/PS/PE lipid at 1 mg/ml or lipid buffer for 2 minutes at 20°C. HD exchange was initiated by the addition of 36 µl of D_2O buffer (final D_2O concentration of 69%). The reaction proceeded for 3, 30, and 300s at 20°C. All conditions and timepoints were generated in independent triplicate. All exchange reactions were terminated by the addition of ice-cold quench buffer to give a final concentration 0.6 M guanidine-HCl and 0.9% formic acid. Samples were flash frozen in liquid nitrogen immediately after quenching and stored at −80°C until injected onto the ultra-performance liquid chromatography (UPLC) system for proteolytic cleavage, peptide separation, and injection onto a Quadrupole Time of Flight (QTOF) for mass analysis, described below.

2.3.7 HDX-MS analysis: Protein digestion and tandem MS data collection

Protein samples were rapidly thawed and injected onto an integrated fluidics system containing an HDx-3 PAL liquid handling robot and climate-controlled (2°C) chromatography system (LEAP Technologies), a Dionex Ultimate 3000 UHPLC system, and an Impact HD QTOF mass spectrometer (Bruker). The protein was run over one immobilized pepsin column (Trajan; ProDx protease column, 2.1 mm x 30 mm PDX.PP01-F32) at 200 µl/min for 3 min at 10°C. The resulting peptides were collected and desalted on a C18 trap column [Acquity UPLC BEH C18 1.7 mm column (2.1 x 5 mm); Waters 186003975]. The trap was subsequently eluted in line with an ACQUITY 1.7 µm particle, 100 x 1 mm^2 C18 UPLC column (Waters 186002352), using a gradient of 3-35% B (buffer A, 0.1% formic acid; buffer B, 100% acetonitrile) over 11 min immediately followed by a gradient of 35-80% B over 5 minutes. MS experiments acquired over a mass range from 150 to 2200 mass/charge ratio (m/z) using an electrospray ionization source operated at a temperature of 200°C and a spray voltage of 4.5 kV.

HDX-MS analysis: Peptide identification

Peptides were identified from the nondeuterated samples of p110α/p85α complex for WT and other mutants using data-dependent acquisition following tandem MS (MS/MS) experiments (0.5-s precursor scan from 150 to 2000 m/z: 12 0.25s fragment scans from 150 to 2000 m/z). MS/MS datasets were analyzed using PEAKS7 (PEAKS) a protein identification database, and peptide identification was carried out by using a false discovery–based approach, with a threshold set to 1% using a database of purified proteins and known contaminants found in SF9 cells[97]. The search parameters were set with a precursor tolerance of 20 parts per million, fragment mass error 0.02 Da, and charge states from 1 to 8.

HDX-MS analysis: Mass analysis of peptide centroids and measurement of deuterium incorporation

HD-Examiner Software (Sierra Analytics) was used to automatically calculate the level of deuterium incorporation into each peptide. All peptides were manually inspected for correct charge state, correct retention time, and appropriate selection of isotopic distribution. Deuteration levels were calculated using the centroid of the experimental isotope clusters. HDX-MS results are presented with no correction for back exchange shown in the Source data, with the only correction being applied correcting for the deuterium oxide percentage of the buffer used in the exchange (69% for p110α core experiments, 69% for WT vs M1043L, H1047R and ΔC, 75% for WT vs G1049R, 81% for WT vs N1068fs and 69% for WT kinase active vs kinase dead). Attempts to generate a fully deuterated class I PI3K sample were unsuccessful, which is common for large macromolecular complexes. Therefore, all deuterium exchange values are relative.

Differences in exchange in a peptide were considered significant if they met all three of the following criteria: ≥5% change in exchange, ≥0.4 Da difference in exchange, and a P-value of <0.01 using a two-tailed Student's t test. The raw HDX data are shown in two different formats.

The raw data for all analysed peptides is available in the source data. The differences in deuterium exchange are visualised in different ways. To allow for visualization of differences across conditions, we used number of deuteron difference (#D) plots (Figs. 2.2C, 2.3D, 2.4A-E, Appendix 3C-E, Appendix 4A+C, Appendix 5A, Appendix 6D-F). These plots show the total difference in deuterium incorporation over the entire HDX time course, with each point indicating a single peptide. These graphs are

calculated by summing the differences at every time point for each peptide and propagating the error. For a selection of peptides, we are showing the %D incorporation over a time course, which allows for comparison of multiple conditions at the same time for a given region (Figs. 2.2D+2.3E, Appendix 3E, Appendix 4 B and D, Appendix 5B+C, Appendix 6G). Samples were only compared when they were set at the same time and were never compared to experiments completed with a different final D_2O level. The data analysis statistics for all HDX-MS experiments are in table S1 according to published guidelines. The HDX-MS proteomics data generated in this study have been deposited to the ProteomeXchange Consortium via the PRIDE partner repository[98] with the dataset identifier PXD031080.

2.4 Results

2.4.1 Disengagement of ABD/p85 co-relates with membrane recruitment

To investigate the role of ABD/p85 in controlling PI3K enzyme activity, we needed a construct that allowed us to interrogate the dynamic effects of full ABD disengagement. We engineered and purified the catalytic core of p110α (106-1068, referred to as p110α core) along with the full-length complex of p110α-p85α (full set of all constructs purified for this study and SDS-page gels are shown in Appendix A and B respectively). Attempts to purify the p110α core construct was unsuccessful, and we were only able to successfully purify this construct when it contained a kinase dead mutation (D915N). To validate that the D915N p110α construct did not cause any significant changes in protein conformation or membrane binding, we carried out HDX-MS experiments on WT and kinase dead p110α-p85α complexes bound to a PDGFR bis-phosphorylated pY peptide

(referred to going forward as pY) composed of PDGFR residues 735–767 with phosphorylation present at Y740 and Y751 in the presence and absence of membrane vesicles (5% PIP_2, 30% PS, 65% PE, referred to afterwards as PIP_2/PS/PE). HDX-MS is a technique that measures the exchange rate of amide hydrogens, and as the rate is dependent on the presence and stability of secondary structure, it is an excellent probe of protein conformational dynamics, and we have extensively used it to study PI3K activation[71,72,76,79,85]. There were no significant changes in conformation in the kinase dead p110α compared to wild-type, and both had equivalent membrane binding to lipid membranes (Appendix Fig 3).

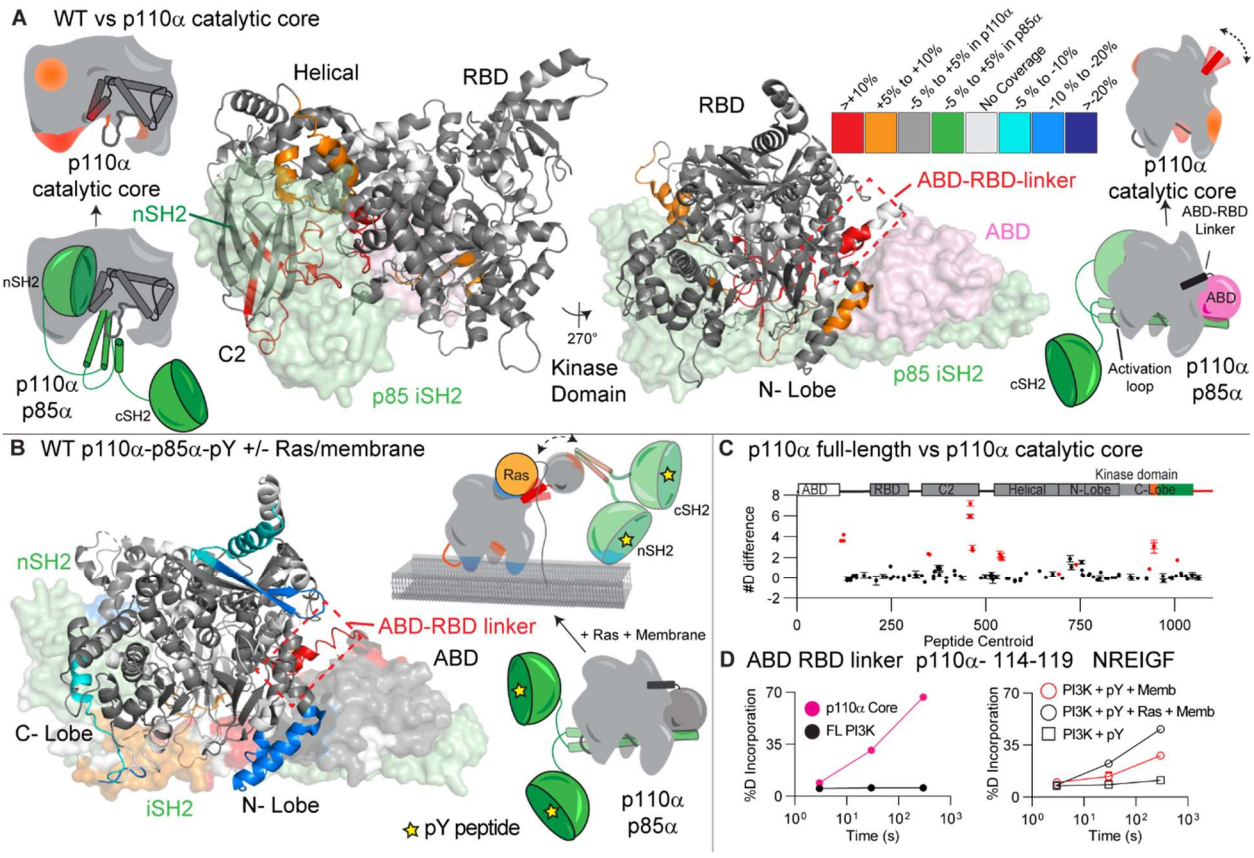

Figure 2.2. Conformational changes in p110α core compared to full length p110α- p85α, and comparison to changes upon pY/Ras membrane recruitment

A. Peptides in p110α that showed significant differences in HDX (greater than 0.4 Da and 5% difference, with a two tailed t-test p<0.01) between the catalytic core and the full-length complex

are mapped on the structure of p110α-p85α complex (PDB: 4OVU) according to the legend. The regions of the ABD (pink) and p85 (green) that are missing in the p110α core are shown as a surface. Cartoon models representing the differences between states are shown next to the structures. A more extensive set of peptides are shown in Fig Appendix4.
B. Peptides in p110α that showed significant differences in both p110α and p85α between free (with pY) and membrane-bound (pY, membrane Ras) (data adapted from Siempelkamp et al JBC, 201712) are mapped onto the structure of p110α-p85α (PDB: 4OVU) according to the legend.
C. The number of deuteron difference for all peptides analyzed over the entire deuterium exchange time course for p110α core compared to full length p110α- p85α. Peptides colored in red are those that had a significant change (greater than 0.4 Da and 5% difference at any timepoint, with a two tailed t-test $p<0.01$). Error bars are S.D. (n=3).
D. Selected p110α peptide in the ABD-RBD linker that showed increases in exchange in p110α core compared to full length p110α-p85α (left), and upon membrane binding of full length PI3K (right, data adapted from Siempelkamp et al JBC, 2017 12). Error bars are S.D. (n=3), with smaller than the size of the point. A more extensive set of peptides comparing the full length p110α-p85α with p110α core are shown in Fig. Appendix4.

We carried out HDX-MS experiments to identify conformational changes that occur in the catalytic core of p110α upon removal of the ABD and p85α regulatory subunit. We compared H/D exchange differences for both the p110α core and the full-length complex of p110α-p85α. The full details of HDX-MS data processing are in Table S1. For the p110α core construct there was significantly increased exchange (for all HDX-MS experiments this is defined as differences at any time point >5%, >0.4 Da, and a p-value less than 0.01 for a two-tailed t-test) in the ABD-RBD linker (114-119), C2 domain (347-355 and 444-475), helical domain (524-551), N-lobe of the kinase domain (691-697, 735-744), the activation loop (930-937) and the C-lobe of the kinase domain (1002-1013) (Fig. 2.2A-D,Appendix fig D). All significant differences in the catalytic core of p110α were in regions that were either in contact with ABD or p85α. This dataset allowed us to compare changes to those we previously observed upon membrane recruitment by both pY, and membrane bound Ras of the full length p110α-p85α complex (Fig. 2.2B)[72]. Intriguingly, we find that the region of the ABD-RBD linker in contact with the ABD domain (114-119)

had similar increases in exchange between WT p110α-p85α and either the p110α core or upon pY/HRas mediated membrane recruitment (Fig. 2.2D). There is a small increase in exchange in this region upon pY binding alone, but this was minor compared to the effect upon membrane binding[76,79]. The increase in region 114-119 was greater when bound to pY/HRas membranes compared to pY mediated membrane binding alone, suggesting this increase is dependent on the amount of membrane binding (Fig. 2.2D). This is also the case for increases in exchange observed upon membrane binding in the N-terminal and C-terminal ends of the iSH2 domain that are in contact with the C2 domain (470-476, 556-570, Appendix Fig B), showing the clear link between increases in the ABD-RBD linker and at the C2-iSH2 interface.

This data comparing the full-length heterodimer vs p110α core allowed us to define the effect of ABD removal on the contact site at the ABD-RBD linker. This region still is protected from exchange at early time points, suggesting presence of secondary structure, however, it is much more dynamic in the absence of the ABD. Comparing this to previous HDX-MS experiments examining pY-Ras membrane recruitment of p110α -p85α [72], showed that the exchange rate of the core is similar to the p110α -p85α membrane bound state, suggesting a correlative ABD disengagement occurring with membrane binding. This is supported by our previous observation of increased membrane binding for oncogenic mutants at the C2-iSH2 or ABD interfaces (N345K, G106V and G118D) that would be expected to promote ABD / iSH2 disengagement[76]. An important note is that this data does not support complete dissociation of the p110-p85 complex (due to the extremely high affinity interaction of the ABD to the iSH2[99]), but instead the ABD-p85 becoming mobile relative to the p110α catalytic core.

2.4.2 Enhanced membrane binding of p110α catalytic core

Our hypothesis that disengagement of the ABD and the regulatory subunit p85α subunit is required for membrane binding suggested that there should be differential membrane binding of the p110α core compared to full length p110α/p85α. We used protein-lipid Fluorescent Resonance Energy Transfer (FRET) assays (Fig. 2. 3A) to compare membrane recruitment of p110α core to full length p110α-p85α in the presence and absence of 1 μM pY. This assay was carried out on two different lipids: one roughly mimicking the plasma membrane (5% PIP_2, 10% Dansyl PS, 15% PS, 40% PE, 15% PC, 10% cholesterol, and 5% sphingomyelin, Fig. 2. 3B) and another optimised for maximal PI3K recruitment (5% PIP_2, 10% Dansyl-PS, 25% PS and 60% PE). While pY was required for robust binding of full length p110α-p85α, it was dispensable for p110α core association, which is expected due to the lack of SH2 domains required for pY binding (Fig. 2. 3B). The p110α core showed increased membrane recruitment for both lipid mixtures compared to the pY activated p110α/p85α complex. To determine the role of free p85α in PI3K membrane recruitment, we also purified recombinant free p85α and analyzed the protein-lipid FRET signal. There was a weak FRET signal for p85α alone, with no change upon pY binding (Fig 2.3 C). This signal was significantly lower than the p110α/p85α complex, indicating a limited role of p85α membrane recruitment, and suggests that membrane binding of PI3K is mainly driven by interactions with the p110α catalytic core.

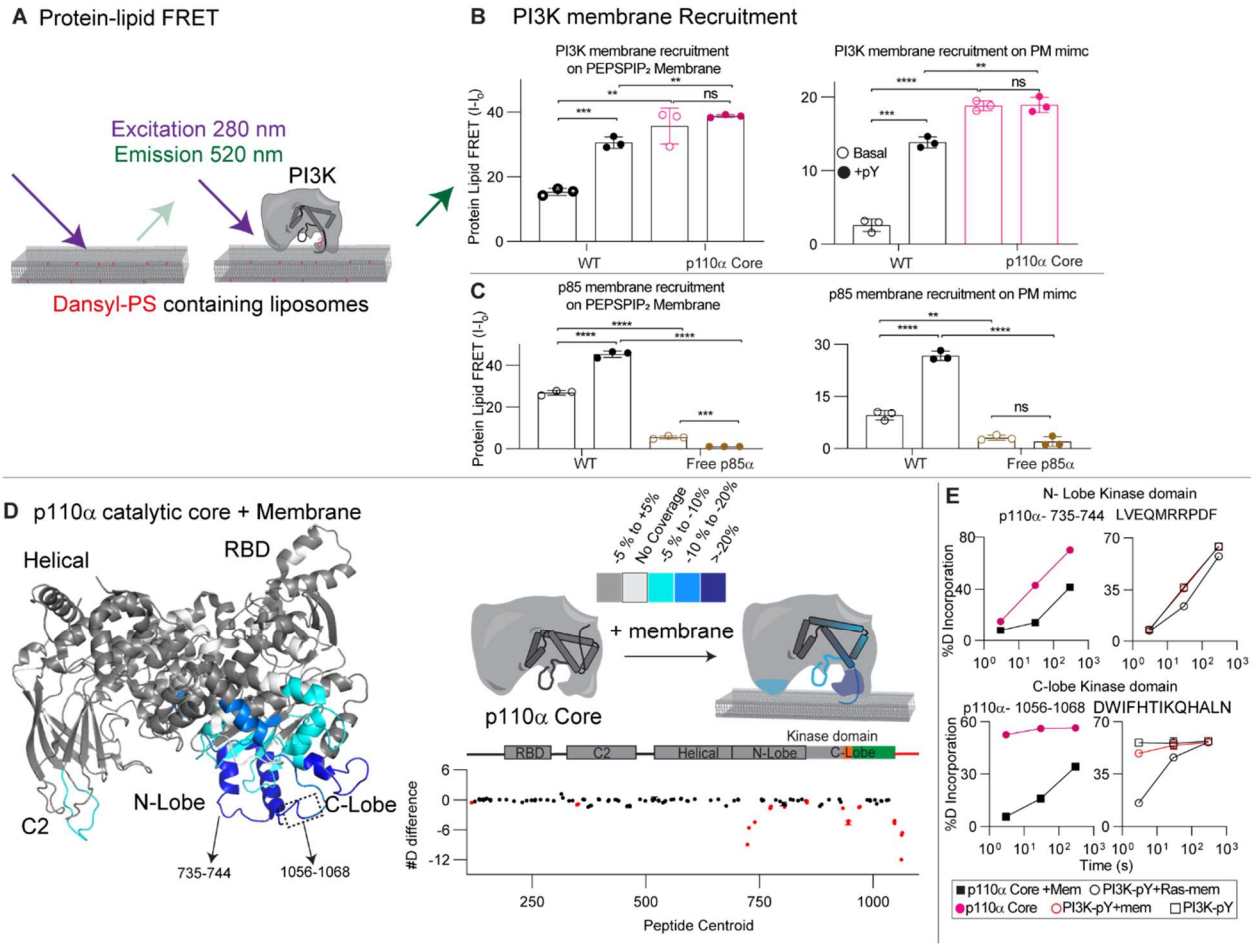

Fig 2.3. Enhanced membrane binding of p110α core compared to full length p110α/p85α, and mapping of the p110α membrane binding interface

A. Cartoon schematic describing the protein-lipid FRET assay, where tryptophan's in the protein are excited at 280 nm, with emission at 350 nm, which upon membrane binding can excite the dansyl moiety in dansyl phosphatidylserine lipids, leading to emission at 520 nm.

B. Protein-Lipid FRET testing membrane recruitment of p110α on PIP2/PS/PE and PM mimic membranes. FRET assays were performed with saturating concentrations of PI3K (0.5 μM) and 33.33 μg of lipid (error bars are S.D., n=3). Two tailed p-values represented by the symbols as follows: ****<0.0001, ***<0.001; **<0.01; n.s.>0.05.

C. Protein-Lipid FRET testing membrane recruitment of p85α on PIP2/PS/PE and PM mimic membranes. FRET assays were performed with saturating concentrations of p85 (0.5 μM) and 33.33 μg of lipid (error bars are S.D., n=3). Two tailed p-values represented by the symbols as follows: ****<0.0001, ***<0.001; **<0.01; *<0.05; n.s.>0.05.

D. Peptides in p110α core that showed significant differences in HDX (greater than 0.4 Da and 5% difference, with a two tailed t-test p<0.01) upon binding to 100 nm extruded 5% PIP_2/PS/PE vesicles were mapped onto the catalytic core of p110α (PDB: 3HHM) according to the legend.

E. The number of deuteron difference for all peptides analyzed over the entire deuterium exchange time course for p110α core upon binding membranes. Peptides colored in red are those

that had a significant change (greater than 0.4 Da and 5% difference at any timepoint, with a two tailed t-test p<0.01). Error bars are S.D. (n=3). A more complete set of peptides comparing the full length p110α-p85α with p110α core are shown in Appendix4, with the full list of all peptides and their deuterium incorporation in the source data file.
F. Selected p110α peptide in the kinase domain that showed decreases in exchange in p110α core upon binding membranes (left), and pY or pY-Ras mediated membrane binding of full length p110α-p85α (right, data adapted from Siempelkamp et al JBC, 2017 [72]).

2.4.3 Defining the membrane binding surface of p110α core

We have extensively characterised the membrane binding of the p110α/p85α complex using HDX-MS, however, the disengagement of the ABD and p85 from the catalytic core has likely complicated the analysis of membrane binding regions. We carried out HDX-MS experiments of p110α core in the presence and absence of 5% PIP_2/PS/PE membranes to fully understand the molecular underpinnings of p110α membrane binding. We observed protection in the ABD-RBD linker (114-119), C2 (343-355), N-lobe kinase domain (713-734,735-744,799-811 and 850-859), Activation loop (930-961) and the C-terminus of the C-lobe kinase domain (1039-1055 and 1056-1068) (Fig. 2.3 A-C). The largest differences occurred in the C-terminus, and N-lobe, with only minor differences in the C2 domain. However, the region of the C2 domain that interacts with the membrane has limited secondary structure (see Fig Appendix 4), which can make tracking transient membrane differences using HDX challenging. Previous HDX-MS experiments testing N345K p110α-p85α binding to membranes showed this same region being protected by membranes[76]. Overall, this supports a model where p110α binds membrane at a surface composed of the C2 domain, the kα1-kα2 helices (720-744) and the 859-872 region of the N-lobe, the activation loop, along with the C-terminal tail. Intriguingly, the kα1-kα2 helices in the N-lobe interact with the ABD, and the 343-355 region of the C2 domain binds the N+C termini of the iSH2 domain, which provides a

putative molecular explanation for why disengagement of the ABD and p85 leads to increased membrane association.

When comparing our data to the full set of missense oncogenic mutations in the ABD, ABD-RBD linker, C2, helical, and the N-lobe of the kinase domain we find that all mutations found in >30 tumours except one (E726K) are located at either the ABD or p85 interfaces. We had previously observed that mutations in the ABD-RBD linker caused similar conformational changes to those located at the C2-iSH2 interface, with this being explained by both mutations leading to disengagement of the ABD and p85 from the catalytic core[76].

2.4.4 Conformational changes in oncogenic mutations C-terminus of the kinase domain

While the disengagement of the ABD and p85 being involved in membrane binding provides a molecular rationale for activation by oncogenic mutations in the ABD, C2, and helical domains, it does not fully explain the molecular mechanism of mutations in the C-lobe of the kinase domain. Our previous HDX-MS analysis of the kinase domain mutant, H1047R, showed increased exposure throughout regions of the N-lobe and C-lobe of the kinase domain, with this resulting in a dramatic increase in membrane binding[76]. In high resolution structures the C-terminus of p110α makes extensive contacts with helices that make up the regulatory motif (kα8 and kα11) and sits on top of the C-terminus of the activation loop (Fig. 2.1E)[94,100–102]. One of the primary interactions is an extensive interface between Trp1051 of the C-terminus and His1047 as well as hydrophobic residues lining kα8 and kα11 of the kinase domain (Met1043, Phe977,980 and 1039).

This region is also in contact with Leu956 in the C-terminal end of the activation loop. This orientation positions the membrane binding WIF motif (residues 1057-1059) distant from the membrane binding interface. When comparing these WT p110α structures to the H1047R crystal structure (3HHM), there is a significant reorganisation of the C-terminus, with all contacts between the C-terminus and kα8 and kα11 disrupted, and the WIF motif oriented at the putative membrane surface (Fig. 2.1D)[77]. This is putatively mediated by mutation of His1047 preventing the C-terminal interaction due to the increased size of the Arg residue compared to His preventing formation of the inhibitory C-terminal conformation (Fig. 2.1E) and orienting the lipid binding WIF motif (hydrophobic residues that participate in membrane recruitment) at the membrane interface.

To understand the regulatory mechanisms underlying the inhibitory interface with the C-terminus we analysed the most frequent oncogenic mutants that occur at or near this interface. While H1047R/L is the most frequent mutation (>6000 from the COSMIC database), there are multiple frequent missense mutations in this region, including M1043L/I/V (>300), G1049R/S (>150), and N1044K/S (>80). In addition, we analyzed an activating frameshift variant that alters the C-terminus by replacing the terminal N with a KLKR extension, which was recently identified in tumour samples (N1068KLKR, referred to afterwards as N1068fs)[90]. To understand if these mutants were activated in a similar way to H1047R, we purified the four p110α mutant complexes (M1043L, H1047R, G1049R, and N1068fs) all bound to full length p85α.

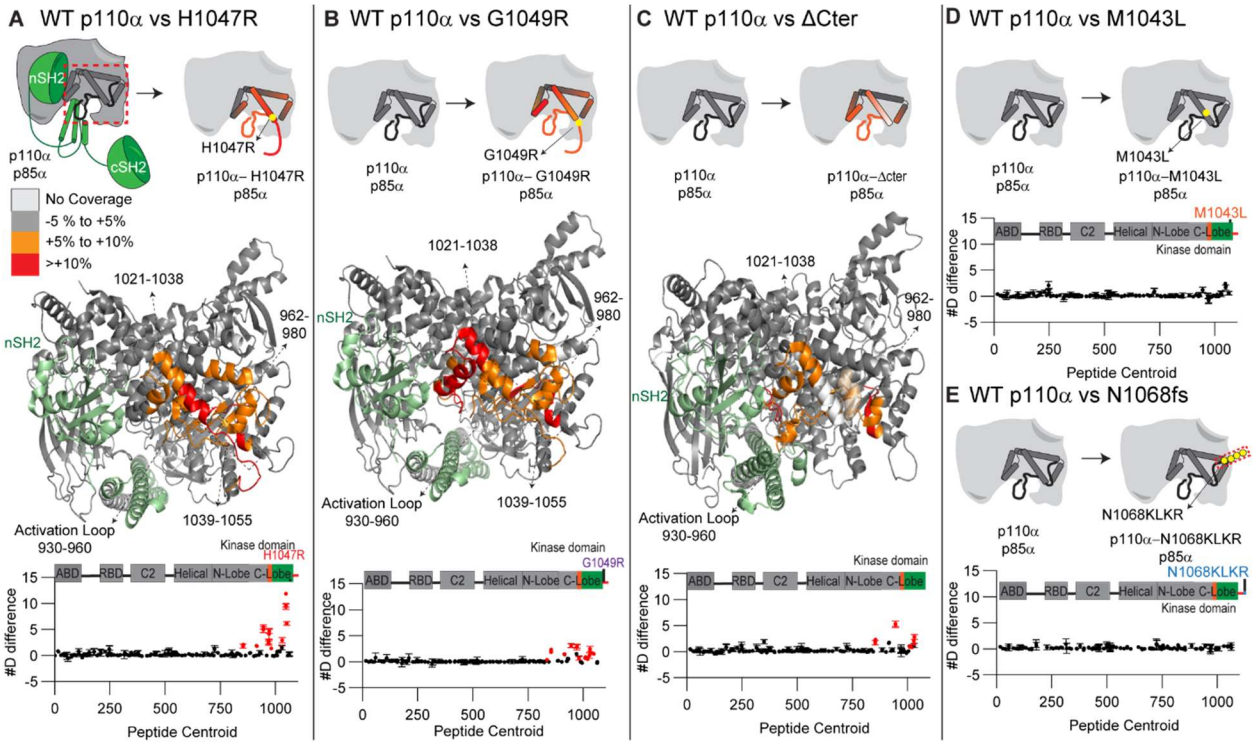

Fig 2.4. Structural difference between various c-terminal mutants of p110α compared to WT p110α/p85α, and mapping of the p110α membrane binding interface

A-C. HDX comparing p110α/p85α WT vs H1047R (**A**), G1049R (**B**) and ΔCter (1-1048) (**C**). Significant differences in deuterium exchange are mapped on to the structure of p110α/p85α H1047R according to the legend (PDB: 3HHM (A+B) and 4OVU (C)). The graph of the #D difference in deuterium incorporation for p110α in each experiment is shown below, with each point representing a single peptide. Peptides colored in red are those that had a significant change in the mutants (greater than 0.4 Da and 5% difference at any timepoint, with a two tailed t-test $p<0.01$). Error bars are S.D. (n=3).

D-E. HDX comparing p110α/p85α WT vs M1043L (D) and N1068fs (E). The graph of the #D difference in deuterium incorporation for p110α in each experiment is shown below, with each point representing a single peptide. For all panels, the HDX-MS data for p85 subunits is shown in Appendix Fig 5, along with representative peptides showing significant changes.

To test if C-terminal mutations worked by disrupting the inhibitory interaction with the C-terminus, we carried out HDX-MS studies on six constructs of full length p110α (WT, M1043L, H1047R, G1049R, N1068fs, and ΔCter), all bound to full length p85α. The use of the ΔCter construct allowed for a direct comparison of removal of the C-terminus,

versus a possible reorientation upon oncogenic mutation. We used kinase active M1043L, H1047R, G1049R, and a kinase dead variant of N1068fs for this comparison.

HDX-MS experiments were carried out for 4-5 timepoints of exchange (3 s at 1°C, 3, 30, 300, and 3000 s at 20°C) for each complex. The full set of all peptides analysed for both p110α and p85α with peptide exchange data presented in Appendix Fig 4. The changes observed for H1047R matched almost exactly our previous studies[76], but this experiment expanded the HDX time course, allowing for a more in-depth analysis of perturbations in conformation.

The H1047R, G1049R, and the ΔCter constructs showed similar significant increases compared to the WT in the kinase domain (Fig. 2.4A-C). These included regions covering 850-858 (hinge between the N and C lobes), the activation loop (930-956), and helices spanning the regulatory arch (1014-1021 in kα10, 1021-1038 in kα11) (Fig. 2.4A-C). Many of these regions correspond directly to the contact site between the C-terminus and kα11. This validates the inhibitory interaction observed in the 4OVU crystal structure, with this interface stabilising helix kα11 and the activation loop. One region in kα8 (962-980) showed a significant change between H1047R, G1049R and WT, which was not observed comparing WT and ΔCter. This helix contacts both the C-terminus and kα11. A possible mechanism explaining this difference is the rotation that occurs in kα11 upon mutation of H1047R. Structures of free p110α lacking the C-terminus do not show this same rotation of the kα11 helix. The rotation of kα11 would alter the interface between kα8 and kα11, leading to increased exchange in kα8. This could be driven by a unique orientation of the C-terminus packing against kα7 in the H1047R or G1049R mutant, which would be lost in the absence of the C-terminus as would occur in

the ΔCter protein. Overall, this data suggests that H1047R and G1049R lead to activation through disruption of the inhibitory conformation of the C-terminal tail, which reorients the lipid binding WIF motif at the membrane binding surface. Both M1043L and N1068fs showed no significant differences compared to WT, suggesting these mutants do not disrupt the inhibitory C-terminal conformation (Fig. 2.4D+E).

We also compared HDX-MS differences in full-length p110α-p85α between WT, H1047R and ΔC in the presence and absence of pY (Appendix Fig 5). The binding of pY led to significant increases for all three constructs at interfaces that have been previously described (ABD-RBD linker, C2-iSH2, nSH2-helical). However, intriguingly there were unique differences upon pY binding for the ΔCter and H1047R constructs at the interface of the regulatory arch with the nSH2 domain (1014-1021, kα10). This is intriguing as it suggests that the opening of this portion of the regulatory motif only occurs upon both disengagement of the nSH2 domain (mediated by pY binding) and disengagement of the inhibitory C-terminus (Appendix Fig 5).

2.4.5 Membrane binding of c-terminal mutants in p110α

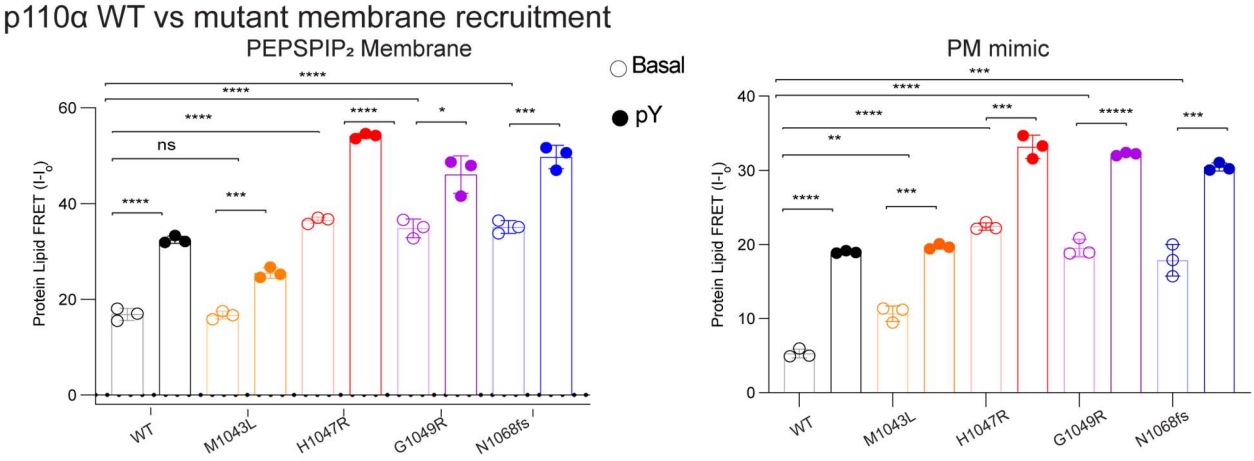

Fig 2.5: Protein-Lipid FRET assay performed with different p110α constructs under basal and pY activated states on PM mimic liposomes (5% PIP2, 10% Dansyl PS, 15 % PS, 40% PE, 10% cholesterol, 15% PC and 5% SM) and PEPSPIP$_2$ (5% PIP2, 10% Dansyl PS, 25 % PS, 65% PE) liposomes. Experiments were carried out at saturating concentrations of PI3K (1μM) and 33.33 μg/ml of lipid vesicles (error bars are S.D., n=3). Two tailed p-values represented by the symbols as follows: ****<0.0001, ***<0.001; **<0.01; *<0.05; n.s.>0.05.

For these mutants, we had difficulty in obtaining sufficient yield of the proteins for extensive biophysical analysis. To circumvent this, we used the kinase dead variants to characterize their membrane binding using protein-lipid FRET using both PM mimic and optimised binding lipids. Membrane binding was enhanced for mutants upon addition of pY, with greater binding for the optimised lipids over the PM mimic. H1047R, G1049R, and N1068fs all showed significantly increased membrane binding over WT both with and without pY (Fig. 2.5), while the M1043 mutant only showed a slight increase in membrane binding without pY for the PM mimic vesicles (Fig. 2.5).

2.5 Discussion

Understanding how p110α is regulated and how oncogenic *PIK3CA* mutants alter this regulation is essential in the development of novel PI3K therapeutics. Due to the critical homeostatic roles that WT p110α plays in growth, development, and metabolism[103], as well as the cell intrinsic[104,105] and systematic[106] negative feedback loops that oppose PI3K pharmacological inhibition, there are extensive advantages to selectively targeting mutant p110α over WT p110α. Therefore, defining the exact molecular basis underlying mutant specific conformational changes may reveal opportunities for mutant-selective drug design. Oncogenic mutants in p110α span multiple domains of the catalytic subunit, with foci occurring at the ABD, ABD-RBD linker,

C2-iSH2 interface, nSH2-helical interface, and the N+C lobes of the kinase domain[95]. While most mis-sense oncogenic mutations discovered in tumours are at hot-spot locations (E542K, E545K, H1047R), more than 25% of all mutations in *PIK3CA* occur outside the hotspots. Extensive biochemical[76] and cellular experiments[107,108] have defined that PIK3CA mutations activate lipid kinase activity by different mechanisms. This together with the recent discovery that multiple mutations in PIK3CA occur *in cis*[93], where hotspot and rare mutations are found in the same gene, highlights the need to fully understand how multiple oncogenic mutations can synergically activate PI3K lipid kinase activity. Here using a suite of biochemical and biophysical approaches we propose a unifying molecular model for how all *PIK3CA* mutations can lead to increased kinase activity, as well as how different oncogenic mutations *in cis* can increase oncogenicity.

We wanted to define how extensive oncogenic gain of function *PIK3CA* mutations at both the ABD interface and the C2-iSH2 interface activate lipid kinase activity. The critical role of the ABD in regulating p110α kinase activity was originally suggested by its direct interaction with the N-lobe of the kinase domain[75,109]. We previously observed exposure occurring at the ABD interface (ABD-RBD linker) upon phosphopeptide pY binding[76,79], and more extensive exposure at the ABD interface upon membrane binding[72,76]. Cryo EM analysis of p110α with p85α revealed disengagement of the ABD and p85 subunit from the catalytic core of p110α upon binding phosphorylated peptide[87]. To fully define the relative role of ABD disengagement in PI3K activation on membranes we generated the p110α catalytic core and directly compared its exchange to the full length p110α-p85α. Increased exposure was seen at all contact interfaces with both p85 and the ABD. Intriguingly, we found that the p110α catalytic core (p110α core)

showed H/D exchange rates at the ABD-RBD linker that almost exactly matched those observed upon Ras and pY mediated membrane binding of WT p110α-p85α[72]. Importantly, we did not observe similar rates when comparing phosphopeptide bound p110α-p85α, suggesting that complete ABD disengagement only occurred when p110α is membrane bound which is in contrast from what was suggested from the cryo-EM model of PI3Kα in the presence of pY peptides.

We previously observed that mutations at the ABD interface exposed the C2-iSH2 interface, and *vice versa*[76]. As the ABD will always remain tightly bound to the iSH2 domain, its disengagement would likely occur simultaneously with disruption of the C2-iSH2 interface. For these mutants, full disruption of the ABD and C2-iSH2 interfaces occurred only upon removal of the nSH2 (through pY binding), with no requirement for membrane. This reveals an unexpected inhibitory role of the nSH2 domain, whereby packing against the helical, kinase, and C2 domains of p110α and the iSH2 of p85α, it can stabilise the interface with the iSH2 domain, which prevents ABD disengagement from the catalytic core of p110α. Intriguingly, ABD disengagement is likely involved in membrane recruitment for all class IA PI3Ks, as HDX-MS experiments on membranes showed exposure in the iSH2 and the ABD-RBD linker of p110β[110] and p110δ[85,111]. These changes were also seen in primary immunodeficiency mutations of p110δ[112] and in activating *PIK3R1* truncations at the N+C termini of the iSH2 involved in immunodeficiencies and oncogenic transformation[71,111]. An interesting implication in this model is that unique class IA regulatory subunits may have distinctive propensities for ABD-p85 disengagement, which may partially explain a unique role for regulatory subunits oncogenic transformation[113]. This will require further study to investigate

regulatory subunit isoform differences in disengagement. Together this highlights the key role of ABD disengagement in PI3K activation, and how oncogenic mutants can alter this regulation.

We next wanted to understand how ABD and p85 disengagement is involved in membrane binding of PI3K. We hypothesized that the free catalytic core of p110α may more efficiently bind to lipid membranes. Our protein-lipid FRET experiments with p110α Core over the pY activated full length p110α-p85α showed enhanced membrane binding similar with our previous studies on the catalytic core construct of p110δ[85]. To understand the mechanism for how this occurs we mapped the membrane binding interface of p110α core using HDX-MS. We observed decreased exchange at the C2 and the N-lobe and C-Lobe of the kinase domain. Many of these changes were not observed in the full-length heterodimer upon binding membranes, with these regions located at either the ABD (kα1-kα2 helices of N-lobe) or iSH2 (C2 domain) interfaces. This suggests that some of the membrane binding regions of p110α are shielded by the ABD or p85 subunit, and disengagement of these regions allows for efficient membrane binding. This model also suggests that the role of phosphopeptide binding in membrane recruitment is two-fold as it both breaks an inhibitory contact between the nSH2 and the regulatory motif of the kinase domain and breaks the nSH2 contact with the helical domain allowing for disengagement of the ABD and p85 subunits from the catalytic core, exposing membrane binding surfaces of p110α (Fig. 2.6).

One of the largest decreases in exchange observed upon membrane binding was in the C-terminus of p110α, specifically at the membrane binding WIF motif. In high resolution structures of inhibited p110α, the C-terminus is pointed away from the putative

membrane binding surface[100], with the C-terminus pointed towards the membrane surface in the structure of H1047R p110α[77] due to a ~180° rotation at the end of the kα11 helix. The C-terminus in the WT structures makes a set of contacts the regulatory motif helices (kα8- kα11) located after the activation loop and contacts the C-terminus of the activation loop. The regulatory motif helices and the C-terminus encompass the activation loop and make extensive contacts proposed to maintain an inactive conformation. The regulatory motif is also directly in contact with the nSH2 domain of regulatory subunits. Sequestering the C-terminus in a inhibited conformation is a conserved aspect of regulation across all class I PI3Ks, with the inhibited conformation of the C-terminus of p110β and p110δ binding to the cSH2 of regulatory subunits[85,114], and p110γ having its C-terminus inhibited by an inhibitory tryptophan lock which does not require regulatory subunits[92]. Removal of the C-terminus causes a substantial rearrangement of the activation loop, and a rotation of the kα11 helix[115]. Most of the frequent mutations in the C-terminus of p110α would be expected to disrupt this inhibitory contact, either through steric hindrance (M1043I/L, H1047R, G1049R) or disruption of key hydrogen bonds (N1044S). One of the only frequent oncogenic mutations that is not at either the regulatory C-terminus or an interface with the ABD or p85 is located at the loop between kα1-kα2 in the N-lobe (E726K) in a location at the membrane binding surface. This mutant likely drives increased lipid kinase activity through enhanced membrane binding of negatively charged lipids through this charge reversal mutant.

To test if conformational changes in H1047R were caused by disruption of the inhibitory contacts with the C-terminus, we compared the H/D exchange rates of H1047R and a deletion of the C-terminus to the WT protein. The H1047R and C-terminal deletion

showed similar increases in exchange in the kα11 helix in contact with the inhibited C-terminus. This suggests a key role of the H1047R mutant is to disrupt inhibitory contacts between the C-terminus and orient the C-terminus in a productive conformation for membrane binding. In addition to this membrane binding role, the removal of the C-terminus also leads to a reorientation of the activation loop, and increased activity towards both ATP hydrolysis and soluble PIP_3 substrate[116]. Therefore, mutations that disrupt this inhibitory C-terminal contact (H1047R, G1049R) activate lipid kinase activity by two unique mechanisms they reorient the WIF motif towards the membrane binding surface, increasing membrane binding, while also causing the activation loop to adapt a catalytically competent conformation. A putative mechanism explaining this is that the 1068fs replaces the terminal Asn, with a set of positive and hydrophobic residues (KLKR), which all would contribute enhanced membrane binding. So, while the 1068fs mutant does not reorient the membrane binding interface, it likely interacts more extensively, increasing membrane residency time, and increasing PIP_3 production. The M1043L mutant has a much smaller effect on membrane binding. Comparing the structure of WT p110α to H1047R p110α shows a rotation of the kα11 helix in the mutant, with the M1043 residue rotating into where the W1051 from the C-terminus is located in the WT structure[77]. We expect that reorientation of the C-terminus is required for full activity, and therefore we propose that the enhanced membrane binding of M1043L (and potentially M1043I/V) is driven by the added steric bulk of the branched chain amino acids, which may more efficiently reorient the C-terminus upon membrane binding. Further structural studies of the M1043 mutants on membrane surfaces will be required to fully access the molecular basis of activation.

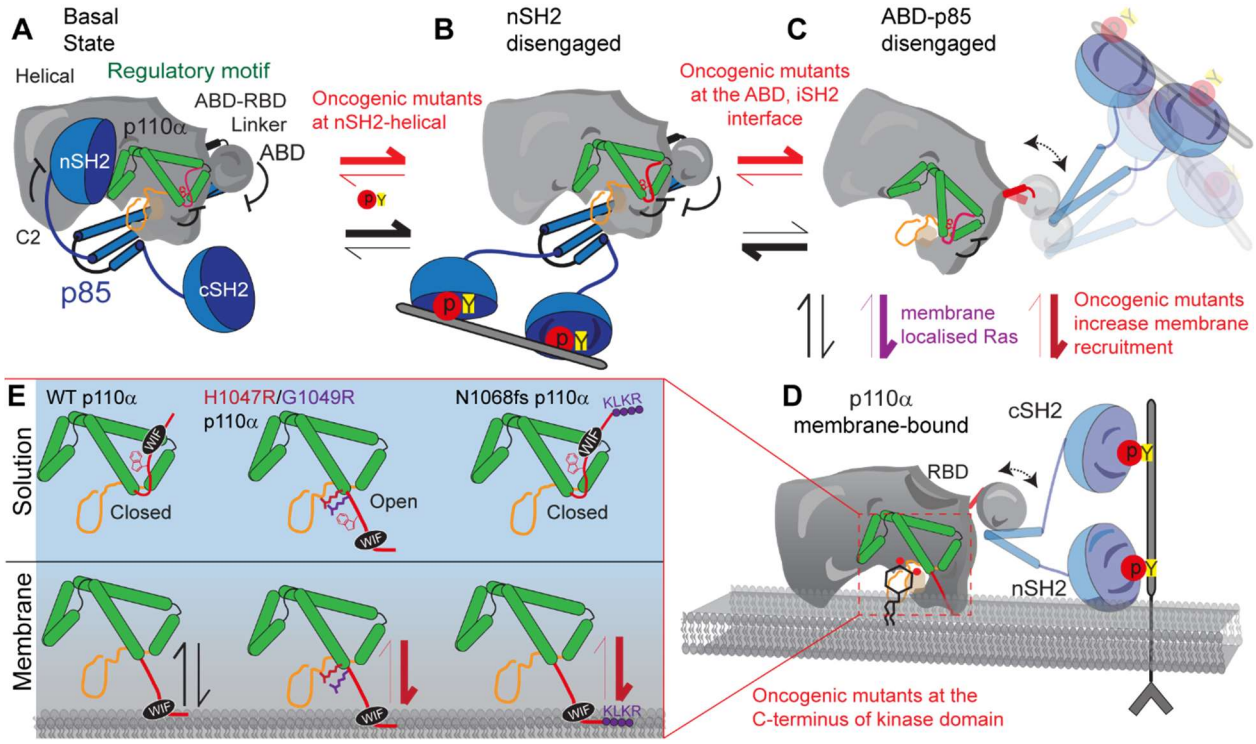

Fig 2.6. Summary of molecular mechanisms of PI3K inhibition by the ABD and regulatory subunit, and how activation occurs in the wild-type enzyme (black and purple arrows) as well as how oncogenic mutations can alter this process (red arrows).
A cartoon model representing the fully inhibited state is shown in panel A, with the nSH2 disengaged state shown in **B** (driven by either pY binding or helical domain mutants), and the ABD-p85 disengaged state shown in **C** (driven by oncogenic mutants at the C2-iSH2 interface and the ABD-interface). The fully active membrane bound state with a reoriented C-terminus is shown in **D.**
E. Different molecular mechanisms driving activation of C-terminal mutations in PIK3CA. The regulatory motif is colored green, with the C-terminus colored red, and the activation loop in black (inactive) or red (orange). The C-terminus when in its closed conformation has the membrane binding WIF motif oriented away from the membrane surface. Membrane binding requires the reorientation of this tail, with the membrane itself likely involved in this conformational change. Mutations that disrupt this interface (H1047R, G1049R) are in an open conformation, leading to greatly increased membrane binding. In the N1068fs mutant there is no change in conformation in solution, but the added KLKR motif dramatically increases membrane recruitment.

Overall, integrating our experimental efforts with the extensive previous biophysical and biochemical analysis of p110α mutants we can propose a unifying model for how p110α is inhibited by regulatory subunits, and how it can be activated both by activating partners and oncogenic mutants (Fig. 2.6). Activation of p110α/p85α by bis-

phosphorylated receptors and their adaptors leads to breaking of the inhibitory nSH2 contacts with the p110α subunit. Helical domain mutants (E542K, E545K) mimic this conformational change (red equilibrium arrows between Fig. 2.6A-2.6B). The removal of the nSH2 partially destabilises the iSH2-C2 and ABD-kinase interfaces, but in the wild type complex the equilibrium is mainly towards a closed p85-ABD engaged complex (black arrows). The pYXXM binding surface of the nSH2 exposed in helical mutants leads to greatly enhanced recruitment to RTKs and their adaptors[117]. Oncogenic mutations that occur at the ABD or iSH2 interfaces in p110α (red equilibrium arrows between Fig 2.6B-2.6C) shifts the equilibrium towards the disengaged state, leading to increased affinity for membranes. Full membrane recruitment still depends on the opening of the C-terminus of p110α. In the wild type complex, membrane recruitment requires additional signalling inputs from Ras GTPases. Oncogenic mutants in the kinase domain lead in increased membrane binding either through reorientation of the WIF binding motif and the activation loop (i.e. H1047R, G1049R), or by altering residues at the membrane interface that can more extensively interact with negatively charged membranes (i.e. E726K, 1068fs) (red equilibrium arrows between Fig. 2.6C-2.6D, and 2.6E). Together, this model can account for the putative mechanism of activation for >98% of all PIK3CA mutants reported in the COSMIC database, and for why double PIK3CA mutants lead to increased oncogenicity (Fig. 4.1).

Extensive efforts have focused on the development of p110α selective inhibitors. *PIK3CA* mutant selective inhibitors would likely have major advantages in cancer treatment as they can evade feedback mechanisms that counteract pharmacological inhibition of WT *PIK3CA*. Mutant selective inhibitors have been discovered that lead to

selective degradation of E545K and H1047R over WT[58], along with recent reports of H1047R selective inhibitors. Our data showing very similar conformational changes in H1047R and G1049R suggest that 1047R/L selective small molecules may also be useful in targeting G1049R/S. There also could be advantages of generating tool compounds that activate PI3K activity, with small molecules that disrupt the ABD or p85 interfaces likely acting as activators. Our findings provide a molecular framework for the future development of the next generation of PI3K modulators as therapeutics.

Chapter 3: Molecular basis for regulation of PI3Kγ by PKCβ mediated phosphorylation

Contributions:

JEB, HR-P and MKR designed all biophysical/biochemical experiments. Protein expression using Sf9 was done by HR-P, MKR and MAHP. Protein purifications were done by HR-P with assistance from MKR and by NH and ES for phosphorylation set-up. Phosphorylation setups were done by NH and ES, and phosphorylation set-up with NB was done by HR-P. HDX-MS samples were prepared by HR-P and BEM. HDX-MS analysis was done by HHR-P, MLJ and JEB. BLI experiments were done by HR-P. HR-P and JEB wrote the manuscript with input from all authors.

3.1 Abstract

PI3Kγ is key to the regulation of immune cell responses activated by G protein-coupled receptors (GPCRs) and GTP loaded Ras. PI3Kγ can form two distinct complexes, with the p110γ catalytic subunit binding to either p101 or p84 regulatory subunits. The propensity of their activation is dependent on the regulatory subunit, with p110γ-p101 complex being robustly recruited by Gβγ of GPCRs while the p110γ-p84 complex requires Ras as a co-stimulator. Apart from activation signals and cancer linked mutations, PI3Kγ has also been shown to be regulated by phosphorylation events downstream of FcεRI. This event leads to the activation of PKCβ, that phosphorylates p110γ in the helical domain and has been shown to modulate enzyme activity. The effect of this phosphorylation on regulatory subunit binding and the structural changes linked to enhanced enzyme activity remains elusive. Using a combination of hydrogen-deuterium exchange mass spectrometry (HDX-MS), biochemical assays, and other biophysical approaches we have characterized the molecular basis of this allosteric modulation upon

phosphorylation. We find that this event is specific to p110γ-p84 complex and increases sensitivity to activation signals. We have also identified a nanobody that has been shown to specifically target p110γ/p84 complex, to also prevent the phosphorylation at the helical domain. Overall, our work provides molecular details into the regulation of PI3Kγ pathway through allosteric modulation and its effect on regulatory partner binding.

3.2 Introduction

The class I phosphoinositide 3-kinase (PI3K) family are bipartite enzyme complexes that regulate several important cellular processes including growth, proliferation, transcription, cytoskeletal dynamics, and membrane trafficking. These enzymes are recruited to the plasma membrane by myriad cell membrane receptors such as RTK, GPCRs and Ras superfamily of GTPases leading to the generation of phosphatidylinositol 3,4,5-trisphosphate (PIP_3) molecule. They are divided into subclasses based on their regulatory partners as class IA consisting of p110α, p110β, and p110δ, and a single isozyme in class IB, p110γ. p110γ can bind to two different regulatory subunits namely p101 and p84 (also called p87) adaptor subunit.

p110γ is encoded by *PIK3CG* and is found to be enriched in leukocytes. This enzyme governs several important immune cell functions [118] such as, cytokine production [30], and reactive oxygen species (ROS) generation. These are critical processes for the innate and adaptive immune systems. The differences in regulation of PI3Kγ pathway stems from the differences in binding of the two different regulatory subunits to p110γ. Although both p84 and p101 bind to p110γ at the same regions, the residues at the binding interfaces vary which leads to differential binding effects[8]. Work

with mouse neutrophils have shown that p110γ/p101 and p110γ/p84 control distinct functions of the PI3Kγ pathway. The p110γ/p101 complex has been shown to promote cell migration whereas p110γ/p84 complex leads to Reactive Oxygen Species production[34]. These signaling outputs are dependent on PI3Kγ activation which occurs downstream of G-Protein Coupled Receptors (GPCRs), Ras superfamily of GTPases and post-translational modifications. Activation of the p110γ-p101 complex is dependent on Gβγ[7], whereas the p110γ-p84 complex requires Ras as a co-stimulator[8,35].

We have extensively characterized the molecular basis of interaction with both the regulatory subunits[7,8]. The p110γ catalytic subunit is composed of an adaptor binding subunit (ABD), a Ras binding domain (RBD) that mediates activation downstream of Ras, a C2 domain, a helical domain that is involved in transducing confirmational changes and binding to Gβγ, and a bi-lobal kinase domain (Fig 3.1A). The cryo-EM structure of p110γ revealed that it binds to the regulatory subunit through interactions with the C2 domain, and the linkers between the RBD-C2 and C2-helical. While the difference in regulation arises from altered binding sites between p84 and p101, and their sensitivity to activation signals, post-translational modifications have also been implicated to alter the PI3Kγ pathway. p110γ has also been shown to be activated downstream of FcεRI. This event leads to accumulation of Ca^{2+} from store operated Ca^{2+} channels (SOCE), which activates protein kinase C β (PKCβ) leading to phosphorylation of p110γ in the helical domain at S582. This modification was discovered in mast cells that do not contain p101 and has been shown to enhance the enzyme activity and promote dissociation of the p84 subunit.[31]. The helical domain is structurally connected to a region of the kinase domain C-terminal to the activation loop, referred to as the regulatory motif (Fig 3.1B).

The C-terminal regulatory motif of all class I PI3Ks undergo conformational change that promote membrane binding[19]. They also showed using in-vivo phosphorylated S582 and phosphomimic mutants that phosphorylation in p110γ helical domain enhances the lipid kinase activity, however the full molecular mechanism underlying this event and its consequences on adaptor binding remains elusive.

PI3Kγ has been shown to be a promising therapeutic target in several human diseases including cancer and inflammation. PI3Kγ complexes play a prominent role in regulating immunity and inflammation which is achieved through migration of immune cell types such as neutrophils and macrophages at the site of inflammation. PI3Kγ has been shown to be a key player in promoting several auto-immune disorders such as Lupus, allergy, cardiovascular diseases, and obesity related changes in metabolism[51,53,119,120]. Inhibition of PI3Kγ signalling has been shown to be beneficial against cancer in combination with checkpoint inhibitors[121]. Loss of PI3Kγ activity has been shown to block metastasis which is mediated by macrophages in several tumour models[122]. Here, using a combination of hydrogen deuterium exchange mass spectrometry (HDX-MS), and biochemical assays, we provide a molecular model for phosphorylation at the helical domain leading to allosteric changes in the kinase domain. We also show that this phosphorylation event is specific to p110γ/p84 complex which has major implications as the regulatory subunits are not equally distributed. Finally, we characterize the effects of a nanobody that can bind to the helical domain and block Ras mediated recruitment of p110γ/p84 complex, to also prevent phosphorylation at the helical domain.

3.3 Materials and methods

3.3.1 Plasmid Generation

PI3Kγ constructs without the regulatory subunit p110γ full length was encoded in a pACEBac vector while the complexes were expressed from biGBac vectors. For purification, a 10× histidine tag, a 2× strep tag, and a tobacco etch virus protease cleavage site were cloned to the N terminus of the regulatory subunits for the complex and to p110γ for constructs without regulatory subunits. Plasmids harboring full-length PKCβ was inserted into the pFastBac1 vector to allow baculovirus expression in *Spodoptera frugiperda* (Sf9) cells. The plasmids containing PKCβ isoform also expressed intra-protein 10X histidine tag, followed by a 2X Strep tag, followed by a Tobacco Etch Virus protease cleavage site N-terminal to the kinase domain. DNA oligonucleotides spanning the desired region were ordered (Sigma). PCR reactions were performed, and PCR purified (Q5 High-Fidelity 2X MasterMix, New England Biosciences #M0492L; QiaQuick PCR Purification Kit, Qiagen #28104). Single colonies were grown overnight and purified using QIAprep Spin Miniprep Kit (Qiagen #27104). Plasmid identity was confirmed by Sanger Sequencing (Eurofins Genomics).

3.3.2 Virus Generation and Amplification

Virus generation and amplification for PI3Kγ constructs were carried out according to our standard protocol. The plasmids encoding genes for insect cell expression were transformed into DH10MultiBac cells (MultiBac, Geneva Biotech) to generate baculovirus plasmid (bacmid) containing the genes of interest. Successful generation was identified by blue-white screening and the bacmid was purified using a standard isopropanol-ethanol extraction method. Bacteria were grown overnight (16 hours) in 3-5 mL 2xYT

(BioBasic #SD7019). Cells were spun down and the pellet was resuspended in 300 µL of 50 mM Tris-HCl, pH 8.0, 10 mM EDTA, 100 mg/mL RNase A. The pellet was lysed by the addition of 300 µL of 1% sodium dodecyl sulfate (SDS) (W/V), 200 mM NaOH, and the reaction was neutralized by addition of 400 µL of 3.0 M potassium acetate, pH 5.5. Following centrifugation at 21130 RCF and 4^{o}C (Rotor #5424 R), the supernatant was mixed with 800 µL isopropanol to precipitate bacmid DNA. Following centrifugation, the pelleted bacmid DNA was washed with 500 µL 70% Ethanol three times. The pellet was then air dried for 1 minute and re-suspended in 50 µL Buffer EB (10 mM Tris-Cl, pH 8.5; All buffers from QIAprep Spin Miniprep Kit, Qiagen #27104). Purified bacmid was then transfected into Sf9 cells. 2 mL of Sf9 cells at 0.6X10^{6} cells/mL were aliquoted into a 6-well plate and allowed to attach to form a confluent layer. Transfection reactions were prepared mixing 8-12 µg of bacmid DNA in 100 µL 1xPBS and 12 µg polyethyleneimine (Polyethyleneimine ‘‘Max’’ MW 40.000, Polysciences #24765, USA) in 100 µL 1xPBS and the reaction was allowed to proceed for 20-30 minutes before addition to an Sf9 monolayer containing well. Transfections were allowed to proceed for 5-6 days before harvesting virus containing supernatant as a P1 viral stock.

Viral stocks were further amplified by adding P1 to Sf9 cells at ~2x10^{6} cells/mL (2/100 volume ratio). This amplification was allowed to proceed for 4-5 days and resulted in a P2 stage viral stock that was used in final protein expression. Harvesting of P2 viral stocks was carried out by centrifuging cell suspensions in 50 mL Falcon tubes at 2281 RCF (Beckman GS-15). To the supernatant containing virus, 5-10% inactivated fetal bovine serum (FBS; VWR Canada #97068-085) was added and the stock was stored at 4 ^{o}C.

3.3.3 Expression and purification of PI3Kγ constructs*:*

All PI3Kγ, p101 and full-length PKCβ constructs were expressed in Sf9 insect cells using the baculovirus expression system. Following 55 hours of expression, cells were harvested by centrifuging at 1680 rcf (Eppendorf Centrifuge 5810 R) and the pellets were snap-frozen in liquid nitrogen. The complex was purified identically through a combination of nickel affinity, streptavidin affinity and size exclusion chromatographic techniques.

The frozen pellets were resuspended in lysis buffer containing 20 mM Tris pH 8, 10 mM Imidazole, 100 mM NaCl, 5% glycerol [v/v], 2 mM βME, protease inhibitor [Protease Inhibitor Cocktail Set III, Sigma]) and sonicated for 2 min (15 s on, 15 s off, level 4.0, Misonix sonicator 3000). Triton-X was added to the lysate at a final concentration of 0.1% and then clarified by spinning at 14, 000 rpm for 45 min (Beckman Coulter JA-20 rotor). The supernatant was loaded onto a 5 ml crude Ni-NTA column (GE healthcare) equilibrated in NiNTA A buffer containing 20 mM Tris pH 8, 100 mM NaCl, 10 mM Imidazole and 5% glycerol [v/v]. The column was washed using high salt buffer containing 20 mM Tris, 1 M NaCl, 10 mM imidazole, 5% glycerol [v/v] followed by NiNTA buffer wash (20 mM Tris pH 8, 100 mM NaCl, 21 mM imidazole and 5% glycerol). The protein was eluted using 100% NiNTA B buffer (20 mM Tris pH 8, 100 mM NaCl, 200 mM imidazole and 5% glycerol). The eluent was loaded onto a 5 mL StrepTrap™ HP column (GE Healthcare) equilibrated in gel filtration buffer (20mM Tris pH 8.5, 100 mM NaCl, 50 mM ammonium sulfate and 0.5 mM TCEP). The column was washed with the same buffer and loaded with tobacco etch virus protease for cleavage of protein tags. After cleavage on the column overnight, the protein was eluted in gel filtration buffer. For the complex

with nanobody, the eluted protein was incubated with two-fold molar excess of purified nanobody on ice for 15 minutes. The protein was concentrated in a 50,000 MWCO Amicon Concentrator (Millipore) to <1 mL and injected onto a Superdex™ 200 10/300 GL Increase size-exclusion column (GE Healthcare) equilibrated in gel filtration buffer. After size exclusion, the protein was concentrated, aliquoted, frozen, and stored at -80^{o}C. For PKCβ, strep eluent was concentrated using 30,000 MWCO Amicon Concentrator (Millipore) to <200 µL, frozen and stored at -80^{o}C.

To purify phosphorylated p110γ, purified PKCβ was added to the strep column at a molar ratio of 1:3 (PKCβ: p110) along with LipTEV, 20 mM MgCl2 and 1mM ATP and allowed to incubate on ice for 3 hours. The protein was eluted by passing 7 ml of gel filtration buffer and treated with a second dose of PKCβ (same ratio as above) and allowed to incubate on ice for another 3 hours. For non-phosphorylated p110, same protocol was followed with the exception in the addition of PKCβ. Both the proteins were concentrated in a 50,000 MWCO Amicon Concentrator (Millipore) to <1 mL and injected onto a Superdex™ 200 10/300 GL Increase size-exclusion column (GE Healthcare) equilibrated in gel filtration buffer. After size exclusion, the protein was concentrated, aliquoted, frozen, and stored at -80^{o}C.

3.3.4 Expression and Purification of lipidated Gβγ for kinase activity assays

Full length, lipidated human Gβγ (Gβ1γ2) was expressed in Sf9 insect cells and purified as described previously[123]. After 65 hours of expression, cells were harvested, and the pellets were frozen as described above. Pellets were resuspended in lysis buffer (20 mM HEPES pH 7.7, 100 mM NaCl, 10 mM βME, protease inhibitor (Protease Inhibitor Cocktail

Set III, Sigma)) and sonicated for 2 minutes (15s on, 15s off, level 4.0, Misonix sonicator 3000). The lysate was spun at 500 RCF (Eppendorf Centrifuge 5810 R) to remove intact cells and the supernatant was centrifuged again at 25,000 RCF for 1 hour (Beckman Coulter JA-20 rotor). The pellet was resuspended in lysis buffer and sodium cholate was added to a final concentration of 1% and stirred at 4oC for 1 hour. The membrane extract was clarified by spinning at 10,000 RCF for 30 minutes (Beckman Coulter JA-20 rotor). The supernatant was diluted 3 times with NiNTA A buffer (20 mM HEPES pH 7.7, 100 mM NaCl, 10 mM Imidazole, 0.1% C12E10, 10mM βME) and loaded onto a 5 mL HisTrap™ FF crude column (GE Healthcare) equilibrated in the same buffer. The column was washed with NiNTA A, 6% NiNTA B buffer (20 mM HEPES pH 7.7, 25 mM NaCl, 250 mM imidazole pH 8.0, 0.1% C12E10, 10 mM βME) and the protein was eluted with 100% NiNTA B. The eluent was loaded onto HiTrapTM Q HP anion exchange column equilibrated in Hep A buffer (20 mM Tris pH 8.0, 8 mM CHAPS, 2 mM Dithiothreitol (DTT)). A gradient was started with Hep B buffer (20 mM Tris pH 8.0, 500 mM NaCl, 8 mM CHAPS, 2 mM DTT) and the protein was eluted in ~50% Hep B buffer. The eluent was concentrated in a 30,000 MWCO Amicon Concentrator (Millipore) to < 1 mL and injected onto a Superdex^{TM} 75 10/300 GL size exclusion column (GE Healthcare) equilibrated in Gel Filtration buffer (20 mM HEPES pH 7.7, 100 mM NaCl, 10 mM CHAPS, 2 mM TCEP). Fractions containing protein were pooled, concentrated, aliquoted, frozen, and stored at -80^{o}C.

3.3.5 Expression and purification of nanobody

Nanobody NB7-PIK3CG with a C-terminal 6X His tag was expressed from a pMESy4 vector in the periplasm of WK6 *E. coli*. A 1L culture was grown to OD_{600} of 0.7 in Terrific Broth containing 0.1% glucose and 2 mM MgCl2 in the presence of 100 µg/mL ampicillin and was induced with 0.5 mM isopropyl-β-D-thiogalactoside (IPTG). Cells were harvested the following day by centrifuging at 2500 RCF (Eppendorf Centrifuge 5810 R) and the pellet was snap-frozen in liquid nitrogen. The frozen pellet was resuspended in 15 mL of buffer containing 200 mM Tris pH 8.0, 0.5mM ethylenediaminetetraacetic acid (EDTA) and 500 mM Sucrose and was mixed for 1 hour at 4°C. To this mixture, 30 mL of resuspension buffer diluted four times in water was added and mixed for 45 minutes at 4°C to induce osmotic shock. The lysate was clarified by centrifuging at 14,000 rpm for 30 minutes (Beckman Coulter JA-20 rotor). Imidazole was added to the supernatant to final concentration of 10mM loaded onto a 5 mL HisTrap™ FF crude column (GE Healthcare) equilibrated in NiNTA A buffer (20 mM Tris pH 8.0, 100 mM NaCl, 20 mM imidazole pH 8.0, 5% (v/v) glycerol, 2 mM β-mercaptoethanol (βME)). The column was washed with high salt NiNTA A buffer (20 mM Tris pH 8.0, 1 M NaCl, 20 mM imidazole pH 8.0, 5% (v/v) glycerol, 2 mM βME), NiNTA A buffer, 6% NiNTA B buffer (20 mM Tris pH 8.0, 100 mM NaCl, 250 mM imidazole pH 8.0, 5% (v/v) glycerol, 2 mM βME) and the protein was eluted with 100% NiNTA B. The eluent was concentrated in a 10,000 MWCO Amicon Concentrator (Millipore) to <1 mL and injected onto a Superdex™ 75 10/300 GL Increase size-exclusion column (GE Healthcare) equilibrated in gel filtration buffer (20mM Tris pH 8.5, 100 mM NaCl, 50 mM Ammonium Sulfate and 0.5 mM tris(2-carboxyethyl) phosphine (TCEP)). Following size exclusion, the protein was concentrated, frozen and stored at -80°C.

3.3.6 Lipid vesicle preparation

Lipid vesicles containing 5% brain phosphatidylinositol 4,5- bisphosphate (PIP2), 20% brain phosphatidylserine (PS), 35% egg-yolk phosphatidylethanolamine (PE), 10% egg-yolk phosphatidylcholine (PC), 25% cholesterol and 5% egg-yolk sphingomyelin (SM) were prepared by mixing the lipids solutions in organic solvent. The solvent was evaporated in a stream of argon following which the lipid film was desiccated in a vacuum for 45 minutes. The lipids were resuspended in lipid buffer (20 mM HEPES pH 7.0, 100 mM NaCl and 10 % glycerol) and the solution was sonicated for 15 minutes. The vesicles were subjected to five freeze thaw cycles and extruded 11 times through a 100-nm filter (T&T Scientific: TT-002-0010). The extruded vesicles were sonicated again for 5 minutes, aliquoted and stored at -80°C. Final vesicle concentration was 5 mg/mL.

3.3.7 Kinase Assays

All kinase assays were done using Transcreener ADP2 Fluorescence Intensity (FI) assays (Bellbrook labs) which measures ADP production. PM-mimic vesicles [5% phosphatidylinositol 4,5-bisphosphate (PI(4,5) P2), 20% phosphatidylserine (PS), 10% phosphatidylcholine (PC), 35% phosphatidylethanolamine (PE), 25% cholesterol, 5% sphingomyelin (SM)] at final concentration of 0.5 mg/mL and ATP at a final concentration of 100 μM . For assays measuring stimulation with $G\beta\gamma$, 1.5 μM of the activator was used in the reaction. 2 μL of 2X substrate solution containing vesicles, the appropriate concentration of $G\beta\gamma$ was mixed with 2 μL of 2X kinase solution and the reaction was allowed to proceed for 60 minutes. The reactions were stopped with 4 μL of 2X stop and

detect solution containing Stop and Detect buffer, 8 nM ADP Alexa Fluor 594 Tracer and 93.7 µg/mL ADP2 Antibody IRDye QC-1 and incubated for 50 minutes. The fluorescence intensity was measured using a SpectraMax M5 plate reader at excitation 590 nm and emission 620 nm. This data was normalized against the measurements obtained for 100 µM ATP and 100 µM ADP. The % ATP turnover was interpolated from a standard curve (0.1-100 µM ADP). This was then used to calculate the specific activity of the enzyme.

3.3.8 Biolayer interferometry

Biolayer interferometry was performed using Octet K2 (Fortebio *Inc.*). His-tagged nanobody was immobilized on an Anti-Penta-His biosensor for 600 s, and the sensor was dipped into solutions of phos or non phosphorylated p110γ at 35 nM final concentration diluted in kinetics buffer (KB) containing 20 mM tris (pH 8.5), 100 mM NaCl, 50 mM ammonium sulfate, 0.1% bovine serum albumin, and 0.02% Tween 20. The association step was allowed to proceed for 600 s followed by a dissociation step in KB without protein for 600 s. The average K_d (dissociation constant) was calculated from the three binding curves based on their global fit to a 1:1 binding model.

3.3.9 Phosphorylation set-up

To test PKC phosphorylation with various p110γ constructs (shown in figure 3.1 E and Figure 3.3), we carried out phosphorylation reactions 20°C in 20 µL with final concentrations of 500 nM PI3K by in the presence of 1mM ATP and 20 mM $MgCl_2$. The samples were made up to 50 µL with distilled water and the reaction was quenched with

the addition of 20 µL of ice-cold acidic quench buffer. After quenching, samples were immediately frozen in liquid nitrogen and stored at -80°C. The samples were subjected to MS/MS analysis and the peptides were identified by using PEAKS7 (PEAKS) and a false discovery rate was set at 0.1% using a database of purified proteins and known contaminants. The phosphorylated peptide sequences were identified by surveying the Serine residues from the phosphorylation region and the rest of the protein. This was then integrated with the extracted ion chromatograms of the phosphorylated and the unphosphorylated peptides. The area under these curves were calculated which was then used to calculate the ratio of the two species.

3.3.10 Hydrogen Deuterium eXchange Mass Spectrometry

Sample Preparation: Exchange reactions to assess differences in p110γ upon phosphorylation were carried out at 18°C in 10 µL volumes with final concentrations of 1.5 uM for both apo and phosphorylated p110γ. A total of two conditions were assessed: p110γ apo and PKCβ phosphorylated p110γ. The hydrogen-deuterium exchange reaction was initiated by the addition of 8 µL D_2O buffer (94.3% D_2O, 100 mM NaCl, 20 mM HEPES pH 7.5) to the 2 µL protein for a final D_2O concentration of 75.5%. Exchange was carried out over five time points (0.3s, 3s, 30s, 300s and 3000s) and the reaction was quenched with addition of 60 µL of ice-cold acidic quench buffer (0.7 M guanidine-HCl, 1% formic acid). After quenching, samples were immediately frozen in liquid nitrogen and stored at -80°C. All reactions were carried out in triplicate.

Protein Digestion and MS/MS Data Collection: Protein samples were rapidly thawed and injected onto an integrated fluidics system containing a HDx-3 PAL liquid handling robot and climate-controlled chromatography system (LEAP Technologies), a Dionex Ultimate 3000 UHPLC system, as well as an Impact HD QTOF Mass spectrometer (Bruker). The protein was run over two immobilized pepsin columns (Applied Biosystems; Poroszyme™ Immobilized Pepsin Cartridge, 2.1 mm x 30 mm; Thermo-Fisher 2-3131-00; at 10°C and 2°C respectively) at 200 µL/min for 3 minutes. The resulting peptides were collected and desalted on a C18 trap column [Acquity UPLC BEH C18 1.7 mm column (2.1 x 5 mm); Waters 186003975]. The trap was subsequently eluted in line with an ACQUITY 1.7 µm particle, 100 x 1 mm2 C18 UPLC column (Waters 186002352), using a gradient of 3-35% B (buffer A, 0.1% formic acid; buffer B, 100% acetonitrile) over 11 min immediately followed by a gradient of 35-80% B over 5 minutes. MS experiments acquired over a mass range from 150 to 2200 mass/charge ratio (m/z) using an electrospray ionization source operated at a temperature of 200°C and a spray voltage of 4.5 kV.

Peptide Identification: Peptides were identified using data-dependent acquisition following tandem MS/MS experiments (0.5 s precursor scan from 150-2000 m/z; twelve 0.25 s fragment scans from 150-2000 m/z). MS/MS datasets were analyzed using PEAKS7 (PEAKS), and a false discovery rate was set at 0.1% using a database of purified proteins and known contaminants. Same approach was used to identify phosphorylated and non-phosphorylated peptides for our in-vitro phosphorylation experiments.

Mass Analysis of Peptide Centroids and Measurement of Deuterium Incorporation: HD-Examiner Software (Sierra Analytics) was used to automatically calculate the level of

deuterium incorporation into each peptide. All peptides were manually inspected for correct charge state, correct retention time, and appropriate selection of isotopic distribution. Deuteration levels were calculated using the centroid of the experimental isotope clusters. HDX-MS results are presented with no correction for back exchange shown in the Source data, with the only correction being applied correcting for the deuterium oxide percentage of the buffer used in the exchange (65.5%). Changes in any peptide at any time point greater than specified cut-offs (4% and 0.3 Da) and with an unpaired, two-tailed t-test value of $p<0.01$ was considered significant. The search parameters were set with a precursor tolerance of 20 parts per million, fragment mass error 0.02 Da, and charge states from 1 to 8, with a selection criterion of peptides that had a −10logP score of >.

3.4 Results

3.4.1 PKCβ phosphorylates p110γ at S582 and S594/595

We have previously characterized the phosphorylation event and implications of it in bone marrow-derived mast cells. PI3Kγ has been shown to be an enhancer IgE/antigen output. In response to the clustering of IgE receptors and Ca^{2+} influx from store operated Ca^{2+} channels, PKCβ has been shown to phosphorylate p110γ at S582 which has been shown to be essential for mast cell degranulation (Fig 3.1D). This event led to the activation of PKCβ and established a direct link with FcεRI and PI3K signalling. We observed that the phosphorylation event in the helical domain led to enhanced enzyme activity using in-vivo bone marrow derived mast cells. The protein structure reveals that the phosphorylation site is in close proximity to the C2-helical linker which could potentially alter the binding

of the regulatory subunit (Fig 3.1C). The helical domain is structurally linked to the regulatory motif through a series of short heat repeat helices, with the helix 624-630 directly contacting the kα9 of the regulatory motif. This should allow allosteric modulation of the protein upon phosphorylation. We have also previously shown using HDX-MS that the binding of the regulatory subunit, either p84 or p101 led to stabilization in the helical domain, with this effect being exaggerated with p101, suggesting that this phosphorylation could have differential effect on the two different p110γ complexes[8]. Moreover, structures of p110γ reveal that S582 points inward, this implies that the residue must rotate to accommodate the phosphate group (Fig 3.1C). In-order for the phosphorylation event to occur, we believe that the helical domain must undergo dynamic unfolding for the serine to accommodate the phosphate group.

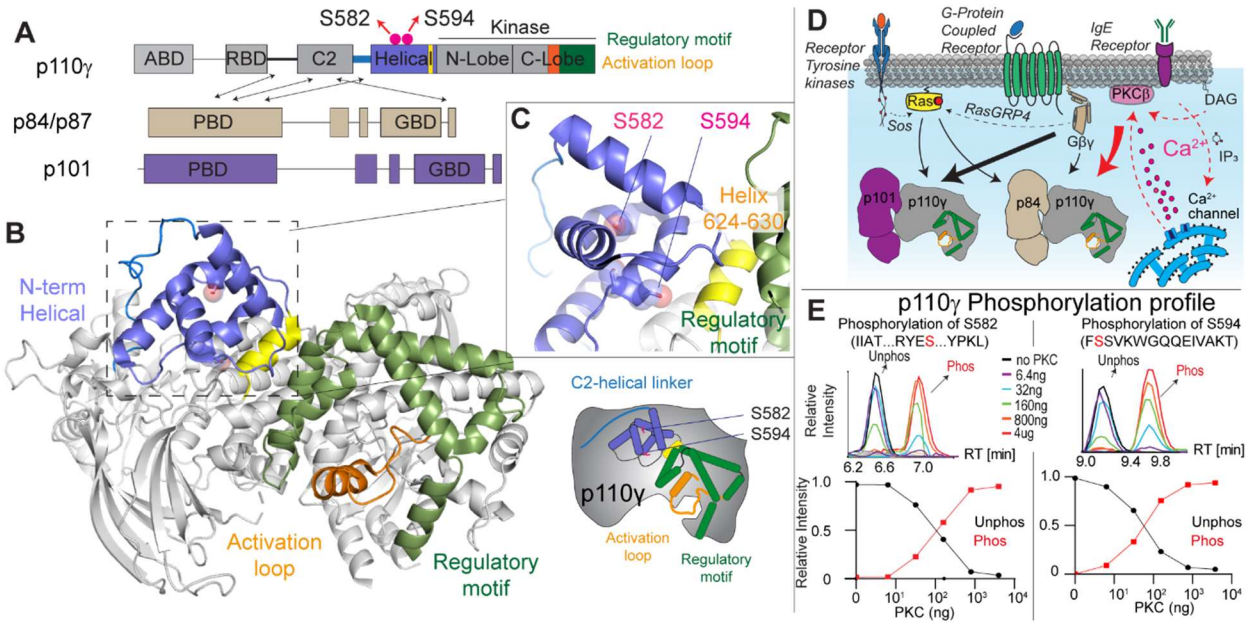

Figure 3.1. Structure of p110γ and location of phosphorylation sites
A. Domain schematics of p110γ with helical domain (blue), activation loop (orange), and regulatory motif (green) of p110 annotated. Same color scheme has been used to map these features on the structures below. The domain architecture of its regulatory subunits p84 and p101 are also annotated. The arrows indicate the sites of interaction.

B. Phosphorylation sites mapped on the structure of p110γ (PDB: 7MEZ). The regions are colored based on domain schematics featured in fig 3.1A. Cartoon schematic of p110γ with various regions indicated. This cartoon view was used to map all further HDX-MS experiments.
C. Orientation of S582 and S594/595 in p110γ (PDB:7MEZ)
D. Cartoon schematic of different pathways associated with PI3Kγ pathway. The red arrows indicate IgE mediated activation of PKCβ and subsequent phosphorylation of p110γ/p84 complex.
E. Ratio of the intensity of extracted ion traces of different phosphorylation site peptides (Left to Right: S582 and S594/S595) from p110γ samples treated with increasing concentration of PKCβ. The extracted traces can be seen in Appendix Fig 7.

To characterize this event, we purified full-length p110γ and the kinase domain of PKCβ (as the full-length is unable to bind p110γ in the absence of a pseudo substrate). We setup *in-vitro* phosphorylation, p110γ was incubated with increasing concentration of PKCβ in the presence of 20 mM $MgCl_2$ and 1 mM ATP. The reaction was carried out for one hour at 4°C and subjected to MS/MS analysis. The phosphorylated peptides were identified as mentioned above. Surprisingly, we identified a novel second site in the helical domain that undergoes simultaneous phosphorylation at S594/S595. Phosphorylation was measured by identifying and calculating the ratios of the population of phosphorylated and non-phosphorylated peptides. Free p110γ underwent phosphorylation by PKC and both the sites showed similar trends in phosphorylation (Fig 3.1E). We have used similar approach to calculate the % of phosphorylation for further experiments.

3.4.2 Phosphorylation leads to allosteric changes in the kinase domain

To understand the biochemical and structural changes caused by phosphorylation, we purified apo and phosphorylated p110γ. We set-up *in vitro*-phosphorylation as mentioned before, followed by size exclusion chromatography. Both the proteins eluted at the same volume (Fig 3.2A) and the phosphorylation percentage was calculated to

be >95%. We characterized the lipid kinase activity of p110γ on a PM mimic liposomes in the presence or absence of Gβγ to determine changes in enzyme activity upon phosphorylation. We noticed that the phosphorylated p110γ has two-fold higher activity compared to apo protein (Fig 3.2B). Interestingly we saw similar 2-fold increase in their activation with Gβγ.

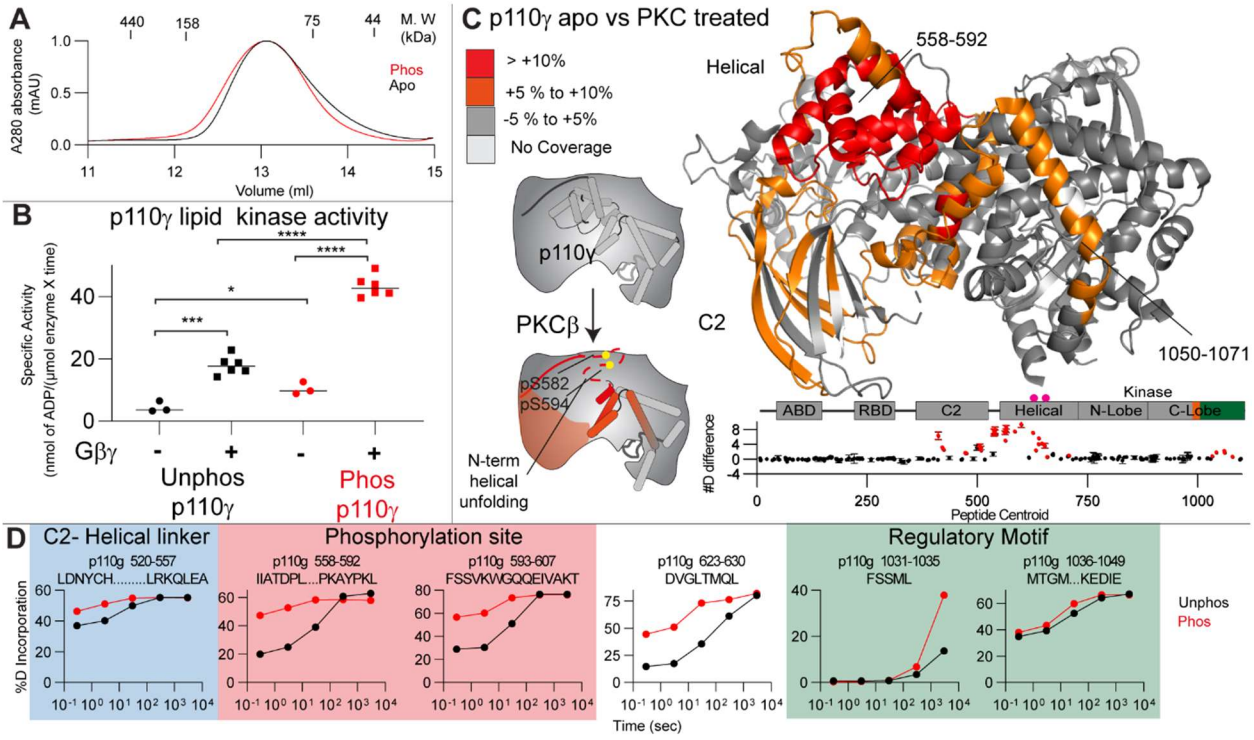

Figure 3. 2. Phosphorylation at the helical domain leads to opening of the regulatory motif
A. Gel filtration elution profile of different p110γ (i.e., apo and phosphorylated). An SDS–polyacrylamide gel electrophoresis image of the p110γ is shown in Appendix figure 1.
B. Lipid kinase assay performed with different p110γ constructs (error bars are S.D., n=6). Experiments were performed with 2.25 to 0.25 µM PI3K, 1.5 µM of Gβγ, and 100 µM ATP in the presence of 0.5 mg/ml of PM mimic liposomes (20% phosphatidylserine, 50% phosphatidylethanolamine, 10% cholesterol, 10% phosphatidylcholine, 5% sphingomyelin, and 5% PIP2). Two tailed p-values represented by the symbols are as follows: ****<0.0001, ***<0.001; *<0.05; n.s.>0.05. Phosphorylated p110γ showed two-fold increase in enzyme activity under basal and Gβγ activated states.
C-D. HDX-MS comparing apo and phosphorylated p110γ. Significant differences in deuterium exchange are mapped on to the structure and cartoon of p110γ according to the legend (PDB: 7MEZ). The graph of the #D difference in deuterium incorporation for p110γ, with each point

representing a single peptide. Peptides colored in red are those that had a significant change in the mutants (greater than 0.4 Da and 5% difference at any timepoint, with a two tailed t-test $p<0.01$). Error bars are S.D. (n=3). **(D)** Changes in percent deuterium exchange for selected peptides. Error bars represent SD (n = 3). A more extensive set of peptides are shown in Appendix Fig 7

To examine the changes caused by the phosphorylation event, we carried out HDX-MS comparing the phosphorylated and apo protein. HDX experiments were carried out for five time points (3s at 1C, 3s, 30s, 300s, 3000s at 20°C) for both the proteins. The peptide exchange data presented is in Appendix Fig 7. Phosphorylated protein showed exposures in the helical domain, C2 and regulatory arch of the kinase domain (Fig 3.2C). This includes regions surrounding the phosphorylation site in the helical domain (550-607), the helices spanning 624-660 of the helical domains that forms direct contact with Kα9 of the regulatory motif, and parts of regulatory arch (1031-1084) consisting of helices Kα9, 10, 11 and 12. The other changes includes C2 (414-428, 467-480 and 498-515) and C2-Helical linker (520-551) which interact with Gβγ. The class IA PI3K C2 domain has been shown to form the membrane binding interface[124] while in class IB it forms interactions with the GBD of the regulatory subunits[83]. Although S582 and S594/595 are not in direct contact with the kinase domain, phosphorylation at these sites transduces conformational changes causing increased kinase activity. Previous HDX experiments comparing PI3K on a membrane have revealed exposures in the helical domain upon membrane recruitment [125]. This increase in activity upon phosphorylation could be explained by the unwinding of helical domain which provides a novel mechanistic role of the helical domain in regulating the activity of PI3Ks.

3.4.3 PKCβ phosphorylation in specific to PI3Kγ/p84 pathway

We hypothesized that p110γ/p84 complex could be vulnerable to phosphorylation downstream of PKCβ, due to the transient nature of their interaction while p110γ/p101 complex could be resistant. To test the ability of p110γ/p84 complex vs p110γ/p101 complex to be phosphorylated by PKCβ, we carried out in-vitro phosphorylation setups with different PI3Kγ variants. To setup phosphorylation of the PI3Kγ variants (p110γ/p84 and p110γ/p101), we followed a similar approach as mentioned above in Fig 3.1E. The reaction was carried out for one hour at 4°C and subjected to MS/MS analysis. We noticed that p110γ/p84 readily underwent phosphorylation at the helical domain with both the sites showing similar trends in phosphorylation (Fig 3.3F) while p110γ/p101 was resistant to phosphorylation even at high concentrations of PKC (Fig 3.3C). Overall, this data supports our hypothesis that p110γ/p84 complex is vulnerable to phosphorylation because transient nature of their interaction that allows the opening of helical domain thus allowing PKCβ-p110 interaction.

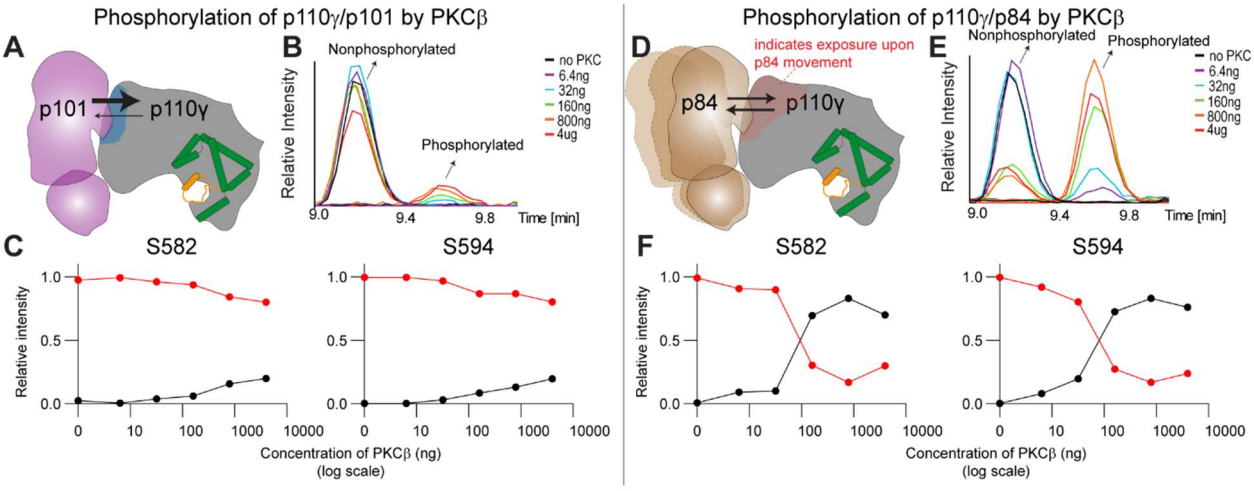

Figure 3.3 PKC mediated phosphorylation is specific to p110γ/p84 complex

A. Cartoon model of p110γ/p101 complex with the arrows indicating that the equilibrium favours the complex formation
B. Extracted ion traces for S582 peptides for p110γ/p101 complex

C. Ratio of the intensity of extracted ion traces of different phosphorylation site peptides (Left to Right: S582 and S594/S595) from p110γ/p101 samples treated with increasing concentration of PKCβ
D. Cartoon model of p110γ/p84 complex with the arrows indicating the transient nature of the complex.
E. Extracted ion traces for S582 peptides for p110γ/p84complex
F. Ratio of the intensity of extracted ion traces of different phosphorylation site peptides (Left to Right: S582 and S594/S595) from p110γ/p84 samples treated with increasing concentration of PKCβ

3.4.4 A nanobody that blocks PKC mediated phosphorylation and specifically prevents the activity of p110γ/p84 complex

Our lab has previously characterized a nanobody that specifically blocks activation downstream of Ras for PI3Kγ complexes [126]. HDX-MS characterization of the nanobody bound to p110γ-p84 showed protections throughout the helical domain, with the largest decrease being localized in the RBD, which is essential for Ras binding (196–211), and regions of the regulatory motif (1035-1050). While this nanobody has no effect on Gβγ mediated activation, it completely kills activation by Ras for both the complexes. The p110γ/p101 complex could be activated by Gβγ because of the additional Gβγ binding site in p101, whereas the p110γ/p84 complex requires Ras for membrane recruitment and subsequent activation by Gβγ. This previously published kinase assay testing p110γ/p101 and p110γ/p84 complex activation with Gβγ and Ras showed that NB7 completely disrupted activation of p110γ/p84 complex by both Gβγ and Ras.

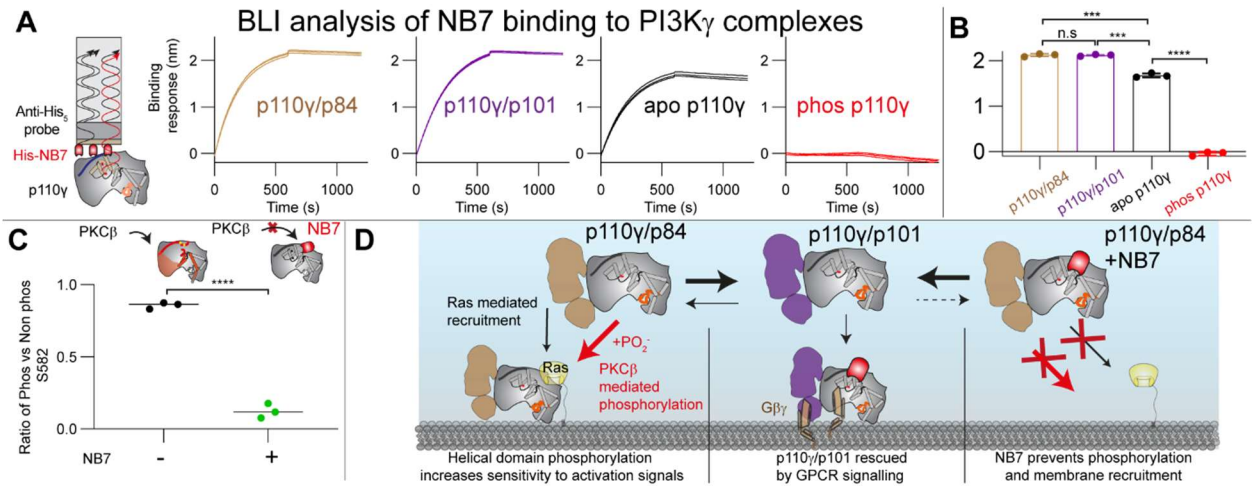

Fig 3.4 NB7 prevents PKC mediated helical domain phosphorylation

A,B. Biolayer interferometry analysis of the binding of the immobilized NB1-PIK3R5 nanobody to various p110γ variants (apo, phos, p110γ/p101 and p110γ/p84). **C.** Ratio of the intensity of extracted ion traces of S582 phosphorylation site peptides from p110γ samples apo vs NB7-bound treated with saturating concentration of PKCβ. **D.** Model showing the modus operandi for NB7 used to target p110γ/p84 complex. NB7 can target Ras mediated recruitment for both p110γ complexes. However due to the additional Gβγ binding site found in p101, p110γ/p101 complex get membrane recruited while the activity of p110γ/p84 is blocked. Binding of NB7 to p110γ/p84 complex kills Ras mediated recruitment which is crucial for this complex and blocks PKCβ mediated phosphorylation.

Next, we wanted to test the binding of NB7 to phosphorylated p110γ. To this end, we used Biolayer Interferometry (BLI) in which we immobilized NB7 to anti-His tips and dipped them into a solution containing apo or phosphorylated p110γ (Fig 3.4B). While NB7 bound to p110γ with high affinity (K_d- 0.6 nM) there was no binding of the phosphorylated p110γ. This could be because the changes caused by phosphorylation in the helical domain and the regulatory motif could alter the binding interface thus preventing NB7 interaction. Next based on our previous HDX-MS data and the structure of the complex, we hypothesized that NB7 should block phosphorylation at the helical domain by PKCβ. To test this, we set-up in-vitro phosphorylation experiments with p110γ and PKCβ in the presence and absence of NB7 at 1:2 of PI3K: NB. The PI3K-NB complex

were allowed to interact for 15 minutes at room temperature followed by PKC phosphorylation at room temperature for one hour. The samples were subjected to MS/MS analysis. The addition of PKC lead to a robust phosphorylation at ~86% with free p110γ sample while the presence of nanobody led to a ~12.4% phosphorylation at saturating concentrations of PKC (500 nM). This ~75% reduction of phosphorylation rate suggests that NB7 could be used to block phosphorylation at S582 and S594/595. (Fig 3.4A).

3.5 Discussion

The PI3Kγ signalling network is critical to the immune functions, and misregulations of this pathway has been implicated in a variety of complex diseases, such as cancer and immune conditions. Critical to this role is the regulation of PI3K signalling by activation signals and PTMs. Here we describe a phosphorylation event that increases sensitivity of p110γ/p84 complex to activation signals. Our work highlights the significance of helical domain in regulating PI3K activity. This discovery has important implications in highlighting the role of allosteric modulation and the role of helical domain in regulating the kinase activity.

We have identified a second phosphorylation site, S594/S595 and shown that the phosphorylation event is specific to the p110γ/p84 complex. However further experiments are required with S594A and S595A mutations to determine the amino acid involved in this novel second phosphorylation. p110γ can form two distinct complexes with either p101 or p84, which allows the enzyme to be activated through unique sets of upstream stimuli. This allows PI3Kγ to control distinct immune functions which has been observed

in mast cells and neutrophils. The p110γ/p101 complex has been shown to promote cell migration whereas the p110γ/p84 complex leads to Reactive Oxygen Species production[34]. This is achieved through the differential ability of the two complexes to be activated by GPCRs. Activation of the p110γ-p101 complex is dependent on Gβγ[6], whereas the p110γ-p84 complex requires Ras as a co-stimulator along with Gβγ for complete activation[35]. The p110γ-p84 complex can also fine tune PI3K signalling by promoting phosphorylation at the helical domain of p110γ through its transient interactions.

Biochemical assays with PI3K complexes using membrane bound Ras and Gβγ showed that the nanobody NB7 blocks Ras mediated recruitment[126]. Interestingly we noticed that this was rescued by Gβγ for p110γ/p101 complex. Based on the HDX-MS comparing p110γ/p84 vs p110γ/p84 bound to NB7[126], it is clear that NB7 binds to the helical domain, ABD-RBD linker and kα11 of the regulatory motif. This explains why NB7 failed to bind to the phosphorylated p110γ as the helical domain and the regulatory motif form the primary binding interfaces. While the NB does not bind at the Ras binding interface, we hypothesize that hindering the movement of the helical domain prevents membrane recruitment. Previous membrane HDX experiments with p110γ/p101 bound to Gβγ showed exposure in the helical domain upon membrane recruitment[125]..

PI3Kγ plays a crucial role in promoting several pathophysiological conditions like cancer, and inflammatory diseases. It has therefore thrusted the development of small molecule inhibitors and is considered an attractive pharmacological target. Upregulation of p101 in murine models of ovarian cancer led to cancer chemoresistance[127]

Neutrophils lacking p84 displayed impaired ROS production[34]. Increased expression of either p110γ or p101 has been shown to cause dysregulated PIP_3 levels leading to cancer[128,129]. Studies have indicated that p84 is commonly downregulated in invasive breast cancer samples[130] . The regulatory subunit p84 undergoes phosphorylation at T607 which has been shown to be important for p110γ-p84 dimerization and the tumour suppressor role of p84[32]. This difference between the two complexes provides a novel platform to specifically target one of the complexes instead of the catalytic site of p110γ. Here, we have characterized a nanobody NB7-PIK3R5 that was previously shown to block Ras mediated activation in p110γ to prevent PKC mediated phosphorylation at the helical domain. Our work highlights the novel role of helical domain in regulating p110γ kinase activity which warrants further biochemical experiments to test Ras binding to NB7 bound p110γ.

Chapter 4: Conclusion and Future directions

4.1 Summary of thesis

PI3Ks are critical for initiating the Akt/mTOR signaling pathway and play fundamental roles in cell proliferation, growth, metabolism, motility, and intracellular trafficking. With their diverse roles in cell signaling, it is not surprising that their dysregulation leads to various disorders, including cancer, and that the PI3K/Akt pathway is the most frequently mutated signaling pathway in all human cancer. This thesis has uncovered exciting and unpredicted roles for PI3K catalytic and regulatory subunits upon activation, PTMS and oncogenic mutations.

PIK3CA, the gene that encodes p110α is the second most frequently mutated oncogene. Since its discovery plethora of studies have been done to understand the regulation of PI3Ks; the role of regulatory subunits binding, activation by various cell surface receptors and the role of oncogenic mutations in hyperactivating the enzymes. The first structure of PI3K was obtained in 1999 which was p110γ in complex with H-Ras. Since then, there have been numerous studies done with class IA PI3Ks in complex with their regulatory partner that have provided molecular insights into their regulation by activation signals. The crystal structure of p110α/p85α with H1047R mutation was obtained in 2009 which revealed the orientation of the c-terminal [22]. The c-terminus of WT was solved in 2014 using x-ray crystallography which showed the c-terminal tail is pointing upward away from the membrane binding interface[131]. Whether this is a true biological phenomenon, or an artifact of crystal packing remained elusive. Moreover, the roles of ABD and p85 in regulating the enzyme activity and membrane recruitment of PI3Ks have not been completely understood.

As a part of my thesis, I have used cutting edge biophysical and biochemical tools including HDX-MS, kinase assays and FRET experiments. My thesis provides the molecular framework that dictates the activation of PI3Kα by all the oncogenic mutations. This also supports our hypothesis that the c-terminal tail has to re-orient to facilitate membrane binding of p110α. This thesis also provides valuable knowledge in defining the role of the ABD and p85 in regulating the enzyme activity. We have also determined the role of p85α in the membrane recruitment of the class IAPI3K isoforms. However, the membrane binding role of other class IA regulatory partners remains unclear. In this final chapter, I will be summarizing my results and the future directions for my work.

4.2 The molecular mechanisms of activation for the oncogenic mutations in PIK3CA

The PI3Kα isoform is critical to maintaining cellular homeostasis and is one of the most frequently mutated oncogenes. This is achieved through recruitment of the enzyme to the plasma membrane by membrane bound activators such as RTK and Ras GTPases or by the oncogenic mutants. Previous HDX-MS experiments from our lab and Roger William's lab have revealed major insights into the regulation of the enzyme[5,17,21]. Upon activation of PI3Kα by pY peptides, apart from the breaking of the nSH2–helical interface (event 1), three other events have been described [21] that include disrupting the iSH2–C2 interface (event 2), movement of the ABD domain relative to the kinase domain (event 3), and interaction of the kinase domain with the membrane (event 4). Based on our HDX-MS data and protein-lipid FRET assays, oncogenic mutations upregulate the enzyme by enhancing one or more of these dynamic events. More recently the cryo-EM structure of p110α/p85α upon pY activation suggested that the ABD/p85

completely disengages from the catalytic core[132]. However, this wasn't supported by previous membrane binding experiments with pY activated p110α/p85α.

Using recombinantly purified catalytic core and a detailed analysis of our previously published HDX-MS data[17], we have shown that the dissociation of ABD/p85 is indeed a true phenomenon that co-relates with membrane recruitment of p110α. The movement of ABD/p85 facilitates membrane binding of p110 through alleviation of inhibition on the N-lobe of kinase domain, activation loop and the iSH2 packed up against the C2 domain. Different PIK3CA mutations activating lipid kinase activity through unique mechanisms is supported by the discovery of tumours harbouring double PIK3CA mutations in cis, with these tumours showing enhanced sensitivity to PI3K inhibition[25]. We also show that upon binding the membrane, the C-terminal tail of p110 undergoes reorganization leading to increased membrane residency. The regulatory motifs of all class IA PI3Ks are maintained in the inactive conformation by inhibitory contacts with the SH2 domains of p85. p110α and p110γ are inhibited by an auto-inhibitory Tryptophan lock found in the c-terminus [5,133]. In the WT complex, membrane recruitment requires additional signalling inputs from Ras GTPases. Oncogenic mutants in the kinase domain lead in increased membrane binding either through reorientation of the WIF binding motif and the activation loop (i.e. H1047R, G1049R), or by altering residues at the membrane interface that can more extensively interact with negatively charged membranes (i.e. E726K, 1068fs). Together, this model can account for the putative mechanism of activation for >98% of all PIK3CA mutants reported in the COSMIC database (Figure 4.1), and for why double PIK3CA mutants lead to increased oncogenicity.

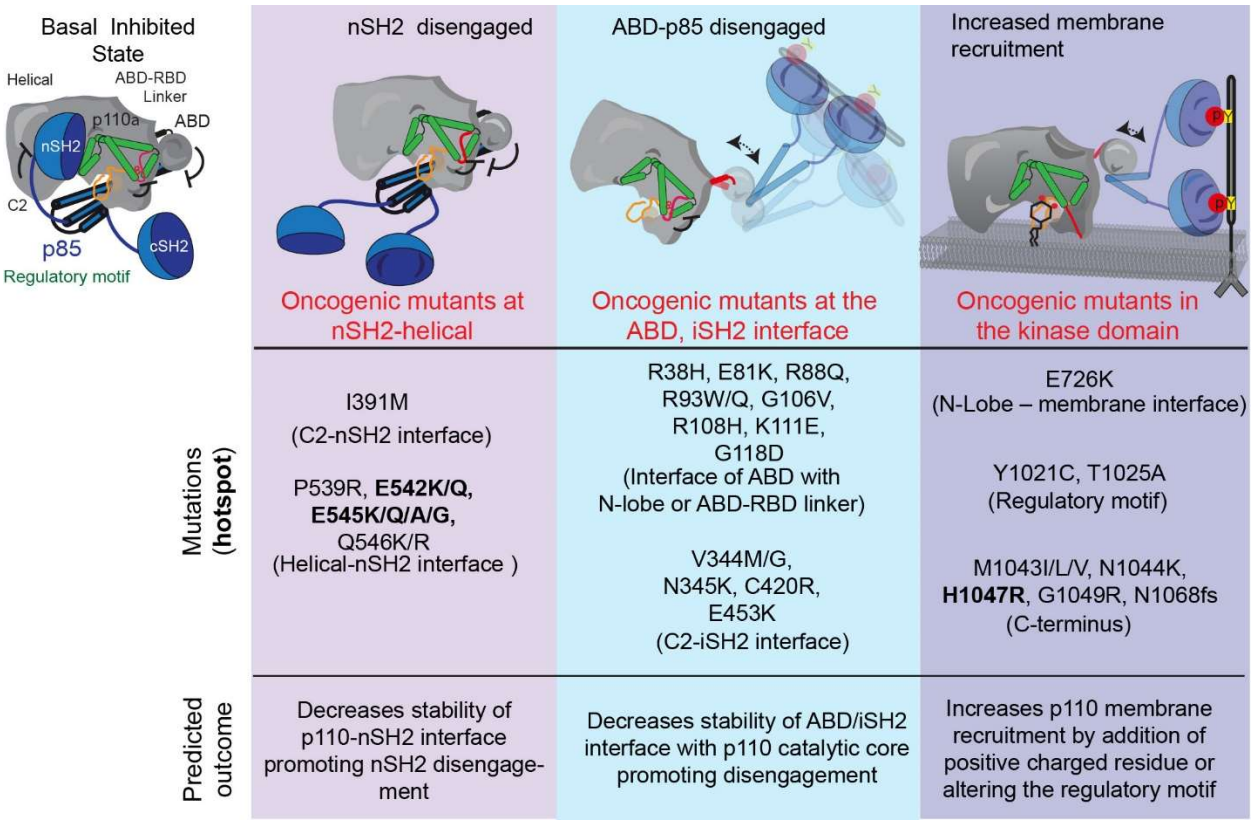

Fig 4.1 Putative mechanism for activation by *PIK3CA* oncogenic mutations

An interesting implication in this model is that unique class IA regulatory subunits may have distinctive propensities for ABD-p85 disengagement, which may partially explain a unique role for regulatory subunits oncogenic transformation. Conventionally, p85α and p85β have been considered to be similar proteins that associate with RTKs and regulate the activity of the catalytic subunits upon activation. Stark differences between p85α and p85β are observed in cancer where PIK3R1 encoding p85α acts as a tumor suppressor, PIK3R2 encoding p85β drives cancer. A comparative examination of p85α and p85β expression levels in a panel of colon and breast cancer samples showed that 50% of tumors have decreased expression levels of p85α and increased levels of p85β[134]. The distinct functions of p85α and p85β are likely to be based on structural differences. Alignment of p85α and p85β showed a high degree

of identity in the C-terminal region consisting of the SH2 domains and a lower homology was observed in the N-terminus consisting of SH3–RhoGap. Structure–function analyses with the deletion of the SH3 domain of p85β is asymptomatic, whereas deletion of this region in p85α showed an increase PI3K pathway activity[135]. Additionally, p85α and p85β also have different intracellular distributions. p85α localizes mainly to internal cell membranes, including the Golgi [134,136], a fraction of p85β localizes to the cytosol, at focal adhesions and the nucleus. These differences suggests that there may be differences in regulation of p110s by the different class IA regulatory subunits, which may play a role in the tumour suppressor activity of p85α and the oncogene activity of p85β. This will require further biochemical and structural studies to investigate regulatory subunit isoform differences in disengagement. The structural changes caused by activation and membrane recruitment p110α/p85α challenges the notion whether similar molecular and structural changes are mediated by the different regulatory subunits and the oncogenic mutations, specifically the G106V mutation (found at the ABD-RBD linker), the mutations in ABD and the C2 domain. HDX-MS with these mutants have suggested that they lead to disengagement of the ABD-p85 from the catalytic core[21]. Further HDX-MS experiments testing these mutants with the different regulatory subunits will help us define the role of different regulatory subunits in controlling class IA PI3K activity. Together this thesis highlights the key role of ABD disengagement, re-orientation of c-terminal tail in PI3K activation, and how oncogenic mutants can alter this regulation.

4.3 Role of PTMs in modulating p110 activity

The p110γ catalytic subunit is completely inactive in the absence of its regulatory subunits[6]. Unlike p110γ, the class IA isoforms (p110α, p110β, p110δ) are

highly active, and the p85 regulatory subunits inhibit the kinase activity and stabilize the catalytic subunit. The propensity for the activation of PI3Kγ complex depends on the regulatory subunit. We have recently shown that p84 forms a transient complex with p110γ compared to p101[8]. p110γ/p84 has been shown to be promote mast cell degranulation downstream of IgE receptors in response to adenosine[137]. This was later shown to activate PI3Kγ pathway independent of GPCR. The binding of Ig to the receptor leads to influx of calcium ions from SOCE which activates PKCβ. Active PKCβ phosphorylates p110γ at S582 found within the helical domain. This modification was shown to promote dissociation of p110γ-p84 complex and enhance the enzyme activity[31]. However, the mechanistic basis for activation by this PTM had remained elusive.

Using cutting-edge techniques that include HDX-MS, BLI, and kinase assays, we have characterized the implications of this activating modification. Using HDX-MS with phosphorylated p110γ, we have shown that the phosphorylation event leads to enhanced activity driven by allosteric changes in the helical domain that gets transduced to the kinase domain. The p110γ/p84 complex is vulnerable to phosphorylation downstream of PKCβ, due to the transient nature of their interaction while the p110γ/p101 complex is resistant. This provides a unique mechanism for why only p110γ/p84 complexes can be activated by PKC. We have also characterized a nanobody that specifically blocks this phosphorylation and could be used to target p110γ/p84 complex. This warrants further in-vivo experiments to assess the specificity and phosphorylation status of p110γ/p84. Further experiments are required to test if binding of NB7 to p110γ prevents complex

formation with Ras. This could be tested in-vitro through protein-protein FRET experiments testing p110:Ras interaction in the presence or absence of the nanobody.

Dysregulation of PI3K signalling pathways by mutations and deletions are implicated in multiple human diseases. Apart from these, the activity can also be modulated by PTMs. Class IA regulatory partner p85α has been identified to undergo several PTMs; by Src kinases, protein kinase (PKA), the p110 catalytic subunit itself, and by protein kinase C (PKC) family members. However, the structural perturbations caused by these PTMs are unknown. In addition, the PTMs in the other regulatory isoforms are still yet to be discovered. Class I PI3Ks have been on the realm of drug discovery programs, due to their relevance in human diseases. With the recent discovery of nanobodies that can modulate the activity of PI3Kα[138], it would be beneficial to recognize nanobodies that can target various PTMs identified for class IA regulatory partner p85α.

4.4 Conclusions

The class I PI3Ks are master regulators of cellular homeostasis, immune functions, migration, and growth. Understanding the molecular basis for the regulation of these complexes by various regulatory mechanisms is critical towards understanding how diverse regulatory inputs from receptors, PTMs and membrane association translate into distinct cellular outputs. Inhibitors targeting p110α are currently developed with the aid of high-resolution structures of these complexes in context of WT and hot spot mutant. This thesis provides the molecular basis for regulation of all oncogenic mutations in PIK3CA which has major implications in the development of mutant specific inhibitors. Moreover, this can be used as a molecular tool to also identify mutations that cause similar structural

perturbations as the hotspot mutations. This may allow to repurpose the same inhibitors for other *PIK3CA* mutants and be useful in the design of targeted therapies with fewer off target effects thus improving patient quality of life. In addition, we have also characterized a nanobody that not only can target and block Ras mediated recruitment of specifically p110γ/p84 complex, it can also be used to prevent PKC mediated phosphorylation.

References

[1] Y. Posor, W. Jang, V. Haucke, Phosphoinositides as membrane organizers, Nat. Rev. Mol. Cell Biol. (2022). https://doi.org/10.1038/s41580-022-00490-x.

[2] F. Gulluni, M.C. De Santis, J.P. Margaria, M. Martini, E. Hirsch, Class II PI3K Functions in Cell Biology and Disease, Trends Cell Biol. 29 (2019) 339–359. https://doi.org/10.1016/j.tcb.2019.01.001.

[3] B. Bilanges, Y. Posor, B. Vanhaesebroeck, PI3K isoforms in cell signalling and vesicle trafficking, Nat. Rev. Mol. Cell Biol. 20 (2019) 515–534. https://doi.org/10.1038/s41580-019-0129-z.

[4] M.K. Rathinaswamy, J.E. Burke, Class I phosphoinositide 3-kinase (PI3K) regulatory subunits and their roles in signaling and disease, Adv. Biol. Regul. 75 (2020) 100657. https://doi.org/10.1016/j.jbior.2019.100657.

[5] J.E. Burke, R.L. Williams, Synergy in activating class I PI3Ks, Trends Biochem. Sci. 40 (2015) 88–100. https://doi.org/10.1016/j.tibs.2014.12.003.

[6] N.K. Rynkiewicz, K.E. Anderson, S. Suire, D.M. Collins, E. Karanasios, O. Vadas, R. Williams, D. Oxley, J. Clark, L.R. Stephens, P.T. Hawkins, Gβγ is a direct regulator of endogenous p101/p110γ and p84/p110γ PI3Kγ complexes in mouse neutrophils, Sci. Signal. 13 (2020) eaaz4003. https://doi.org/10.1126/scisignal.aaz4003.

[7] M.K. Rathinaswamy, U. Dalwadi, K.D. Fleming, C. Adams, J.T.B. Stariha, E. Pardon, M. Baek, O. Vadas, F. DiMaio, J. Steyaert, S.D. Hansen, C.K. Yip, J.E. Burke, Structure of the phosphoinositide 3-kinase (PI3K) p110γ-p101 complex reveals molecular mechanism of GPCR activation, Sci. Adv. 7 (2021) eabj4282. https://doi.org/10.1126/sciadv.abj4282.

[8] M.K. Rathinaswamy, M.L. Jenkins, X. Zhang, J.T. Stariha, H. Ranga-Prasad, U. Dalwadi, K.D. Fleming, C.K. Yip, R.L. Williams, J.E. Burke, Molecular basis for differential activation of p101 and p84 complexes of PI3Kγ by Ras and GPCRs, Biochemistry, 2022. https://doi.org/10.1101/2022.07.29.502076.

[9] M.E. Pacold, S. Suire, O. Perisic, S. Lara-Gonzalez, C.T. Davis, E.H. Walker, P.T. Hawkins, L. Stephens, J.F. Eccleston, R.L. Williams, Crystal Structure and Functional Analysis of Ras Binding to Its Effector Phosphoinositide 3-Kinase γ, Cell. 103 (2000) 931–944. https://doi.org/10.1016/S0092-8674(00)00196-3.

[10] M. Zhang, H. Jang, R. Nussinov, The structural basis for Ras activation of PI3Kα lipid kinase, Phys. Chem. Chem. Phys. 21 (2019) 12021–12028. https://doi.org/10.1039/C9CP00101H.

[11] K. Rostislavleva, N. Soler, Y. Ohashi, L. Zhang, E. Pardon, J.E. Burke, G.R. Masson, C. Johnson, J. Steyaert, N.T. Ktistakis, R.L. Williams, Structure and flexibility of the endosomal Vps34 complex reveals the basis of its function on membranes, Science. 350 (2015) aac7365. https://doi.org/10.1126/science.aac7365.

[12] N. Miled, Y. Yan, W.-C. Hon, O. Perisic, M. Zvelebil, Y. Inbar, D. Schneidman-Duhovny, H.J. Wolfson, J.M. Backer, R.L. Williams, Mechanism of Two Classes of Cancer Mutations in the Phosphoinositide 3-Kinase Catalytic Subunit, Science. 317 (2007) 239–242. https://doi.org/10.1126/science.1135394.

[13] O. Vadas, J.E. Burke, X. Zhang, A. Berndt, R.L. Williams, Structural Basis for Activation and Inhibition of Class I Phosphoinositide 3-Kinases, Sci. Signal. 4 (2011). https://doi.org/10.1126/scisignal.2002165.

[14] I. Echeverria, Y. Liu, S.B. Gabelli, L.M. Amzel, Oncogenic mutations weaken the interactions that stabilize the p110α-p85α heterodimer in phosphatidylinositol 3-kinase α, FEBS J. 282 (2015) 3528–3542. https://doi.org/10.1111/febs.13365.

[15] M. Fox, H.R. Mott, D. Owen, Class IA PI3K regulatory subunits: p110-independent roles and structures, Biochem. Soc. Trans. 48 (2020) 1397–1417. https://doi.org/10.1042/BST20190845.

[16] M.-J. Park, R. Sheng, A. Silkov, D.-J. Jung, Z.-G. Wang, Y. Xin, H. Kim, P. Thiagarajan-Rosenkranz, S. Song, Y. Yoon, W. Nam, I. Kim, E. Kim, D.-G. Lee, Y. Chen, I. Singaram, L. Wang, M.H. Jang, C.-S. Hwang, B. Honig, S. Ryu, J. Lorieau, Y.-M. Kim, W. Cho, SH2 Domains Serve as Lipid-Binding Modules for pTyr-Signaling Proteins, Mol. Cell. 62 (2016) 7–20. https://doi.org/10.1016/j.molcel.2016.01.027.

[17] B.D. Siempelkamp, M.K. Rathinaswamy, M.L. Jenkins, J.E. Burke, Molecular mechanism of activation of class IA phosphoinositide 3-kinases (PI3Ks) by membrane-localized HRas, J. Biol. Chem. 292 (2017) 12256–12266. https://doi.org/10.1074/jbc.M117.789263.

[18] G. Gangadhara, G. Dahl, T. Bohnacker, R. Rae, J. Gunnarsson, S. Blaho, L. Öster, H. Lindmark, K. Karabelas, N. Pemberton, C. Tyrchan, M. Mogemark, M.P. Wymann, R.L. Williams, M.W.D. Perry, T. Papavoine, J. Petersen, A class of highly selective inhibitors bind to an active state of PI3Kγ, Nat. Chem. Biol. 15 (2019) 348–357. https://doi.org/10.1038/s41589-018-0215-0.

[19] M.K. Rathinaswamy, Z. Gaieb, K.D. Fleming, C. Borsari, N.J. Harris, B.E. Moeller, M.P. Wymann, R.E. Amaro, J.E. Burke, Disease-related mutations in PI3Kγ disrupt regulatory C-terminal dynamics and reveal a path to selective inhibitors, ELife. 10 (2021) e64691. https://doi.org/10.7554/eLife.64691.

[20] J.E. Burke, R.L. Williams, Dynamic steps in receptor tyrosine kinase mediated activation of class IA phosphoinositide 3-kinases (PI3K) captured by H/D exchange (HDX-MS), Adv. Biol. Regul. 53 (2013) 97–110. https://doi.org/10.1016/j.jbior.2012.09.005.

[21] J.E. Burke, O. Perisic, G.R. Masson, O. Vadas, R.L. Williams, Oncogenic mutations mimic and enhance dynamic events in the natural activation of phosphoinositide 3-kinase p110α (*PIK3CA*), Proc. Natl. Acad. Sci. 109 (2012) 15259–15264. https://doi.org/10.1073/pnas.1205508109.

[22] D. Mandelker, S.B. Gabelli, O. Schmidt-Kittler, J. Zhu, I. Cheong, C.-H. Huang, K.W. Kinzler, B. Vogelstein, L.M. Amzel, A frequent kinase domain mutation that changes the interaction between PI3Kα and the membrane, Proc. Natl. Acad. Sci. 106 (2009) 16996–17001. https://doi.org/10.1073/pnas.0908444106.

[23] W.-C. Hon, A. Berndt, R.L. Williams, Regulation of lipid binding underlies the activation mechanism of class IA PI3-kinases, Oncogene. 31 (2012) 3655–3666. https://doi.org/10.1038/onc.2011.532.

[24] J.M. Spangle, T. Von, D.C. Pavlick, A. Khotimsky, J.J. Zhao, T.M. Roberts, PIK3CA C-terminal frameshift mutations are novel oncogenic events that sensitize tumors to PI3K-α inhibition, Proc. Natl. Acad. Sci. 117 (2020) 24427–24433. https://doi.org/10.1073/pnas.2000060117.

[25] N. Vasan, P. Razavi, J.L. Johnson, H. Shao, H. Shah, A. Antoine, E. Ladewig, A. Gorelick, T.-Y. Lin, E. Toska, G. Xu, A. Kazmi, M.T. Chang, B.S. Taylor, M.N. Dickler, K. Jhaveri, S. Chandarlapaty, R. Rabadan, E. Reznik, M.L. Smith, R. Sebra, F. Schimmoller, T.R. Wilson, L.S. Friedman, L.C. Cantley, M. Scaltriti, J. Baselga, Double *PIK3CA* mutations in cis increase oncogenicity and sensitivity to PI3Kα inhibitors, Science. 366 (2019) 714–723. https://doi.org/10.1126/science.aaw9032.

[26] J.Y. Lee, Y.-H. Chiu, J. Asara, L.C. Cantley, Inhibition of PI3K binding to activators by serine phosphorylation of PI3K regulatory subunit p85α Src homology-2 domains, Proc. Natl. Acad. Sci. 108 (2011) 14157–14162. https://doi.org/10.1073/pnas.1107747108.

[27] M.J. Layton, M. Saad, N.L. Church, R.B. Pearson, C.A. Mitchell, W.A. Phillips, Autophosphorylation of serine 608 in the p85 regulatory subunit of wild type or cancer-associated mutants of phosphoinositide 3-kinase does not affect its lipid kinase activity, BMC Biochem. 13 (2012) 30. https://doi.org/10.1186/1471-2091-13-30.

[28] P. Mellor, L.A. Furber, J.N.K. Nyarko, D.H. Anderson, Multiple roles for the p85α isoform in the regulation and function of PI3K signalling and receptor trafficking, Biochem. J. 441 (2012) 23–37. https://doi.org/10.1042/BJ20111164.

[29] C.F. de la Cruz-Herrera, M. Baz-Martínez, V. Lang, A. El Motiam, J. Barbazán, R. Couceiro, M. Abal, A. Vidal, M. Esteban, C. Muñoz-Fontela, A. Nieto, M.S. Rodríguez, M. Collado, C. Rivas, Conjugation of SUMO to p85 leads to a novel mechanism of PI3K regulation, Oncogene. 35 (2016) 2873–2880. https://doi.org/10.1038/onc.2015.356.

[30] M. Laffargue, R. Calvez, P. Finan, A. Trifilieff, M. Barbier, F. Altruda, E. Hirsch, M.P. Wymann, Phosphoinositide 3-Kinase γ Is an Essential Amplifier of Mast Cell Function, Immunity. 16 (2002) 441–451. https://doi.org/10.1016/S1074-7613(02)00282-0.

[31] R. Walser, J.E. Burke, E. Gogvadze, T. Bohnacker, X. Zhang, D. Hess, P. Küenzi, M. Leitges, E. Hirsch, R.L. Williams, M. Laffargue, M.P. Wymann, PKCβ Phosphorylates PI3Kγ to Activate It and Release It from GPCR Control, PLoS Biol. 11 (2013) e1001587. https://doi.org/10.1371/journal.pbio.1001587.

[32] M.E. Turvey, M. Klingler-Hoffmann, P. Hoffmann, S.R. McColl, p84 forms a negative regulatory complex with p110γ to control PI3Kγ signalling during cell migration, Immunol. Cell Biol. 93 (2015) 735–743. https://doi.org/10.1038/icb.2015.35.

[33] P. Castel, E. Toska, J.A. Engelman, M. Scaltriti, The present and future of PI3K inhibitors for cancer therapy, Nat. Cancer. 2 (2021) 587–597. https://doi.org/10.1038/s43018-021-00218-4.

[34] A. Deladeriere, L. Gambardella, D. Pan, K.E. Anderson, P.T. Hawkins, L.R. Stephens, The regulatory subunits of PI3Kγ control distinct neutrophil responses, Sci. Signal. 8 (2015). https://doi.org/10.1126/scisignal.2005564.

[35] B. Kurig, A. Shymanets, T. Bohnacker, Prajwal, C. Brock, M.R. Ahmadian, M. Schaefer, A. Gohla, C. Harteneck, M.P. Wymann, E. Jeanclos, B. Nürnberg, Ras is an indispensable coregulator of the class I $_{B}$ phosphoinositide 3-kinase p87/p110γ, Proc. Natl. Acad. Sci. 106 (2009) 20312–20317. https://doi.org/10.1073/pnas.0905506106.

[36] C.C. Dibble, S.A. Barritt, G.E. Perry, E.C. Lien, R.C. Geck, S.E. DuBois-Coyne, D. Bartee, T.T. Zengeya, E.B. Cohen, M. Yuan, B.D. Hopkins, J.L. Meier, J.G. Clohessy, J.M. Asara, L.C. Cantley, A. Toker, PI3K drives the de novo synthesis of coenzyme A from vitamin B5, Nature. 608 (2022) 192–198. https://doi.org/10.1038/s41586-022-04984-8.

[37] N. Vasan, L.C. Cantley, At a crossroads: how to translate the roles of PI3K in oncogenic and metabolic signalling into improvements in cancer therapy, Nat. Rev. Clin. Oncol. 19 (2022) 471–485. https://doi.org/10.1038/s41571-022-00633-1.

[38] Y. Samuels, Z. Wang, A. Bardelli, N. Silliman, J. Ptak, S. Szabo, H. Yan, A. Gazdar, S.M. Powell, G.J. Riggins, J.K.V. Willson, S. Markowitz, K.W. Kinzler, B. Vogelstein, V.E. Velculescu, High Frequency of Mutations of the *PIK3CA* Gene in Human Cancers, Science. 304 (2004) 554–554. https://doi.org/10.1126/science.1096502.

[39] M.H. Bailey, C. Tokheim, E. Porta-Pardo, S. Sengupta, D. Bertrand, A. Weerasinghe, A. Colaprico, M.C. Wendl, J. Kim, B. Reardon, P.K.-S. Ng, K.J. Jeong, S. Cao, Z. Wang, J. Gao, Q. Gao, F. Wang, E.M. Liu, L. Mularoni, C. Rubio-Perez, N. Nagarajan, I. Cortés-Ciriano, D.C. Zhou, W.-W. Liang, J.M. Hess, V.D. Yellapantula, D. Tamborero, A. Gonzalez-Perez, C. Suphavilai, J.Y. Ko, E. Khurana, P.J. Park, E.M. Van Allen, H. Liang, M.S. Lawrence, A. Godzik, N. Lopez-Bigas, J. Stuart, D. Wheeler, G. Getz, K. Chen, A.J. Lazar, G.B. Mills, R. Karchin, L. Ding, S.J. Caesar-Johnson, J.A. Demchok, I. Felau, M. Kasapi, M.L. Ferguson, C.M. Hutter, H.J. Sofia, R. Tarnuzzer, Z. Wang, L. Yang, J.C. Zenklusen, J. (Julia) Zhang, S. Chudamani, J. Liu, L. Lolla, R. Naresh, T. Pihl, Q. Sun, Y. Wan, Y. Wu, J. Cho, T. DeFreitas, S. Frazer, N. Gehlenborg, G. Getz, D.I. Heiman, J. Kim, M.S. Lawrence, P. Lin, S. Meier, M.S. Noble, G. Saksena, D. Voet, H. Zhang, B. Bernard, N. Chambwe, V. Dhankani, T. Knijnenburg, R. Kramer, K. Leinonen, Y. Liu, M. Miller, S. Reynolds, I. Shmulevich, V. Thorsson, W. Zhang, R. Akbani, B.M. Broom, A.M. Hegde, Z. Ju, R.S. Kanchi, A. Korkut, J. Li, H. Liang, S. Ling, W. Liu, Y. Lu, G.B. Mills, K.-S. Ng, A. Rao, M. Ryan, J. Wang, J.N. Weinstein, J. Zhang, A. Abeshouse, J. Armenia, D. Chakravarty, W.K. Chatila, I. de Bruijn, J. Gao, B.E. Gross, Z.J. Heins, R. Kundra, K. La, M.

Ladanyi, A. Luna, M.G. Nissan, A. Ochoa, S.M. Phillips, E. Reznik, F. Sanchez-Vega, C. Sander, N. Schultz, R. Sheridan, S.O. Sumer, Y. Sun, B.S. Taylor, J. Wang, H. Zhang, P. Anur, M. Peto, P. Spellman, C. Benz, J.M. Stuart, C.K. Wong, C. Yau, D.N. Hayes, J.S. Parker, M.D. Wilkerson, A. Ally, M. Balasundaram, R. Bowlby, D. Brooks, R. Carlsen, E. Chuah, N. Dhalla, R. Holt, S.J.M. Jones, K. Kasaian, D. Lee, Y. Ma, M.A. Marra, M. Mayo, R.A. Moore, A.J. Mungall, K. Mungall, A.G. Robertson, S. Sadeghi, J.E. Schein, P. Sipahimalani, A. Tam, N. Thiessen, K. Tse, T. Wong, A.C. Berger, R. Beroukhim, A.D. Cherniack, C. Cibulskis, S.B. Gabriel, G.F. Gao, G. Ha, M. Meyerson, S.E. Schumacher, J. Shih, M.H. Kucherlapati, R.S. Kucherlapati, S. Baylin, L. Cope, L. Danilova, M.S. Bootwalla, P.H. Lai, D.T. Maglinte, D.J. Van Den Berg, D.J. Weisenberger, J.T. Auman, S. Balu, T. Bodenheimer, C. Fan, K.A. Hoadley, A.P. Hoyle, S.R. Jefferys, C.D. Jones, S. Meng, P.A. Mieczkowski, L.E. Mose, A.H. Perou, C.M. Perou, J. Roach, Y. Shi, J.V. Simons, T. Skelly, M.G. Soloway, D. Tan, U. Veluvolu, H. Fan, T. Hinoue, P.W. Laird, H. Shen, W. Zhou, M. Bellair, K. Chang, K. Covington, C.J. Creighton, H. Dinh, H. Doddapaneni, L.A. Donehower, J. Drummond, R.A. Gibbs, R. Glenn, W. Hale, Y. Han, J. Hu, V. Korchina, S. Lee, L. Lewis, W. Li, X. Liu, M. Morgan, D. Morton, D. Muzny, J. Santibanez, M. Sheth, E. Shinbrot, L. Wang, M. Wang, D.A. Wheeler, L. Xi, F. Zhao, J. Hess, E.L. Appelbaum, M. Bailey, M.G. Cordes, L. Ding, C.C. Fronick, L.A. Fulton, R.S. Fulton, C. Kandoth, E.R. Mardis, M.D. McLellan, C.A. Miller, H.K. Schmidt, R.K. Wilson, D. Crain, E. Curley, J. Gardner, K. Lau, D. Mallery, S. Morris, J. Paulauskis, R. Penny, C. Shelton, T. Shelton, M. Sherman, E. Thompson, P. Yena, J. Bowen, J.M. Gastier-Foster, M. Gerken, K.M. Leraas, T.M. Lichtenberg, N.C. Ramirez, L. Wise, E. Zmuda, N. Corcoran, T. Costello, C. Hovens, A.L. Carvalho, A.C. de Carvalho, J.H. Fregnani, A. Longatto-Filho, R.M. Reis, C. Scapulatempo-Neto, H.C.S. Silveira, D.O. Vidal, A. Burnette, J. Eschbacher, B. Hermes, A. Noss, R. Singh, M.L. Anderson, P.D. Castro, M. Ittmann, D. Huntsman, B. Kohl, X. Le, R. Thorp, C. Andry, E.R. Duffy, V. Lyadov, O. Paklina, G. Setdikova, A. Shabunin, M. Tavobilov, C. McPherson, R. Warnick, R. Berkowitz, D. Cramer, C. Feltmate, N. Horowitz, A. Kibel, M. Muto, C.P. Raut, A. Malykh, J.S. Barnholtz-Sloan, W. Barrett, K. Devine, J. Fulop, Q.T. Ostrom, K. Shimmel, Y. Wolinsky, A.E. Sloan, A. De Rose, F. Giuliante, M. Goodman, B.Y. Karlan, C.H. Hagedorn, J. Eckman, J. Harr, J. Myers, K. Tucker, L.A. Zach, B. Deyarmin, H. Hu, L. Kvecher, C. Larson, R.J. Mural, S. Somiari, A. Vicha, T. Zelinka, J. Bennett, M. Iacocca, B. Rabeno, P. Swanson, M. Latour, L. Lacombe, B. Têtu, A. Bergeron, M. McGraw, S.M. Staugaitis, J. Chabot, H. Hibshoosh, A. Sepulveda, T. Su, T. Wang, O. Potapova, O. Voronina, L. Desjardins, O. Mariani, S. Roman-Roman, X. Sastre, M.-H. Stern, F. Cheng, S. Signoretti, A. Berchuck, D. Bigner, E. Lipp, J. Marks, S. McCall, R. McLendon, A. Secord, A. Sharp, M. Behera, D.J. Brat, A. Chen, K. Delman, S. Force, F. Khuri, K. Magliocca, S. Maithel, J.J. Olson, T. Owonikoko, A. Pickens, S. Ramalingam, D.M. Shin, G. Sica, E.G. Van Meir, H. Zhang, W. Eijckenboom, A. Gillis, E. Korpershoek, L. Looijenga, W. Oosterhuis, H. Stoop, K.E. van Kessel, E.C. Zwarthoff, C. Calatozzolo, L. Cuppini, S. Cuzzubbo, F. DiMeco, G. Finocchiaro, L. Mattei, A. Perin, B. Pollo, C. Chen, J. Houck, P. Lohavanichbutr, A. Hartmann, C. Stoehr, R. Stoehr, H. Taubert, S. Wach, B. Wullich, W. Kycler, D. Murawa, M. Wiznerowicz, K. Chung, W.J. Edenfield, J. Martin, E. Baudin, G. Bubley, R. Bueno, A. De Rienzo, W.G. Richards, S. Kalkanis, T. Mikkelsen, H. Noushmehr, L. Scarpace, N. Girard, M. Aymerich, E. Campo, E. Giné, A.L. Guillermo, N. Van Bang, P.T. Hanh, B.D. Phu, Y. Tang, H. Colman, K. Evason, P.R. Dottino, J.A. Martignetti, H. Gabra, H. Juhl, T. Akeredolu, S. Stepa, D. Hoon, K. Ahn, K.J. Kang, F. Beuschlein, A. Breggia, M. Birrer, D. Bell, M. Borad, A.H. Bryce, E. Castle, V. Chandan, J. Cheville, J.A. Copland, M. Farnell, T. Flotte, N. Giama, T. Ho, M. Kendrick, J.-P. Kocher, K. Kopp, C. Moser, D. Nagorney, D. O'Brien, B.P. O'Neill, T. Patel, G. Petersen, F. Que, M. Rivera, L. Roberts, R. Smallridge, T. Smyrk, M. Stanton, R.H. Thompson, M. Torbenson, J.D. Yang, L. Zhang, F. Brimo, J.A. Ajani, A.M.A. Gonzalez, C. Behrens, J. Bondaruk, R. Broaddus, B. Czerniak, B. Esmaeli, J. Fujimoto, J. Gershenwald, C. Guo, A.J. Lazar, C. Logothetis, F. Meric-Bernstam, C. Moran, L. Ramondetta, D. Rice, A. Sood, P. Tamboli, T.

Thompson, P. Troncoso, A. Tsao, I. Wistuba, C. Carter, L. Haydu, P. Hersey, V. Jakrot, H. Kakavand, R. Kefford, K. Lee, G. Long, G. Mann, M. Quinn, R. Saw, R. Scolyer, K. Shannon, A. Spillane, J. Stretch, M. Synott, J. Thompson, J. Wilmott, H. Al-Ahmadie, T.A. Chan, R. Ghossein, A. Gopalan, D.A. Levine, V. Reuter, S. Singer, B. Singh, N.V. Tien, T. Broudy, C. Mirsaidi, P. Nair, P. Drwiega, J. Miller, J. Smith, H. Zaren, J.-W. Park, N.P. Hung, E. Kebebew, W.M. Linehan, A.R. Metwalli, K. Pacak, P.A. Pinto, M. Schiffman, L.S. Schmidt, C.D. Vocke, N. Wentzensen, R. Worrell, H. Yang, M. Moncrieff, C. Goparaju, J. Melamed, H. Pass, N. Botnariuc, I. Caraman, M. Cernat, I. Chemencedji, A. Clipca, S. Doruc, G. Gorincioi, S. Mura, M. Pirtac, I. Stancul, D. Tcaciuc, M. Albert, I. Alexopoulou, A. Arnaout, J. Bartlett, J. Engel, S. Gilbert, J. Parfitt, H. Sekhon, G. Thomas, D.M. Rassl, R.C. Rintoul, C. Bifulco, R. Tamakawa, W. Urba, N. Hayward, H. Timmers, A. Antenucci, F. Facciolo, G. Grazi, M. Marino, R. Merola, R. de Krijger, A.-P. Gimenez-Roqueplo, A. Piché, S. Chevalier, G. McKercher, K. Birsoy, G. Barnett, C. Brewer, C. Farver, T. Naska, N.A. Pennell, D. Raymond, C. Schilero, K. Smolenski, F. Williams, C. Morrison, J.A. Borgia, M.J. Liptay, M. Pool, C.W. Seder, K. Junker, L. Omberg, M. Dinkin, G. Manikhas, D. Alvaro, M.C. Bragazzi, V. Cardinale, G. Carpino, E. Gaudio, D. Chesla, S. Cottingham, M. Dubina, F. Moiseenko, R. Dhanasekaran, K.-F. Becker, K.-P. Janssen, J. Slotta-Huspenina, M.H. Abdel-Rahman, D. Aziz, S. Bell, C.M. Cebulla, A. Davis, R. Duell, J.B. Elder, J. Hilty, B. Kumar, J. Lang, N.L. Lehman, R. Mandt, P. Nguyen, R. Pilarski, K. Rai, L. Schoenfield, K. Senecal, P. Wakely, P. Hansen, R. Lechan, J. Powers, A. Tischler, W.E. Grizzle, K.C. Sexton, A. Kastl, J. Henderson, S. Porten, J. Waldmann, M. Fassnacht, S.L. Asa, D. Schadendorf, M. Couce, M. Graefen, H. Huland, G. Sauter, T. Schlomm, R. Simon, P. Tennstedt, O. Olabode, M. Nelson, O. Bathe, P.R. Carroll, J.M. Chan, P. Disaia, P. Glenn, R.K. Kelley, C.N. Landen, J. Phillips, M. Prados, J. Simko, K. Smith-McCune, S. VandenBerg, K. Roggin, A. Fehrenbach, A. Kendler, S. Sifri, R. Steele, A. Jimeno, F. Carey, I. Forgie, M. Mannelli, M. Carney, B. Hernandez, B. Campos, C. Herold-Mende, C. Jungk, A. Unterberg, A. von Deimling, A. Bossler, J. Galbraith, L. Jacobus, M. Knudson, T. Knutson, D. Ma, M. Milhem, R. Sigmund, A.K. Godwin, R. Madan, H.G. Rosenthal, C. Adebamowo, S.N. Adebamowo, A. Boussioutas, D. Beer, T. Giordano, A.-M. Mes-Masson, F. Saad, T. Bocklage, L. Landrum, R. Mannel, K. Moore, K. Moxley, R. Postier, J. Walker, R. Zuna, M. Feldman, F. Valdivieso, R. Dhir, J. Luketich, E.M.M. Pinero, M. Quintero-Aguilo, C.G. Carlotti, J.S. Dos Santos, R. Kemp, A. Sankarankuty, D. Tirapelli, J. Catto, K. Agnew, E. Swisher, J. Creaney, B. Robinson, C.S. Shelley, E.M. Godwin, S. Kendall, C. Shipman, C. Bradford, T. Carey, A. Haddad, J. Moyer, L. Peterson, M. Prince, L. Rozek, G. Wolf, R. Bowman, K.M. Fong, I. Yang, R. Korst, W.K. Rathmell, J.L. Fantacone-Campbell, J.A. Hooke, A.J. Kovatich, C.D. Shriver, J. DiPersio, B. Drake, R. Govindan, S. Heath, T. Ley, B. Van Tine, P. Westervelt, M.A. Rubin, J.I. Lee, N.D. Aredes, A. Mariamidze, Comprehensive Characterization of Cancer Driver Genes and Mutations, Cell. 173 (2018) 371-385.e18. https://doi.org/10.1016/j.cell.2018.02.060.

[40] J.G. Tate, S. Bamford, H.C. Jubb, Z. Sondka, D.M. Beare, N. Bindal, H. Boutselakis, C.G. Cole, C. Creatore, E. Dawson, P. Fish, B. Harsha, C. Hathaway, S.C. Jupe, C.Y. Kok, K. Noble, L. Ponting, C.C. Ramshaw, C.E. Rye, H.E. Speedy, R. Stefancsik, S.L. Thompson, S. Wang, S. Ward, P.J. Campbell, S.A. Forbes, COSMIC: the Catalogue Of Somatic Mutations In Cancer, Nucleic Acids Res. 47 (2019) D941–D947. https://doi.org/10.1093/nar/gky1015.

[41] K.C. Kurek, V.L. Luks, U.M. Ayturk, A.I. Alomari, S.J. Fishman, S.A. Spencer, J.B. Mulliken, M.E. Bowen, G.L. Yamamoto, H.P.W. Kozakewich, M.L. Warman, Somatic Mosaic Activating Mutations in PIK3CA Cause CLOVES Syndrome, Am. J. Hum. Genet. 90 (2012) 1108–1115. https://doi.org/10.1016/j.ajhg.2012.05.006.

[42] M.J. Lindhurst, V.E.R. Parker, F. Payne, J.C. Sapp, S. Rudge, J. Harris, A.M. Witkowski, Q. Zhang, M.P. Groeneveld, C.E. Scott, A. Daly, S.M. Huson, L.L. Tosi, M.L. Cunningham, T.N. Darling, J. Geer, Z. Gucev, V.R. Sutton, C. Tziotzios, A.K. Dixon, T. Helliwell, S. O'Rahilly, D.B. Savage, M.J.O. Wakelam, I. Barroso, L.G. Biesecker, R.K. Semple, Mosaic overgrowth with fibroadipose

hyperplasia is caused by somatic activating mutations in PIK3CA, Nat. Genet. 44 (2012) 928–933. https://doi.org/10.1038/ng.2332.
[43] K.M. Keppler-Noreuil, J.J. Rios, V.E.R. Parker, R.K. Semple, M.J. Lindhurst, J.C. Sapp, A. Alomari, M. Ezaki, W. Dobyns, L.G. Biesecker, *PIK3CA* -related overgrowth spectrum (PROS): Diagnostic and testing eligibility criteria, differential diagnosis, and evaluation, Am. J. Med. Genet. A. 167 (2015) 287–295. https://doi.org/10.1002/ajmg.a.36836.
[44] S. Wee, D. Wiederschain, S.-M. Maira, A. Loo, C. Miller, R. deBeaumont, F. Stegmeier, Y.-M. Yao, C. Lengauer, PTEN-deficient cancers depend on PIK3CB, Proc. Natl. Acad. Sci. 105 (2008) 13057–13062. https://doi.org/10.1073/pnas.0802655105.
[45] M.E. Urick, M.L. Rudd, A.K. Godwin, D. Sgroi, M. Merino, D.W. Bell, *PIK3R1* (p85α) Is Somatically Mutated at High Frequency in Primary Endometrial Cancer, Cancer Res. 71 (2011) 4061–4067. https://doi.org/10.1158/0008-5472.CAN-11-0549.
[46] Finding of Rare Disease Genes (FORGE) Canada Consortium, J.-B. Rivière, G.M. Mirzaa, B.J. O'Roak, M. Beddaoui, D. Alcantara, R.L. Conway, J. St-Onge, J.A. Schwartzentruber, K.W. Gripp, S.M. Nikkel, T. Worthylake, C.T. Sullivan, T.R. Ward, H.E. Butler, N.A. Kramer, B. Albrecht, C.M. Armour, L. Armstrong, O. Caluseriu, C. Cytrynbaum, B.A. Drolet, A.M. Innes, J.L. Lauzon, A.E. Lin, G.M.S. Mancini, W.S. Meschino, J.D. Reggin, A.K. Saggar, T. Lerman-Sagie, G. Uyanik, R. Weksberg, B. Zirn, C.L. Beaulieu, J. Majewski, D.E. Bulman, M. O'Driscoll, J. Shendure, J.M. Graham, K.M. Boycott, W.B. Dobyns, De novo germline and postzygotic mutations in AKT3, PIK3R2 and PIK3CA cause a spectrum of related megalencephaly syndromes, Nat. Genet. 44 (2012) 934–940. https://doi.org/10.1038/ng.2331.
[47] L.W.T. Cheung, S. Yu, D. Zhang, J. Li, P.K.S. Ng, N. Panupinthu, S. Mitra, Z. Ju, Q. Yu, H. Liang, D.H. Hawke, Y. Lu, R.R. Broaddus, G.B. Mills, Naturally Occurring Neomorphic PIK3R1 Mutations Activate the MAPK Pathway, Dictating Therapeutic Response to MAPK Pathway Inhibitors, Cancer Cell. 26 (2014) 479–494. https://doi.org/10.1016/j.ccell.2014.08.017.
[48] C.L. Lucas, A. Chandra, S. Nejentsev, A.M. Condliffe, K. Okkenhaug, PI3Kδ and primary immunodeficiencies, Nat. Rev. Immunol. 16 (2016) 702–714. https://doi.org/10.1038/nri.2016.93.
[49] C.L. Lucas, Y. Zhang, A. Venida, Y. Wang, J. Hughes, J. McElwee, M. Butrick, H. Matthews, S. Price, M. Biancalana, X. Wang, M. Richards, T. Pozos, I. Barlan, A. Ozen, V.K. Rao, H.C. Su, M.J. Lenardo, Heterozygous splice mutation in PIK3R1 causes human immunodeficiency with lymphoproliferation due to dominant activation of PI3K, J. Exp. Med. 211 (2014) 2537–2547. https://doi.org/10.1084/jem.20141759.
[50] G.L. Dornan, B.D. Siempelkamp, M.L. Jenkins, O. Vadas, C.L. Lucas, J.E. Burke, Conformational disruption of PI3Kδ regulation by immunodeficiency mutations in *PIK3CD* and *PIK3R1*, Proc. Natl. Acad. Sci. 114 (2017) 1982–1987. https://doi.org/10.1073/pnas.1617244114.
[51] A. Fougerat, S. Gayral, P. Gourdy, A. Schambourg, T. Rückle, M.K. Schwarz, C. Rommel, E. Hirsch, J.-F. Arnal, J.-P. Salles, B. Perret, M. Breton-Douillon, M.P. Wymann, M. Laffargue, Genetic and Pharmacological Targeting of Phosphoinositide 3-Kinase-γ Reduces Atherosclerosis and Favors Plaque Stability by Modulating Inflammatory Processes, Circulation. 117 (2008) 1310–1317. https://doi.org/10.1161/CIRCULATIONAHA.107.720466.
[52] A.W. Ferrante, Obesity-induced inflammation: a metabolic dialogue in the language of inflammation, J. Intern. Med. 262 (2007) 408–414. https://doi.org/10.1111/j.1365-2796.2007.01852.x.
[53] E. Collmann, T. Bohnacker, R. Marone, J. Dawson, M. Rehberg, R. Stringer, F. Krombach, C. Burkhart, E. Hirsch, G.J. Hollingworth, M. Thomas, M.P. Wymann, Transient targeting of phosphoinositide 3-kinase acts as a roadblock in mast cells' route to allergy, J. Allergy Clin. Immunol. 132 (2013) 959–968. https://doi.org/10.1016/j.jaci.2013.03.008.

[54] B. Nürnberg, S. Beer-Hammer, Function, Regulation and Biological Roles of PI3Kγ Variants, Biomolecules. 9 (2019) 427. https://doi.org/10.3390/biom9090427.
[55] B.D. Hopkins, C. Pauli, X. Du, D.G. Wang, X. Li, D. Wu, S.C. Amadiume, M.D. Goncalves, C. Hodakoski, M.R. Lundquist, R. Bareja, Y. Ma, E.M. Harris, A. Sboner, H. Beltran, M.A. Rubin, S. Mukherjee, L.C. Cantley, Suppression of insulin feedback enhances the efficacy of PI3K inhibitors, Nature. 560 (2018) 499–503. https://doi.org/10.1038/s41586-018-0343-4.
[56] M.M. Kaneda, K.S. Messer, N. Ralainirina, H. Li, C.J. Leem, S. Gorjestani, G. Woo, A.V. Nguyen, C.C. Figueiredo, P. Foubert, M.C. Schmid, M. Pink, D.G. Winkler, M. Rausch, V.J. Palombella, J. Kutok, K. McGovern, K.A. Frazer, X. Wu, M. Karin, R. Sasik, E.E.W. Cohen, J.A. Varner, PI3Kγ is a molecular switch that controls immune suppression, Nature. 539 (2016) 437–442. https://doi.org/10.1038/nature19834.
[57] J. Godfrey, W. Kang, L. Huang, S. Coma, R. Maute, M.P. Chao, J.A. Pachter, S. Smith, J. Kline, Macrophage Activation By Dual PI3K-δ/γ Inhibition Enhances Anti-CD47-Mediated Phagocytosis and Prolongs Survival in DLBCL, Blood. 136 (2020) 40–40. https://doi.org/10.1182/blood-2020-143304.
[58] K.W. Song, K.A. Edgar, E.J. Hanan, M. Hafner, J. Oeh, M. Merchant, D. Sampath, M.A. Nannini, R. Hong, L. Phu, W.F. Forrest, E. Stawiski, S. Schmidt, N. Endres, J. Guan, J.J. Wallin, J. Cheong, E.G. Plise, G.D. Lewis Phillips, L. Salphati, T.P. Heffron, A.G. Olivero, S. Malek, S.T. Staben, D.S. Kirkpatrick, A. Dey, L.S. Friedman, RTK-Dependent Inducible Degradation of Mutant PI3Ka Drives GDC-0077 (Inavolisib) Efficacy, Cancer Discov. (2021). https://doi.org/10.1158/2159-8290.CD-21-0072.
[59] A.J. Takeda, T.J. Maher, Y. Zhang, S.M. Lanahan, M.L. Bucklin, S.R. Compton, P.M. Tyler, W.A. Comrie, M. Matsuda, K.N. Olivier, S. Pittaluga, J.J. McElwee, D.A. Long Priel, D.B. Kuhns, R.L. Williams, P.J. Mustillo, M.P. Wymann, V. Koneti Rao, C.L. Lucas, Human PI3Kγ deficiency and its microbiota-dependent mouse model reveal immunodeficiency and tissue immunopathology, Nat. Commun. 10 (2019) 4364. https://doi.org/10.1038/s41467-019-12311-5.
[60] Marini Thian, Birgit Hoeger, Anton Kamnev, Fiona Poyer, Sevgi Köstel Bal, Michael Caldera, Raúl Jiménez-Heredia, Jakob Huemer, Winfried F. Pickl, Miriam Groß, Stephan Ehl, Carrie L. Lucas, Jörg Menche, Caroline Hutter, Andishe Attarbaschi, Loïc Dupré, Kaan Boztug, Germline biallelic PIK3CG mutations in a multifaceted immunodeficiency with immune dysregulation, Haematologica. 105 (2020) e488. https://doi.org/10.3324/haematol.2019.231399.
[61] Y. Samuels, Z. Wang, A. Bardelli, N. Silliman, J. Ptak, S. Szabo, H. Yan, A. Gazdar, S. Powell, G. Riggins, J. Willson, S. Markowitz, K. Kinzler, B. Vogelstein, V. Velculescu, High frequency of mutations of the PIK3CA gene in human cancers., Science. 304 (2004) 554. https://doi.org/10.1126/science.1096502.
[62] M.S. Lawrence, P. Stojanov, C.H. Mermel, J.T. Robinson, L.A. Garraway, T.R. Golub, M. Meyerson, S.B. Gabriel, E.S. Lander, G. Getz, Discovery and saturation analysis of cancer genes across 21 tumour types, Nature. 505 (2014) 495–501. https://doi.org/10.1038/nature12912.
[63] M.H. Bailey, C. Tokheim, E. Porta-Pardo, S. Sengupta, D. Bertrand, A. Weerasinghe, A. Colaprico, M.C. Wendl, J. Kim, B. Reardon, P.K.-S. Ng, K.J. Jeong, S. Cao, Z. Wang, J. Gao, Q. Gao, F. Wang, E.M. Liu, L. Mularoni, C. Rubio-Perez, N. Nagarajan, I. Cortés-Ciriano, D.C. Zhou, W.-W. Liang, J.M. Hess, V.D. Yellapantula, D. Tamborero, A. Gonzalez-Perez, C. Suphavilai, J.Y. Ko, E. Khurana, P.J. Park, E.M. Van Allen, H. Liang, MC3 Working Group, Cancer Genome Atlas Research Network, M.S. Lawrence, A. Godzik, N. Lopez-Bigas, J. Stuart, D. Wheeler, G. Getz, K. Chen, A.J. Lazar, G.B. Mills, R. Karchin, L. Ding, Comprehensive Characterization of Cancer Driver Genes and Mutations., Cell. 173 (2018) 371-385.e18. https://doi.org/10.1016/j.cell.2018.02.060.
[64] M.D. Goncalves, B.D. Hopkins, L.C. Cantley, Phosphatidylinositol 3-Kinase, Growth Disorders, and Cancer, N. Engl. J. Med. 379 (2018) 2052–2062. https://doi.org/10.1056/NEJMra1704560.

[65] J.E. Burke, Structural Basis for Regulation of Phosphoinositide Kinases and Their Involvement in Human Disease., Mol. Cell. 71 (2018) 653–673. https://doi.org/10.1016/j.molcel.2018.08.005.
[66] J.E. Burke, R.L. Williams, Synergy in activating class I PI3Ks., Trends Biochem. Sci. 40 (2015) 88–100. https://doi.org/10.1016/j.tibs.2014.12.003.
[67] R.R. Madsen, B. Vanhaesebroeck, Cracking the context-specific PI3K signaling code., Sci. Signal. 13 (2020) eaay2940. https://doi.org/10.1126/scisignal.aay2940.
[68] J. Yu, Y. Zhang, J. McIlroy, T. Rordorf-Nikolic, G.A. Orr, J.M. Backer, Regulation of the p85/p110 phosphatidylinositol 3'-kinase: stabilization and inhibition of the p110alpha catalytic subunit by the p85 regulatory subunit., Mol Cell Biol. 18 (1998) 1379–1387.
[69] J. Yu, C. Wjasow, J.M. Backer, Regulation of the p85/p110alpha phosphatidylinositol 3'-kinase. Distinct roles for the n-terminal and c-terminal SH2 domains, J. Biol. Chem. 273 (1998) 30199–30203. https://doi.org/10.1074/jbc.273.46.30199.
[70] C.L. Carpenter, K.R. Auger, M. Chanudhuri, M. Yoakim, B. Schaffhausen, S. Shoelson, L.C. Cantley, Phosphoinositide 3-kinase is activated by phosphopeptides that bind to the SH2 domains of the 85-kDa subunit, J. Biol. Chem. 268 (1993) 9478–9483.
[71] G.L. Dornan, J.T.B. Stariha, M.K. Rathinaswamy, C.J. Powell, M.J. Boulanger, J.E. Burke, Defining How Oncogenic and Developmental Mutations of PIK3R1 Alter the Regulation of Class IA Phosphoinositide 3-Kinases., Struct. Lond. Engl. 1993. 28 (2020) 145-156.e5. https://doi.org/10.1016/j.str.2019.11.013.
[72] B.D. Siempelkamp, M.K. Rathinaswamy, M.L. Jenkins, J.E. Burke, Molecular mechanism of activation of class IA phosphoinositide 3-kinases (PI3Ks) by membrane-localized HRas., J. Biol. Chem. 292 (2017) 12256–12266. https://doi.org/10.1074/jbc.M117.789263.
[73] T.C. Buckles, B.P. Ziemba, G.R. Masson, R.L. Williams, J.J. Falke, Single-Molecule Study Reveals How Receptor and Ras Synergistically Activate PI3Kα and PIP3 Signaling., Biophys J. 113 (2017) 2396–2405. https://doi.org/10.1016/j.bpj.2017.09.018.
[74] C.-H. Huang, D. Mandelker, O. Schmidt-Kittler, Y. Samuels, V.E. Velculescu, K.W. Kinzler, B. Vogelstein, S.B. Gabelli, L.M. Amzel, The structure of a human p110alpha/p85alpha complex elucidates the effects of oncogenic PI3Kalpha mutations, Science. 318 (2007) 1744–1748. https://doi.org/10.1126/science.1150799.
[75] N. Miled, Y. Yan, W.-C. Hon, O. Perisic, M. Zvelebil, Y. Inbar, D. Schneidman-Duhovny, H.J. Wolfson, J.M. Backer, R.L. Williams, Mechanism of two classes of cancer mutations in the phosphoinositide 3-kinase catalytic subunit., Science. 317 (2007) 239–242. https://doi.org/10.1126/science.1135394.
[76] J.E. Burke, O. Perisic, G.R. Masson, O. Vadas, R.L. Williams, Oncogenic mutations mimic and enhance dynamic events in the natural activation of phosphoinositide 3-kinase p110α (PIK3CA)., Proc. Natl. Acad. Sci. U. S. A. 109 (2012) 15259–15264. https://doi.org/10.1073/pnas.1205508109.
[77] D. Mandelker, S.B. Gabelli, O. Schmidt-Kittler, J. Zhu, I. Cheong, C.-H. Huang, K.W. Kinzler, B. Vogelstein, L.M. Amzel, A frequent kinase domain mutation that changes the interaction between PI3Kalpha and the membrane., Proc Natl Acad Sci USA. 106 (2009) 16996–17001. https://doi.org/10.1073/pnas.0908444106.
[78] M. Chakrabarti, S.B. Gabelli, L.M. Amzel, Allosteric Activation of PI3Kα Results in Dynamic Access to Catalytically Competent Conformations, Struct. Lond. Engl. 1993. 28 (2020) 465-474.e5. https://doi.org/10.1016/j.str.2020.01.010.
[79] J.E. Burke, R.L. Williams, Dynamic steps in receptor tyrosine kinase mediated activation of class IA phosphoinositide 3-kinases (PI3K) captured by H/D exchange (HDX-MS)., Adv. Biol. Regul. 53 (2013) 97–110. https://doi.org/10.1016/j.jbior.2012.09.005.

[80] P. Gkeka, T. Evangelidis, M. Pavlaki, V. Lazani, S. Christoforidis, B. Agianian, Z. Cournia, Investigating the structure and dynamics of the PIK3CA wild-type and H1047R oncogenic mutant., PLoS Comput Biol. 10 (2014) e1003895. https://doi.org/10.1371/journal.pcbi.1003895.
[81] E.H. Walker, O. Perisic, C. Ried, L. Stephens, R.L. Williams, Structural insights into phosphoinositide 3-kinase catalysis and signalling., Nature. 402 (1999) 313–320. https://doi.org/10.1038/46319.
[82] K. Rostislavleva, N. Soler, Y. Ohashi, L. Zhang, E. Pardon, J.E. Burke, G.R. Masson, C. Johnson, J. Steyaert, N.T. Ktistakis, R.L. Williams, Structure and flexibility of the endosomal Vps34 complex reveals the basis of its function on membranes., Science. 350 (2015) aac7365. https://doi.org/10.1126/science.aac7365.
[83] M.K. Rathinaswamy, U. Dalwadi, K.D. Fleming, C. Adams, J.T.B. Stariha, E. Pardon, M. Baek, O. Vadas, F. DiMaio, J. Steyaert, S.D. Hansen, C.K. Yip, J.E. Burke, Structure of the phosphoinositide 3-kinase (PI3K) p110γ-p101 complex reveals molecular mechanism of GPCR activation, Sci. Adv. 7 (2021) eabj4282. https://doi.org/10.1126/sciadv.abj4282.
[84] H. Wu, S.C. Shekar, R.J. Flinn, M. El-Sibai, B.S. Jaiswal, K.I. Sen, V. Janakiraman, S. Seshagiri, G.J. Gerfen, M.E. Girvin, J.M. Backer, Regulation of Class IA PI 3-kinases: C2 domain-iSH2 domain contacts inhibit p85/p110alpha and are disrupted in oncogenic p85 mutants., Proc. Natl. Acad. Sci. U. S. A. 106 (2009) 20258–20263. https://doi.org/10.1073/pnas.0902369106.
[85] J.E. Burke, O. Vadas, A. Berndt, T. Finegan, O. Perisic, R.L. Williams, Dynamics of the phosphoinositide 3-kinase p110δ interaction with p85α and membranes reveals aspects of regulation distinct from p110α, Struct. Lond. Engl. 1993. 19 (2011) 1127–1137. https://doi.org/10.1016/j.str.2011.06.003.
[86] X. Zhang, O. Vadas, O. Perisic, K.E. Anderson, J. Clark, P.T. Hawkins, L.R. Stephens, R.L. Williams, Structure of lipid kinase p110β/p85β elucidates an unusual SH2-domain-mediated inhibitory mechanism, Mol. Cell. 41 (2011) 567–578. https://doi.org/10.1016/j.molcel.2011.01.026.
[87] X. Liu, S. Yang, J.R. Hart, Y. Xu, X. Zou, H. Zhang, Q. Zhou, T. Xia, Y. Zhang, D. Yang, M.-W. Wang, P.K. Vogt, Cryo-EM structures of PI3Kα reveal conformational changes during inhibition and activation, Proc. Natl. Acad. Sci. U. S. A. 118 (2021) e2109327118. https://doi.org/10.1073/pnas.2109327118.
[88] B.S. Jaiswal, V. Janakiraman, N.M. Kljavin, S. Chaudhuri, H.M. Stern, W. Wang, Z. Kan, H.A. Dbouk, B.A. Peters, P. Waring, T. Dela Vega, D.M. Kenski, K.K. Bowman, M. Lorenzo, H. Li, J. Wu, Z. Modrusan, J. Stinson, M. Eby, P. Yue, J.S. Kaminker, F.J. de Sauvage, J.M. Backer, S. Seshagiri, Somatic Mutations in p85α Promote Tumorigenesis through Class IA PI3K Activation, Cancer Cell. 16 (2009) 463–474. https://doi.org/10.1016/j.ccr.2009.10.016.
[89] G.L. Dornan, J.E. Burke, Molecular Mechanisms of Human Disease Mediated by Oncogenic and Primary Immunodeficiency Mutations in Class IA Phosphoinositide 3-Kinases., Front. Immunol. 9 (2018) 575. https://doi.org/10.3389/fimmu.2018.00575.
[90] J.M. Spangle, T. Von, D.C. Pavlick, A. Khotimsky, J.J. Zhao, T.M. Roberts, PIK3CA C-terminal frameshift mutations are novel oncogenic events that sensitize tumors to PI3K-α inhibition, Proc. Natl. Acad. Sci. U. S. A. 117 (2020) 24427–24433. https://doi.org/10.1073/pnas.2000060117.
[91] M. Sun, P. Hillmann, B.T. Hofmann, J.R. Hart, P.K. Vogt, Cancer-derived mutations in the regulatory subunit p85 of phosphoinositide 3-kinase function through the catalytic subunit p110, Proc. Natl. Acad. Sci. 107 (2010) 15547–15552. https://doi.org/10.1073/pnas.1009652107.
[92] M.K. Rathinaswamy, Z. Gaieb, K.D. Fleming, C. Borsari, N.J. Harris, B.E. Moeller, M.P. Wymann, R.E. Amaro, J.E. Burke, Disease-related mutations in PI3Kγ disrupt regulatory C-terminal dynamics and reveal a path to selective inhibitors, ELife. 10 (2021) e64691. https://doi.org/10.7554/eLife.64691.

[93] N. Vasan, P. Razavi, J.L. Johnson, H. Shao, H. Shah, A. Antoine, E. Ladewig, A. Gorelick, T.-Y. Lin, E. Toska, G. Xu, A. Kazmi, M.T. Chang, B.S. Taylor, M.N. Dickler, K. Jhaveri, S. Chandarlapaty, R. Rabadan, E. Reznik, M.L. Smith, R. Sebra, F. Schimmoller, T.R. Wilson, L.S. Friedman, L.C. Cantley, M. Scaltriti, J. Baselga, Double PIK3CA mutations in cis increase oncogenicity and sensitivity to PI3Kα inhibitors., Science. 366 (2019) 714–723. https://doi.org/10.1126/science.aaw9032.

[94] M.S. Miller, O. Schmidt-Kittler, D.M. Bolduc, E.T. Brower, D. Chaves-Moreira, M. Allaire, K.W. Kinzler, I.G. Jennings, P.E. Thompson, P.A. Cole, L.M. Amzel, B. Vogelstein, S.B. Gabelli, Structural basis of nSH2 regulation and lipid binding in PI3Kα., Oncotarget. 5 (2014) 5198–5208. https://doi.org/10.18632/oncotarget.2263.

[95] J.G. Tate, S. Bamford, H.C. Jubb, Z. Sondka, D.M. Beare, N. Bindal, H. Boutselakis, C.G. Cole, C. Creatore, E. Dawson, P. Fish, B. Harsha, C. Hathaway, S.C. Jupe, C.Y. Kok, K. Noble, L. Ponting, C.C. Ramshaw, C.E. Rye, H.E. Speedy, R. Stefancsik, S.L. Thompson, S. Wang, S. Ward, P.J. Campbell, S.A. Forbes, COSMIC: the Catalogue Of Somatic Mutations In Cancer., Nucleic Acids Res. 47 (2019) D941–D947. https://doi.org/10.1093/nar/gky1015.

[96] W.C. Hon, A. Berndt, R.L. Williams, Regulation of lipid binding underlies the activation mechanism of class IA PI3-kinases., Oncogene. 31 (2012) 3655–3666. https://doi.org/10.1038/onc.2011.532.

[97] J.M. Dobbs, M.L. Jenkins, J.E. Burke, Escherichia coli and Sf9 Contaminant Databases to Increase Efficiency of Tandem Mass Spectrometry Peptide Identification in Structural Mass Spectrometry Experiments, J. Am. Soc. Mass Spectrom. 31 (2020) 2202–2209. https://doi.org/10.1021/jasms.0c00283.

[98] Y. Perez-Riverol, A. Csordas, J. Bai, M. Bernal-Llinares, S. Hewapathirana, D.J. Kundu, A. Inuganti, J. Griss, G. Mayer, M. Eisenacher, E. Pérez, J. Uszkoreit, J. Pfeuffer, T. Sachsenberg, S. Yilmaz, S. Tiwary, J. Cox, E. Audain, M. Walzer, A.F. Jarnuczak, T. Ternent, A. Brazma, J.A. Vizcaíno, The PRIDE database and related tools and resources in 2019: improving support for quantification data., Nucleic Acids Res. 47 (2019) D442–D450. https://doi.org/10.1093/nar/gky1106.

[99] M.J. Fry, G. Panayotou, R. Dhand, F. Ruiz-Larrea, I. Gout, O. Nguyen, S.A. Courtneidge, M.D. Waterfield, Purification and characterization of a phosphatidylinositol 3-kinase complex from bovine brain by using phosphopeptide affinity columns, Biochem. J. 288 (1992) 383–393. https://doi.org/10.1042/bj2880383.

[100] P. Furet, V. Guagnano, R.A. Fairhurst, P. Imbach-Weese, I. Bruce, M. Knapp, C. Fritsch, F. Blasco, J. Blanz, R. Aichholz, J. Hamon, D. Fabbro, G. Caravatti, Discovery of NVP-BYL719 a potent and selective phosphatidylinositol-3 kinase alpha inhibitor selected for clinical evaluation., Bioorg. Med. Chem. Lett. 23 (2013) 3741–3748. https://doi.org/10.1016/j.bmcl.2013.05.007.

[101] P.A. Barsanti, R.J. Aversa, X. Jin, Y. Pan, Y. Lu, R. Elling, R. Jain, M. Knapp, J. Lan, X. Lin, P. Rudewicz, J. Sim, L. Taricani, G. Thomas, L. Xiao, Q. Yue, Structure-Based Drug Design of Novel Potent and Selective Tetrahydropyrazolo[1,5-a]pyrazines as ATR Inhibitors, ACS Med. Chem. Lett. 6 (2015) 37–41. https://doi.org/10.1021/ml500353p.

[102] W. Han, D.L. Menezes, Y. Xu, M.S. Knapp, R. Elling, M.T. Burger, Z.-J. Ni, A. Smith, J. Lan, T.E. Williams, J. Verhagen, K. Huh, H. Merritt, J. Chan, S. Kaufman, C.F. Voliva, S. Pecchi, Discovery of imidazo[1,2-a]-pyridine inhibitors of pan-PI3 kinases that are efficacious in a mouse xenograft model, Bioorg. Med. Chem. Lett. 26 (2016) 742–746. https://doi.org/10.1016/j.bmcl.2016.01.003.

[103] D.A. Fruman, H. Chiu, B.D. Hopkins, S. Bagrodia, L.C. Cantley, R.T. Abraham, The PI3K Pathway in Human Disease., Cell. 170 (2017) 605–635. https://doi.org/10.1016/j.cell.2017.07.029.

[104] S.-Y. Sun, L.M. Rosenberg, X. Wang, Z. Zhou, P. Yue, H. Fu, F.R. Khuri, Activation of Akt and eIF4E survival pathways by rapamycin-mediated mammalian target of rapamycin inhibition, Cancer Res. 65 (2005) 7052–7058. https://doi.org/10.1158/0008-5472.CAN-05-0917.

[105] A. Chakrabarty, V. Sánchez, M.G. Kuba, C. Rinehart, C.L. Arteaga, Feedback upregulation of HER3 (ErbB3) expression and activity attenuates antitumor effect of PI3K inhibitors, Proc. Natl. Acad. Sci. U. S. A. 109 (2012) 2718–2723. https://doi.org/10.1073/pnas.1018001108.
[106] B.D. Hopkins, C. Pauli, X. Du, D.G. Wang, X. Li, D. Wu, S.C. Amadiume, M.D. Goncalves, C. Hodakoski, M.R. Lundquist, R. Bareja, Y. Ma, E.M. Harris, A. Sboner, H. Beltran, M.A. Rubin, S. Mukherjee, L.C. Cantley, Suppression of insulin feedback enhances the efficacy of PI3K inhibitors., Nature. 560 (2018) 499–503. https://doi.org/10.1038/s41586-018-0343-4.
[107] L. Zhao, P. Vogt, Helical domain and kinase domain mutations in p110alpha of phosphatidylinositol 3-kinase induce gain of function by different mechanisms., Proc. Natl. Acad. Sci. U. S. A. 105 (2008) 2652–2657. https://doi.org/10.1073/pnas.0712169105.
[108] M. Gymnopoulos, M.-A. Elsliger, P.K. Vogt, Rare cancer-specific mutations in PIK3CA show gain of function., Proc. Natl. Acad. Sci. U. S. A. 104 (2007) 5569–5574. https://doi.org/10.1073/pnas.0701005104.
[109] C. Huang, D. Mandelker, O. Schmidt-Kittler, Y. Samuels, V. Velculescu, K. Kinzler, B. Vogelstein, S. Gabelli, L. Amzel, The structure of a human p110alpha/p85alpha complex elucidates the effects of oncogenic PI3Kalpha mutations., Science. 318 (2007) 1744–1748. https://doi.org/10.1126/science.1150799.
[110] H.A. Dbouk, O. Vadas, A. Shymanets, J.E. Burke, R.S. Salamon, B.D. Khalil, M.O. Barrett, G.L. Waldo, C. Surve, C. Hsueh, O. Perisic, C. Harteneck, P.R. Shepherd, T.K. Harden, A.V. Smrcka, R. Taussig, A.R. Bresnick, B. Nürnberg, R.L. Williams, J.M. Backer, G protein-coupled receptor-mediated activation of p110β by Gβγ is required for cellular transformation and invasiveness., Sci. Signal. 5 (2012) ra89–ra89. https://doi.org/10.1126/scisignal.2003264.
[111] G.L. Dornan, B.D. Siempelkamp, M.L. Jenkins, O. Vadas, C.L. Lucas, J.E. Burke, Conformational disruption of PI3Kδ regulation by immunodeficiency mutations in PIK3CD and PIK3R1., Proc Natl Acad Sci USA. 114 (2017) 1982–1987. https://doi.org/10.1073/pnas.1617244114.
[112] A.J. Takeda, Y. Zhang, G.L. Dornan, B.D. Siempelkamp, M.L. Jenkins, H.F. Matthews, J.J. McElwee, W. Bi, F.O. Seeborg, H.C. Su, J.E. Burke, C.L. Lucas, Novel PIK3CD mutations affecting N-terminal residues of p110δ cause activated PI3Kδ syndrome (APDS) in humans., J. Allergy Clin. Immunol. 140 (2017) 1152-1156.e10. https://doi.org/10.1016/j.jaci.2017.03.026.
[113] J. Vallejo-Díaz, M. Chagoyen, M. Olazabal-Morán, A. González-García, A.C. Carrera, The Opposing Roles of PIK3R1/p85α and PIK3R2/p85β in Cancer, Trends Cancer. 5 (2019) 233–244. https://doi.org/10.1016/j.trecan.2019.02.009.
[114] X. Zhang, O. Vadas, O. Perisic, K.E. Anderson, J. Clark, P.T. Hawkins, L.R. Stephens, R.L. Williams, Structure of lipid kinase p110β/p85β elucidates an unusual SH2-domain-mediated inhibitory mechanism, Mol. Cell. 41 (2011) 567–578. https://doi.org/10.1016/j.molcel.2011.01.026.
[115] M. Zhang, H. Jang, R. Nussinov, Structural Features that Distinguish Inactive and Active PI3K Lipid Kinases, J. Mol. Biol. 432 (2020) 5849–5859. https://doi.org/10.1016/j.jmb.2020.09.002.
[116] J.D. Carson, G. Van Aller, R. Lehr, R.H. Sinnamon, R.B. Kirkpatrick, K.R. Auger, D. Dhanak, R.A. Copeland, R.R. Gontarek, P.J. Tummino, L. Luo, Effects of oncogenic p110alpha subunit mutations on the lipid kinase activity of phosphoinositide 3-kinase., Biochem. J. 409 (2008) 519–524. https://doi.org/10.1042/BJ20070681.
[117] D.L. Swaney, D.J. Ramms, Z. Wang, J. Park, Y. Goto, M. Soucheray, N. Bhola, K. Kim, F. Zheng, Y. Zeng, M. McGregor, K.A. Herrington, R. O'Keefe, N. Jin, N.K. VanLandingham, H. Foussard, J. Von Dollen, M. Bouhaddou, D. Jimenez-Morales, K. Obernier, J.F. Kreisberg, M. Kim, D.E. Johnson, N. Jura, J.R. Grandis, J.S. Gutkind, T. Ideker, N.J. Krogan, A protein network map of head and neck cancer reveals PIK3CA mutant drug sensitivity, Science. 374 (2021) eabf2911. https://doi.org/10.1126/science.abf2911.

[118] K. Okkenhaug, Signaling by the Phosphoinositide 3-Kinase Family in Immune Cells, Annu. Rev. Immunol. 31 (2013) 675–704. https://doi.org/10.1146/annurev-immunol-032712-095946.
[119] D.F. Barber, A. Bartolomé, C. Hernandez, J.M. Flores, C. Redondo, C. Fernandez-Arias, M. Camps, T. Rückle, M.K. Schwarz, S. Rodríguez, C. Martinez-A, D. Balomenos, C. Rommel, A.C. Carrera, PI3Kγ inhibition blocks glomerulonephritis and extends lifespan in a mouse model of systemic lupus, Nat. Med. 11 (2005) 933–935. https://doi.org/10.1038/nm1291.
[120] E. Patrucco, A. Notte, L. Barberis, G. Selvetella, A. Maffei, M. Brancaccio, S. Marengo, G. Russo, O. Azzolino, S.D. Rybalkin, L. Silengo, F. Altruda, R. Wetzker, M.P. Wymann, G. Lembo, E. Hirsch, PI3Kγ Modulates the Cardiac Response to Chronic Pressure Overload by Distinct Kinase-Dependent and -Independent Effects, Cell. 118 (2004) 375–387. https://doi.org/10.1016/j.cell.2004.07.017.
[121] O. De Henau, M. Rausch, D. Winkler, L.F. Campesato, C. Liu, D.H. Cymerman, S. Budhu, A. Ghosh, M. Pink, J. Tchaicha, M. Douglas, T. Tibbitts, S. Sharma, J. Proctor, N. Kosmider, K. White, H. Stern, J. Soglia, J. Adams, V.J. Palombella, K. McGovern, J.L. Kutok, J.D. Wolchok, T. Merghoub, Overcoming resistance to checkpoint blockade therapy by targeting PI3Kγ in myeloid cells, Nature. 539 (2016) 443–447. https://doi.org/10.1038/nature20554.
[122] X. Wang, G. Luo, K. Zhang, J. Cao, C. Huang, T. Jiang, B. Liu, L. Su, Z. Qiu, Hypoxic Tumor-Derived Exosomal miR-301a Mediates M2 Macrophage Polarization via PTEN/PI3Kγ to Promote Pancreatic Cancer Metastasis, Cancer Res. 78 (2018) 4586–4598. https://doi.org/10.1158/0008-5472.CAN-17-3841.
[123] T. Kozasa, Purification of G protein subunits from Sf9 insect cells using hexahistidine-tagged alpha and beta gamma subunits, Methods Mol. Biol. Clifton NJ. 237 (2004) 21–38. https://doi.org/10.1385/1-59259-430-1:21.
[124] H. Ranga-Prasad, M.L. Jenkins, M.A. Parson, M.K. Rathinaswamy, J.E. Burke, Oncogenic mutations of *PIK3CA* lead to increased membrane recruitment driven by reorientation of the ABD, p85 and C-terminus, Biochemistry, 2022. https://doi.org/10.1101/2022.04.05.487205.
[125] O. Vadas, H.A. Dbouk, A. Shymanets, O. Perisic, J.E. Burke, W.F. Abi Saab, B.D. Khalil, C. Harteneck, A.R. Bresnick, B. Nürnberg, J.M. Backer, R.L. Williams, Molecular determinants of PI3Kγ-mediated activation downstream of G-protein–coupled receptors (GPCRs), Proc. Natl. Acad. Sci. 110 (2013) 18862–18867. https://doi.org/10.1073/pnas.1304801110.
[126] M.K. Rathinaswamy, K.D. Fleming, U. Dalwadi, E. Pardon, N.J. Harris, C.K. Yip, J. Steyaert, J.E. Burke, HDX-MS-optimized approach to characterize nanobodies as tools for biochemical and structural studies of class IB phosphoinositide 3-kinases, Struct. Lond. Engl. 1993. 29 (2021) 1371-1381.e6. https://doi.org/10.1016/j.str.2021.07.002.
[127] L.Y. Li, H.J. Kim, S.A. Park, S.H. Lee, L.K. Kim, J.Y. Lee, S. Kim, Y.T. Kim, S.W. Kim, E.J. Nam, Genetic Profiles Associated with Chemoresistance in Patient-Derived Xenograft Models of Ovarian Cancer, Cancer Res. Treat. 51 (2019) 1117–1127. https://doi.org/10.4143/crt.2018.405.
[128] C. Johnson, S.J. Marriott, L.S. Levy, Overexpression of p101 activates PI3Kγ signaling in T cells and contributes to cell survival, Oncogene. 26 (2007) 7049–7057. https://doi.org/10.1038/sj.onc.1210504.
[129] S. Kang, A. Denley, B. Vanhaesebroeck, P.K. Vogt, Oncogenic transformation induced by the p110β, -γ, and -δ isoforms of class I phosphoinositide 3-kinase, Proc. Natl. Acad. Sci. 103 (2006) 1289–1294. https://doi.org/10.1073/pnas.0510772103.
[130] METABRIC Group, C. Curtis, S.P. Shah, S.-F. Chin, G. Turashvili, O.M. Rueda, M.J. Dunning, D. Speed, A.G. Lynch, S. Samarajiwa, Y. Yuan, S. Gräf, G. Ha, G. Haffari, A. Bashashati, R. Russell, S. McKinney, A. Langerød, A. Green, E. Provenzano, G. Wishart, S. Pinder, P. Watson, F. Markowetz, L. Murphy, I. Ellis, A. Purushotham, A.-L. Børresen-Dale, J.D. Brenton, S. Tavaré, C. Caldas, S.

Aparicio, The genomic and transcriptomic architecture of 2,000 breast tumours reveals novel subgroups, Nature. 486 (2012) 346–352. https://doi.org/10.1038/nature10983.
[131] P. Furet, V. Guagnano, R.A. Fairhurst, P. Imbach-Weese, I. Bruce, M. Knapp, C. Fritsch, F. Blasco, J. Blanz, R. Aichholz, J. Hamon, D. Fabbro, G. Caravatti, Discovery of NVP-BYL719 a potent and selective phosphatidylinositol-3 kinase alpha inhibitor selected for clinical evaluation, Bioorg. Med. Chem. Lett. 23 (2013) 3741–3748. https://doi.org/10.1016/j.bmcl.2013.05.007.
[132] X. Liu, S. Yang, J.R. Hart, Y. Xu, X. Zou, H. Zhang, Q. Zhou, T. Xia, Y. Zhang, D. Yang, M.-W. Wang, P.K. Vogt, Cryo-EM structures of PI3Kα reveal conformational changes during inhibition and activation, Proc. Natl. Acad. Sci. 118 (2021) e2109327118. https://doi.org/10.1073/pnas.2109327118.
[133] M.K. Rathinaswamy, Z. Gaieb, K.D. Fleming, C. Borsari, N.J. Harris, B.E. Moeller, M.P. Wymann, R.E. Amaro, J.E. Burke, Disease-related mutations in PI3Kγ disrupt regulatory C-terminal dynamics and reveal a path to selective inhibitors, ELife. 10 (2021) e64691. https://doi.org/10.7554/eLife.64691.
[134] I. Cortés, J. Sánchez-Ruíz, S. Zuluaga, V. Calvanese, M. Marqués, C. Hernández, T. Rivera, L. Kremer, A. González-García, A.C. Carrera, p85β phosphoinositide 3-kinase subunit regulates tumor progression, Proc. Natl. Acad. Sci. 109 (2012) 11318–11323. https://doi.org/10.1073/pnas.1118138109.
[135] Y. Ito, P.K. Vogt, J.R. Hart, Domain analysis reveals striking functional differences between the regulatory subunits of phosphatidylinositol 3-kinase (PI3K), p85α and p85β, Oncotarget. 8 (2017) 55863–55876. https://doi.org/10.18632/oncotarget.19866.
[136] J. Luo, S.J. Field, J.Y. Lee, J.A. Engelman, L.C. Cantley, The p85 regulatory subunit of phosphoinositide 3-kinase down-regulates IRS-1 signaling via the formation of a sequestration complex, J. Cell Biol. 170 (2005) 455–464. https://doi.org/10.1083/jcb.200503088.
[137] T. Bohnacker, R. Marone, E. Collmann, R. Calvez, E. Hirsch, M.P. Wymann, PI3Kγ Adaptor Subunits Define Coupling to Degranulation and Cell Motility by Distinct PtdIns(3,4,5)P_3 Pools in Mast Cells, Sci. Signal. 2 (2009). https://doi.org/10.1126/scisignal.2000259.
[138] J.R. Hart, X. Liu, C. Pan, A. Liang, L. Ueno, Y. Xu, A. Quezada, X. Zou, S. Yang, Q. Zhou, S. Schoonooghe, G. Hassanzadeh-Ghassabeh, T. Xia, W. Shui, D. Yang, P.K. Vogt, M.-W. Wang, Nanobodies and chemical cross-links advance the structural and functional analysis of PI3Kα, Proc. Natl. Acad. Sci. 119 (2022) e2210769119. https://doi.org/10.1073/pnas.2210769119.

Table 1- HDX-MS processing details

Experiment	Comparing WT PI3K and p110α core. HDX Stats table for data shown in Figure 2.2 and Figure 2.3.		
Data set	WT	p110α core	p110α core + Memb
HDX reaction details	$\%D_2O$=69% $pH_{(read)}$=7.5 Temp=18ºC	$\%D_2O$=69% $pH_{(read)}$=7.5 Temp=18ºC	$\%D_2O$=69% $pH_{(read)}$=7.5 Temp=18ºC
HDX time course (seconds)	3s, 30s, 300s	3s, 30s, 300s	3s, 30s, 300s
HDX controls	N/A	N/A	N/A
Back-exchange	No correction, deuterium levels are relative	No correction, deuterium levels are relative	No correction, deuterium levels are relative
Replicates	3	3	3
Protein	p110α		
Number of peptides	125	125	125
Sequence coverage	89.9%	89.9%	89.9%
Average peptide /redundancy	Length= 13.9 Redundancy= 1.8	Length= 13.9 Redundancy= 1.8	Length= 13.9 Redundancy= 1.8
Repeatability	Average StDev= 0.6%	Average StDev=0.4%	Average StDev=0.6%

Experiment	Comparing basal PI3K WT vs mutants (H1047R, M1043L and Delta C) and in the presence of pY with H1047R and Delta C. HDX Stats table for data shown in Figure 2.4A, Figure C, Figure D and appendix Figure 5 and 6						
Data set	WT	WT+pY	H1047R	H1047R + pY	M1043L	Delta C	Delta C + pY
HDX reaction details	$\%D_2O$=75% $pH_{(read)}$=7.5 Temp=18ºC	$\%D_2O$=75% $pH_{(read)}$=7.5 Temp=18ºC	$\%D_2O$=75% $pH_{(read)}$=7.5 Temp=18ºC	$\%D_2O$=75% $pH_{(read)}$=7.5 Temp=18ºC	$\%D_2O$=75% $pH_{(read)}$=7.5 Temp=18ºC	$\%D_2O$=75% $pH_{(read)}$=7.5 Temp=18ºC	$\%D_2O$=75% $pH_{(read)}$=7.5 Temp=18ºC
HDX time course (seconds)	3s, 30s, 300s, 3000s at 18ºC 3s at 0 ºC	3s, 30s, 300s, 3000s at 18ºC 3s at 0 ºC	3s, 30s, 300s, 3000s at 18ºC 3s at 0 ºC	3s, 30s, 300s, 3000s at 18ºC 3s at 0 ºC	3s, 30s, 300s, 3000s at 18ºC 3s at 0 ºC	3s, 30s, 300s, 3000s at 18ºC 3s at 0 ºC	3s, 30s, 300s, 3000s at 18ºC 3s at 0 ºC

HDX controls	N/A	N/A	N/A	N/A	N/A	N/A	N/A
Back-exchange	No correction deuterium levels are relative	No correction deuterium levels are relative	No correction deuterium levels are relative	No correction deuterium levels are relative	No correction deuterium levels are relative	No correction deuterium levels are relative	No correction deuterium levels are relative
Replicates	3	3	3	3	3	3	3
Significant differences in HDX	>5% and >0.4 Da and unpaired t-test ≤0.01	>5% and >0.4 Da and unpaired t-test ≤0.01	>5% and >0.4 Da and unpaired t-test ≤0.01	>5% and >0.4 Da and unpaired t-test ≤0.01	>5% and >0.4 Da and unpaired t-test ≤0.01	>5% and >0.4 Da and unpaired t-test ≤0.01	>5% and >0.4 Da and unpaired t-test ≤0.01
Protein							
Number peptides	171	171	170	170	169	164	164
Sequence coverage	95.8%	95.8%	95.8%	95.8%	95.8%	95.8%	95.8%
Average peptide /redundancy	Length= 13.7 Redundancy= 2.1	Length= 13.7 Redundancy= 2.1	Length= 13.7 Redundancy= 2.1	Length= 13.7 Redundancy= 2.1	Length= 13.7 Redundancy= 2.1	Length= 13.7 Redundancy= 2.1	Length= 13.7 Redundancy= 2.1
Repeatability	Average StDev=0.5%	Average StDev=0.5%	Average StDev=0.6%	Average StDev=0.5%	Average StDev=0.5%	Average StDev=0.5%	Average StDev=0.5%
Protein							
Number peptides	117	117	117	117	117	117	117
Sequence coverage	90.3%	90.3%	90.3%	90.3%	90.3%	90.3%	90.3%
Average peptide /redundancy	Length= 16.3 Redundancy= 2.6	Length= 16.3 Redundancy= 2.6	Length= 16.3 Redundancy= 2.6	Length= 16.3 Redundancy= 2.6	Length= 16.3 Redundancy= 2.6	Length= 16.3 Redundancy= 2.6	Length= 16.3 Redundancy= 2.6
Repeatability	Average StDev=0.5%	Average StDev=0.6%	Average StDev=0.6%	Average StDev=0.5%	Average StDev=0.6%	Average StDev=0.6%	Average StDev=0.6%

Experiment	Comparing Kinase Active PI3K and G1049R PI3K. HDX Stats table for data shown in Figure 2.4B and Figure 2.4F and appendix figure 5	
Data set	WT	G1049R
HDX reaction details	$\%D_2O$=76% $pH_{(read)}$=7.5	$\%D_2O$=76% $pH_{(read)}$=7.5

	Temp=18ºC	Temp=18ºC
HDX time course (seconds)	3s, 30s, 300s, 3000s	3s, 30s, 300s, 3000s
HDX controls	N/A	N/A
Back-exchange	No correction, deuterium levels are relative	No correction, deuterium levels are relative
Replicates	3	3
Significant differences in HDX	>5% and >0.4 Da and unpaired t-test ≤0.01	>5% and >0.4 Da and unpaired t-test ≤0.01
Protein	p110α	
Number of peptides	169	169
Sequence coverage	95.2%	95.2%
Average peptide /redundancy	Length=13.7 Redundancy=2.1	Length=13.7 Redundancy=2.1
Repeatability	Average StDev=0.6%	Average StDev=0.5%
Protein	p85	
Number of peptides	114	114
Sequence coverage	89%	89%
Average peptide /redundancy	Length=16.4 Redundancy=2.5	Length=16.4 Redundancy=2.5
Repeatability	Average StDev=0.6%	Average StDev=0.5%

Experiment	Comparing Kinase Active PI3K and Frameshift. HDX Stats table for data shown in Figure 5E	
Data set	WT	Frameshift
HDX reaction details	$\%D_2O$=81% $pH_{(read)}$=7.5 Temp=18ºC	$\%D_2O$=81% $pH_{(read)}$=7.5 Temp=18ºC
HDX time course (seconds)	3s, 30s, 300s, 3000s	3s, 30s, 300s, 3000s
HDX controls	N/A	N/A

Back-exchange	No correction, deuterium levels are relative	No correction, deuterium levels are relative
Replicates	3	3
Significant differences in HDX	>5% and >0.4 Da and unpaired t-test ≤0.01	>5% and >0.4 Da and unpaired t-test ≤0.01
Protein	p110α	
Number of peptides	141	139
Sequence coverage	84.7%	84.7%
Average peptide /redundancy	Length= 13.7 Redundancy= 1.6	Length= 13.7 Redundancy= 1.6
Repeatability	Average StDev=0.9%	Average StDev=0.7%
Protein	p85	
Number of peptides	180	180
Sequence coverage	79%	79%
Average peptide /redundancy	Length= 16 Redundancy= 2.6	Length= 16 Redundancy= 2.6
Repeatability	Average StDev=0.9%	Average StDev=0.6%

Experiment	Comparing Kinase Active PI3K and Kinase Dead (KD) PI3K. HDX Stats table for data shown in Supplemental Figure 3			
Data set	WT	WT+memb	KD	KD + Memb
HDX reaction details	$\%D_2O$=72% $pH_{(read)}$=7.5 Temp=18ºC	$\%D_2O$=72% $pH_{(read)}$=7.5 Temp=18ºC	$\%D_2O$=72% $pH_{(read)}$=7.5 Temp=18ºC	$\%D_2O$=72% $pH_{(read)}$=7.5 Temp=18ºC
HDX time course (seconds)	3s, 300s	3s, 300s	3s, 300s	3s, 300s
HDX controls	N/A	N/A	N/A	N/A
Back-exchange	No correction, deuterium levels are relative	No correction, deuterium levels are relative	No correction, deuterium levels are relative	No correction, deuterium levels are relative
Replicates	3	3	3	3

Significant differences in HDX	>5% and >0.4 Da and unpaired t-test ≤0.01	>5% and >0.4 Da and unpaired t-test ≤0.01	>5% and >0.4 Da and unpaired t-test ≤0.01	>5% and >0.4 Da and unpaired t-test ≤0.01
Protein	p110α			
Number of peptides	133	133	133	133
Sequence coverage	84.9%	84.9%	84.9%	84.9%
Average peptide /redundancy	Length=13.1 Redundancy=1.5	Length=13.1 Redundancy=1.5	Length=13.1 Redundancy=1.5	Length=13.1 Redundancy=1.5
Repeatability	Average StDev=0.7	Average StDev=0.7	Average StDev=1.1%	Average StDev=1.3%
Protein	p85			
Number of peptides	81	81	81	81
Sequence coverage	71.4%	71.4%	71.4%	71.4%
Average peptide /redundancy	Length=15.1 Redundancy=1.6	Length=15.1 Redundancy=1.6	Length=15.1 Redundancy=1.6	Length=15.1 Redundancy=1.6
Repeatability	Average StDev=0.7	Average StDev=0.6%	Average StDev=1.4%	Average StDev=1%

Experiment	Comparing apo and PKC treated p110γ. HDX Stats table for data shown in Figure 3.2 and appendix figure 7	
Protein Data Set	apo p110γ	PKC treated p110γ (phosphorylated p110γ)
HDX reaction details	%D2O=75.5% pH(read)= 7.5 Temp= 18°C	%D2O=75.5% pH(read)= 7.5 Temp= 18°C
HDX time course	0.3s (3s on ice), 3s, 30s, 300s, 3000s	0.3s (3s on ice), 3s, 30s, 300s, 3000s
HDX controls	N/A	N/A
Back-exchange	Corrected based on %D2O	Corrected based on %D2O

Number of peptides	241	241
Sequence coverage	95.5%	95.5%
Average peptide length / Redundancy	Length = 15.2 Redundancy = 3.3	Length = 15.2 Redundancy = 3.3
Replicates	3	3
Repeatability	Average StDev = 0.5%	Average StDev = 0.6%
Significant differences in HDX	>5% and >0.5 Da and unpaired t-test <0.01	>5% and >0.5 Da and unpaired t-test <0.01

Appendix

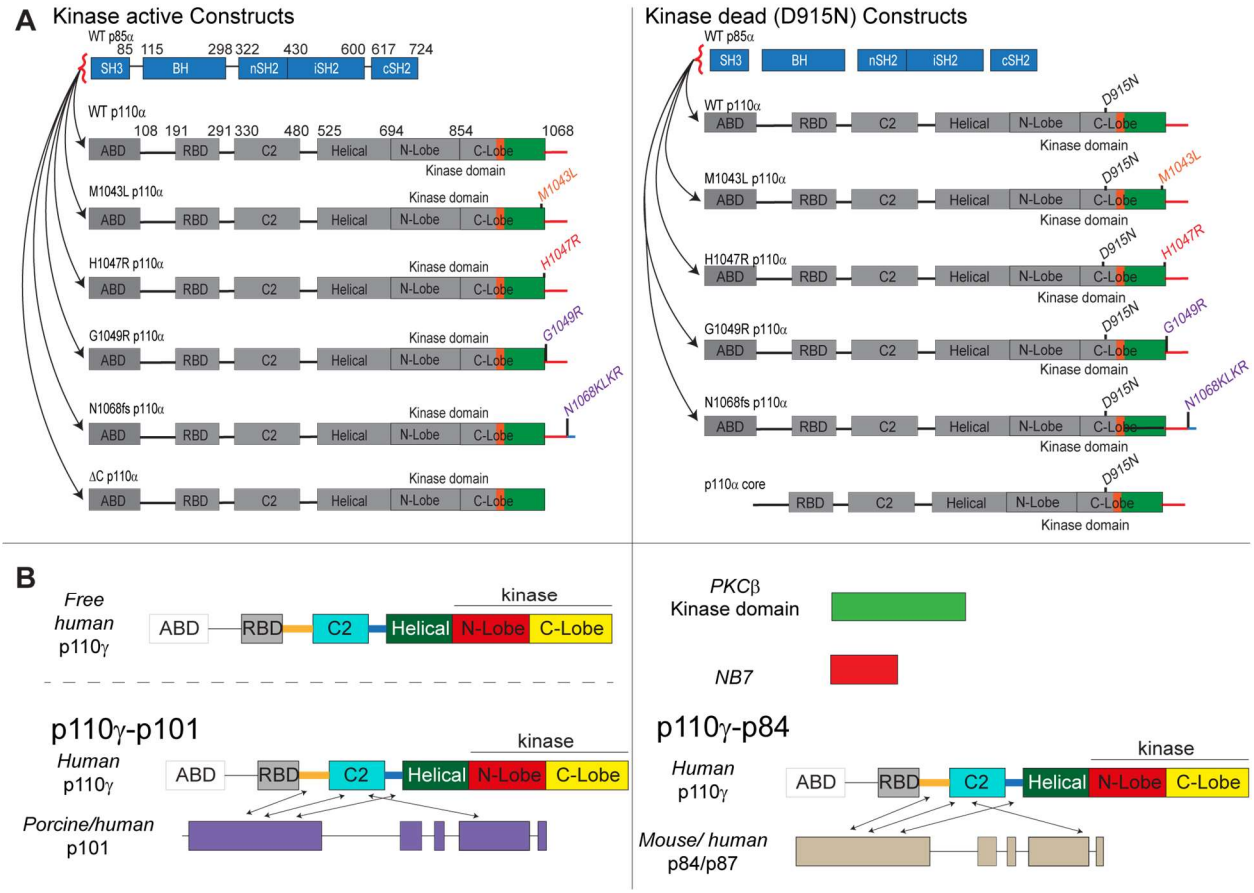

Figure 1: List of constructs used in this thesis

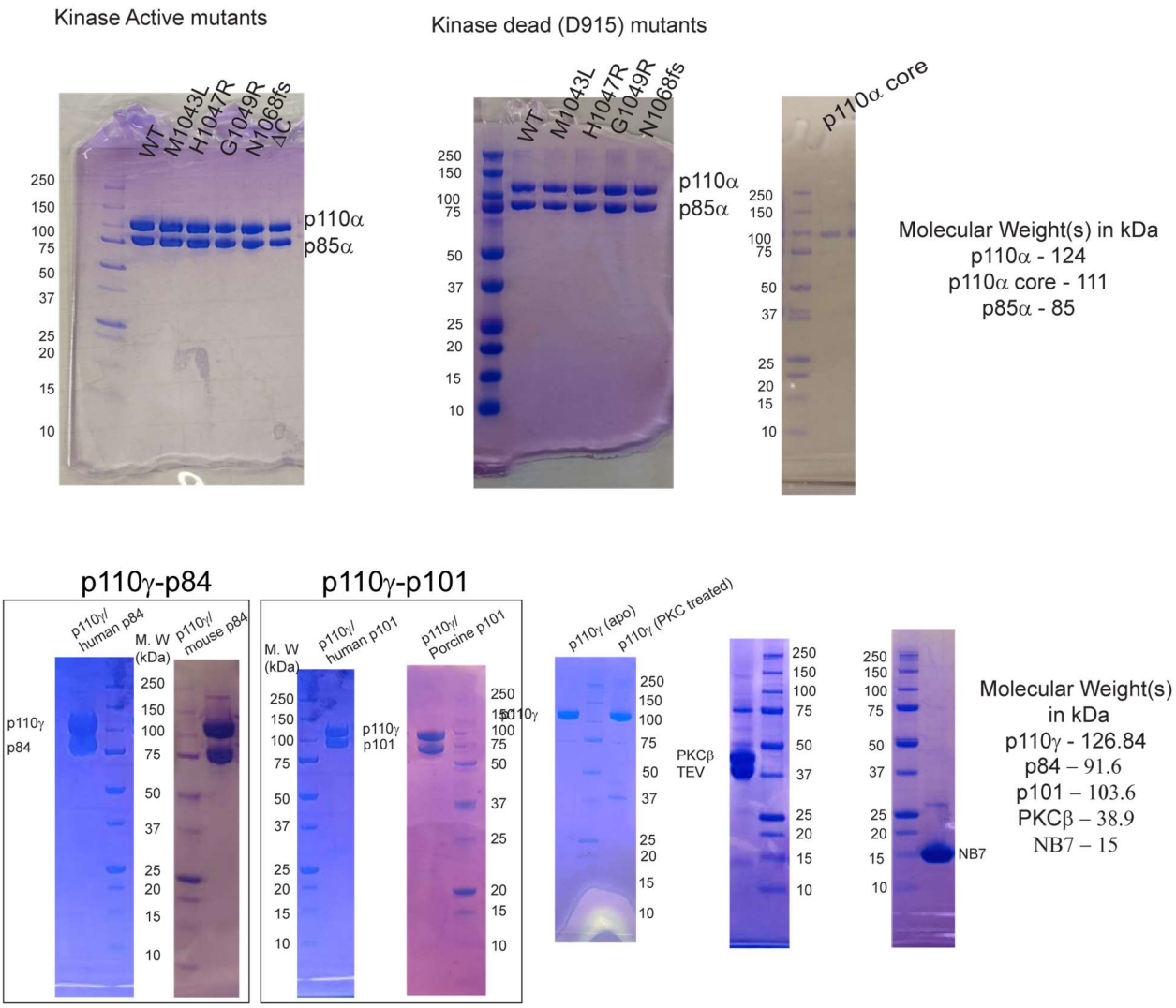

Figure 2: SDS PAGE images indicating the purity of various proteins used in this study.

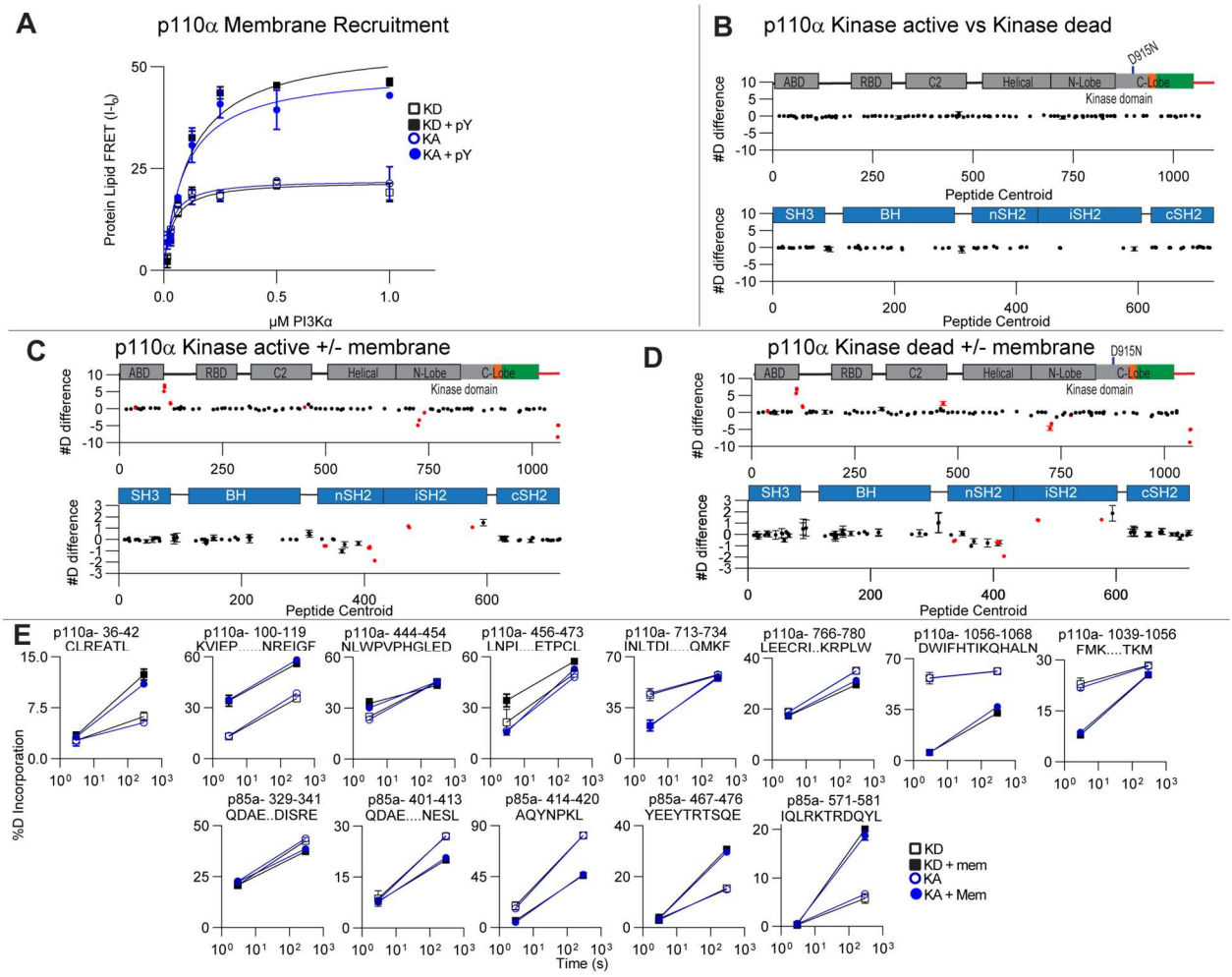

Fig 3 Comparison between kinase active (KA) and kinase dead (KD) p110α

A. Protein-Lipid FRET assay performed with kinase active and kinase dead p110α constructs under basal and pY activated states on liposomes containing 5% PIP2, 10% Dansyl PS, 25 % PS, 65% PE. Experiments were carried out at saturating concentrations of PI3K concentrations ranging from 0.015 to 1μM, 1μM pY, and 33.33 μg/ml of lipid vesicles (error bars are S.D., n=3).

(B-D). The #D difference in deuterium incorporation for p110α and p85α in each experiment, with each point representing a single peptide, with error as SD (n=3). comparing the following conditions: C. p110α/p85α WT kinase active vs kinase dead. D. WT kinase active in solution and membrane. E. WT kinase dead in solution and membrane. Peptides in p110α and p85α that showed significant differences in HDX upon binding to 100 nm extruded 5% PIP2/PS/PE vesicles are colored in red (greater than 0.4 Da and 5% difference at any timepoint, with a two tailed t-test $p<0.01$).

E. %D graphs for a selection of peptides comparing WT kinase active vs Kinase dead under pY active state and membrane bound state. Full HDX-MS data available in source data.

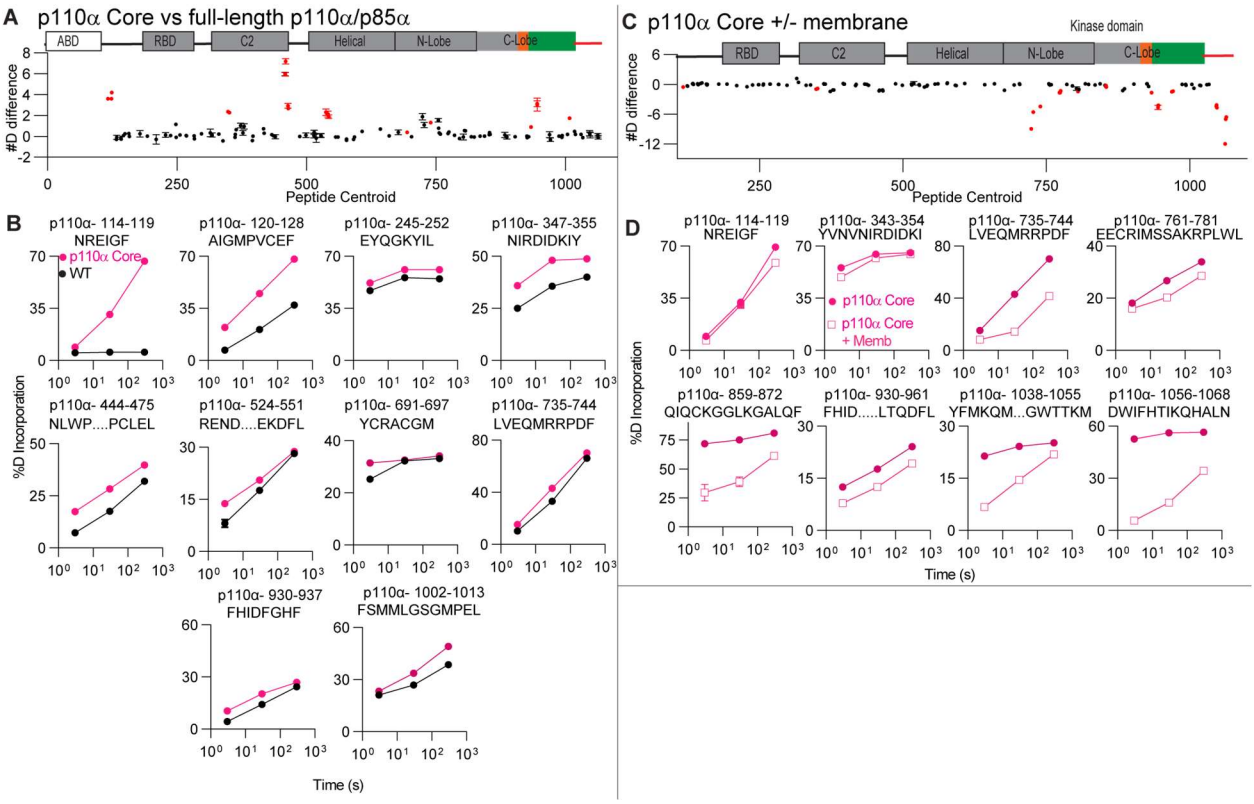

Fig 4 HDX-MS differences for experiments done with ΔABD

A. The #D difference in deuterium incorporation for p110α between p110α core and full-length p110α/p85α complex with error as SD (n=3). Peptides in p110α that showed significant differences in HDX are colored in red (greater than 0.4 Da and 5% difference at any timepoint, with a two tailed t-test p<0.01).

B. %D graphs for a selection of peptides comparing p110α core and full-length p110α/p85α with error as SD (n=3). Full HDX-MS data available in source data.

C. The #D difference in deuterium incorporation for p110α core upon binding 5% PIP2 membranes with error as SD (n=3). Peptides in p110α that showed significant differences in HDX are colored in red (greater than 0.4 Da and 5% difference at any timepoint, with a two tailed t-test p<0.01).

D. %D graphs for a selection of peptides comparing for p110α core in the presence and absence of 5% PIP2 membranes with error as SD (n=3). Note that the intrinsic exchange rate of different regions explains some of the differences in H/D exchange seen upon membrane binding. Regions with stable secondary structure in the absence of membrane are protected primarily at later time point (this is due to membrane binding further stabilising the secondary structure, see 735-744). The C-terminus undergoes a putative disorder-order transition (1056-1068), and shows stabilisation at all time points, with rapid exchange in the absence of membranes. Finally, regions with limited secondary structure (343-354) show protection at only early timepoints of D2O exchange.

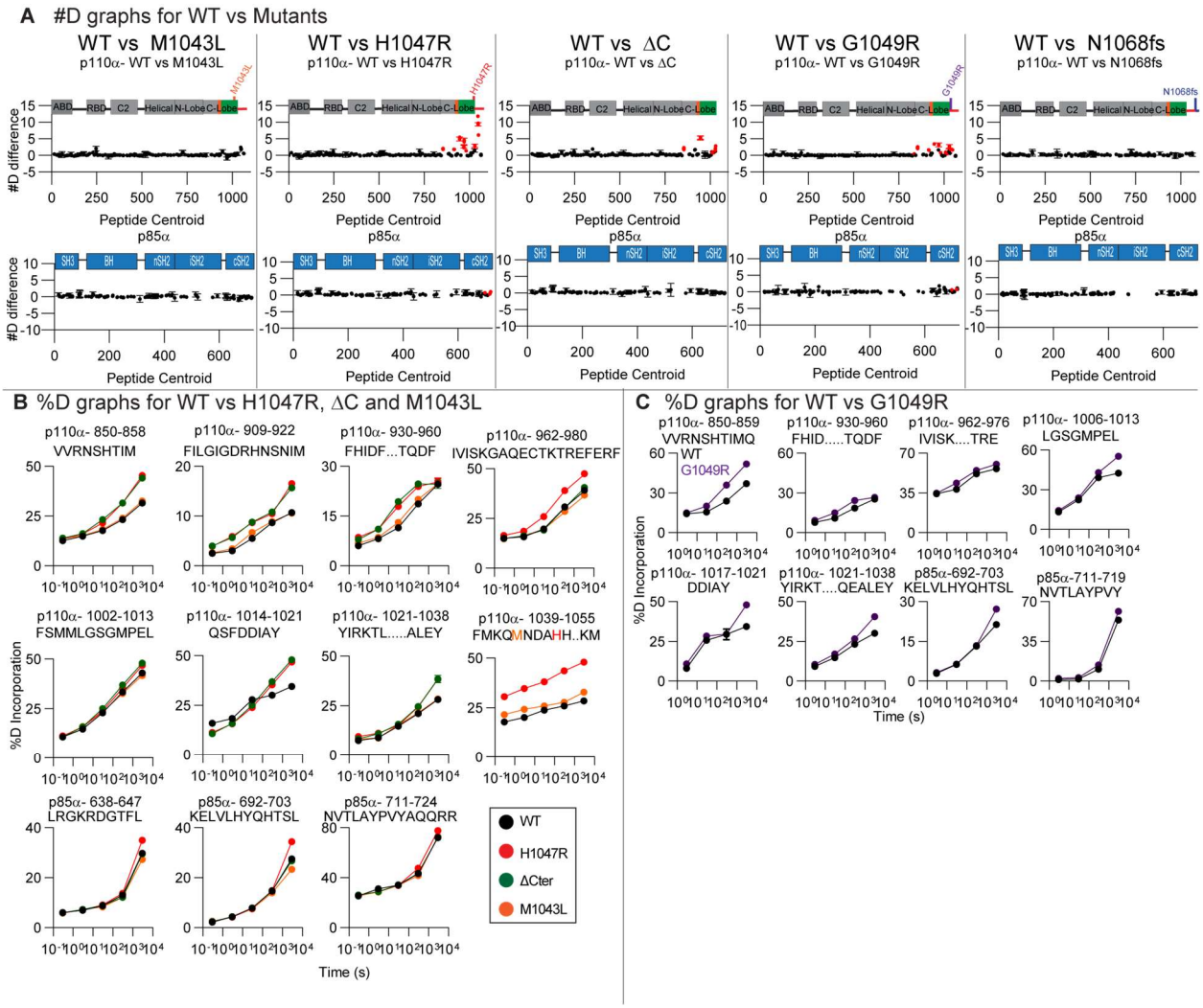

Fig 5 Source data for experiments comparing WT and different c-terminal mutants

A. The #D difference in deuterium incorporation for p110α and p85α in between WT and the indicated p110α mutant or deletion with error as SD (n=3). Peptides in p110α and p85α that showed significant differences in HDX are colored in red (greater than 0.4 Da and 5% difference at any timepoint, with a two tailed t-test p<0.01). Peptide graphs for HDX differences between WT and mutants showing changes in both p110α and p85α **B-C**. % D graphs for a selection of peptides showing significant differences between and WT and mutants.

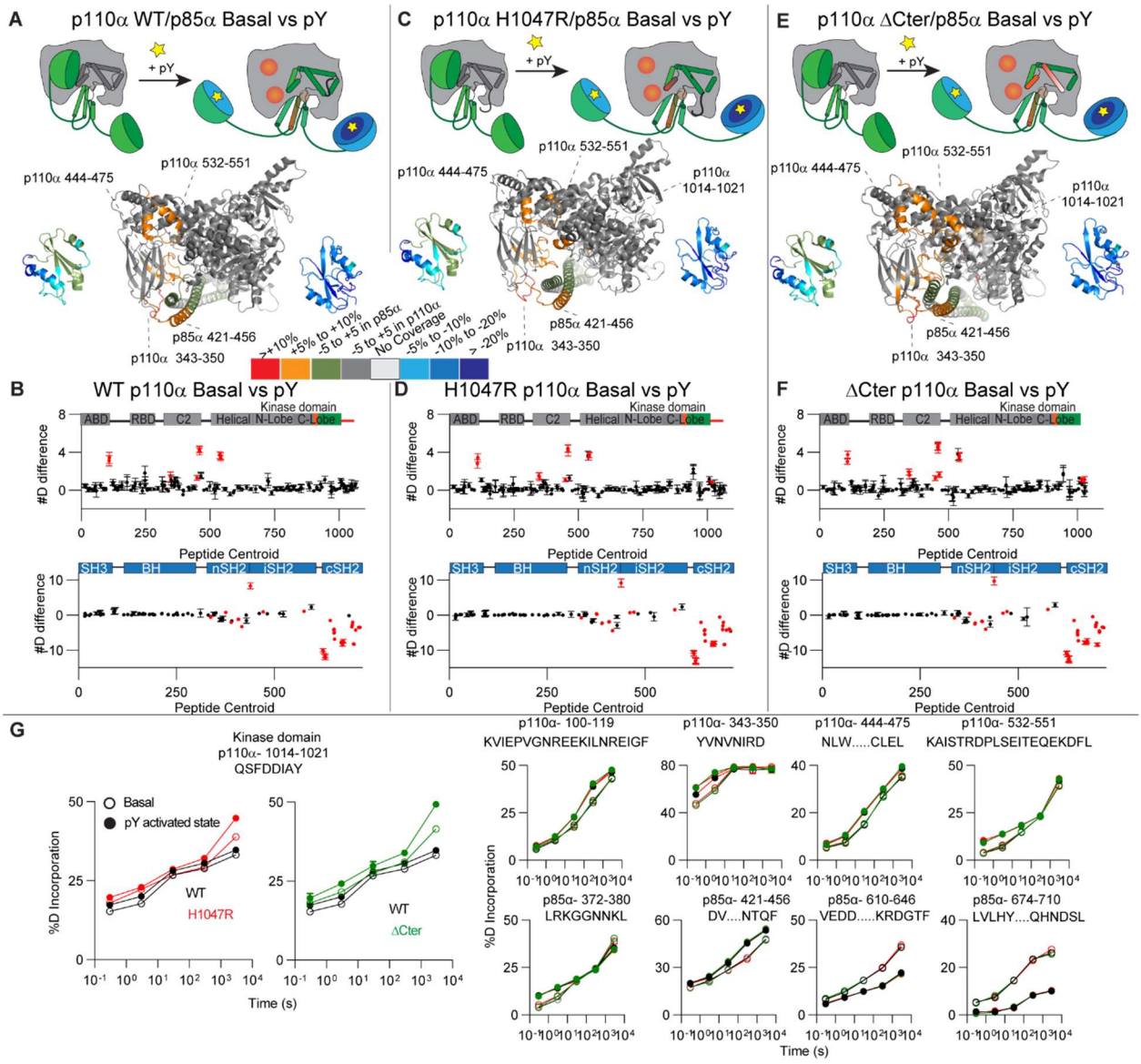

A. Fig 6. Addition of pY leads to increased exposure in the kinase domain.

B. A-C. HDX-MS comparing basal and pY activated states of (A) WT (B) H1047R and (C) the ΔC-terminus. The differences with H1047R were mapped onto p110α/iSH2-nSh2 (PDB: 3HHM) and cSH2 (2Y3A). The differences between WT and ΔCter were mapped onto p110α/iSH2-nSH2 (PDB: 4OVU) and nSH2 (2Y3A)

C. D-F. The #D difference in deuterium incorporation for p110α and p85α upon pY binding for the indicated p110α mutant or deletion with error as SD (n=3). Peptides in p110α and p85α that showed significant differences in HDX are colored in red (greater than 0.4 Da and 5% difference at any timepoint, with a two tailed t-test p<0.01).

D. G. %D graphs for a selection of peptides with differences in exchange. Note that the intrinsic exchange rate of different regions explains some of the differences in H/D exchange seen upon pY binding. Regions with stable secondary structure in the absence of pY are protected primarily at later time points (this is due to pY binding further stabilising the secondary

structure, see 1014-1021). Regions with less stable secondary structure show changes throughout the time course (see peptide 444-475).

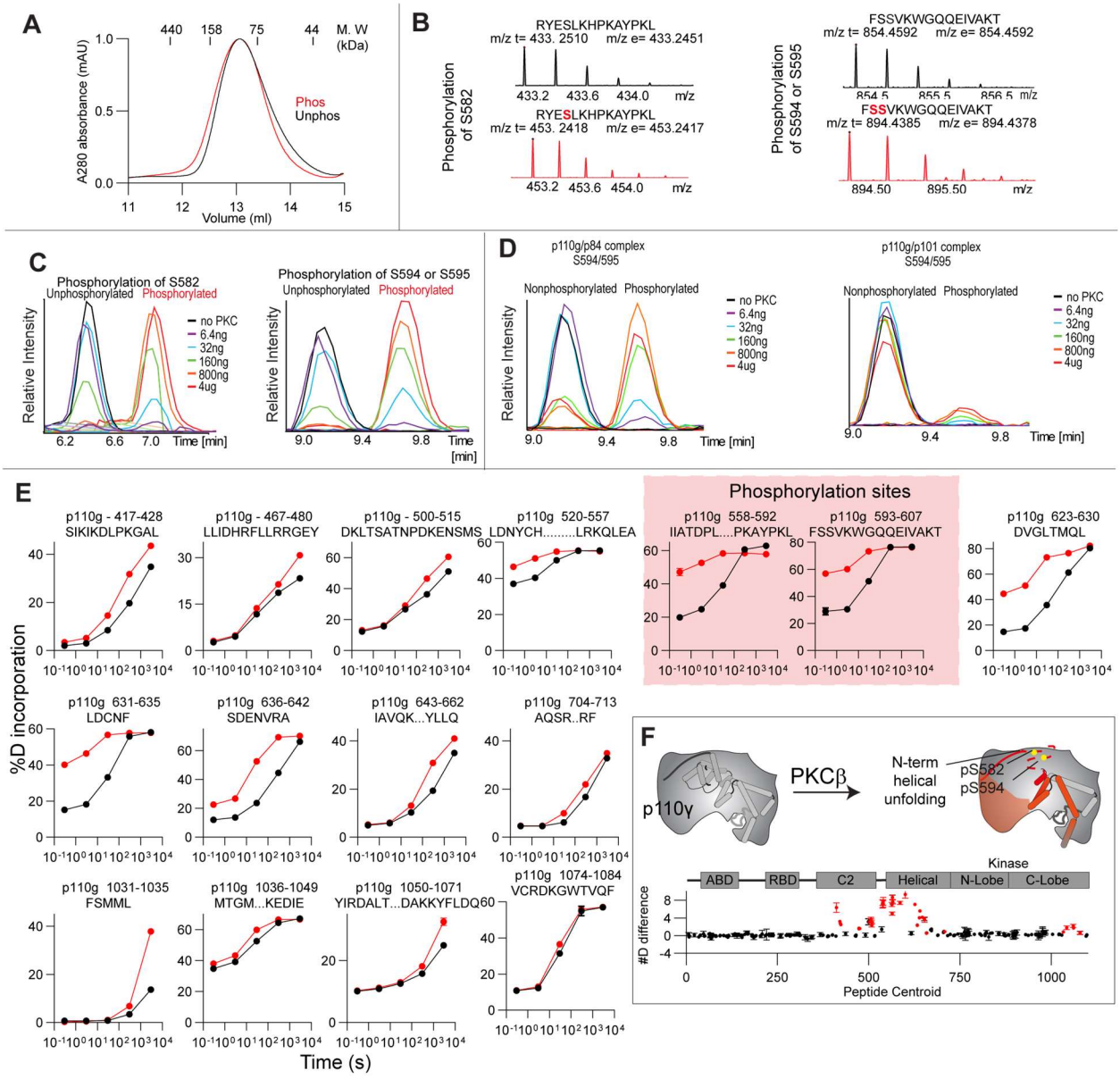

Fig 7. Source data for experiments involving apo vs PKC treated p110γ

E. Gel filtration trace for purified p110γ apo and PKCβ treated p110γ
B and C. Extracted ion traces for S582 and S594/595 peptides for p110γ **D.** Ratio of the intensity of extracted ion traces for S594/S595 from p110γ/p101 and p110γ/p84 samples treated with increasing concentration of PKCβ. **E.** % D graphs for a selection of peptides showing significant differences between apo and phosphorylated p110γ. **F.** The #D difference in deuterium incorporation for p110γ in between apo and phosphorylated state with error as SD (n=3). Peptides

in p110γ that showed significant differences in HDX are colored in red (greater than 0.4 Da and 5% difference at any timepoint, with a two tailed t-test $p<0.01$).